Measurement and modelling of snow properties in urban and suburban Montreal neighbourhoods.

Eric Christensen

Masters of Science

Department of Natural Resource Sciences

McGill University

Montreal,Quebec

October, 2009

A thesis submitted to McGill University, in partial fulfillment of the requirements of the degree of Master of Science

ABSTRACT

Although snow's behaviour is well known in rural contexts through a long standing and widespread network of measurement and recording, the specificity of existing urban datasets to where they were measured limits their applicability to other cities. In this study, snow measurements were performed in urban and suburban Montreal, Québec, Canada over the course of the winter of 2007-2008. Observations of density, depth and albedo showed general trends similar to those expected from rural snow but with density values closer to those measured in other urban studies. Snow properties were scaled up to the convective footprint of an eddy covariance flux tower. Convective fluxes showed little to no relationship with observed snow conditions. Snow evolution data was used in the validation of an offline version of the snow subroutine that is part of the ISBA land surface model. Best results were found for locations subjected to little or no disturbance. Worst results were found for highly disturbed locations.

ABRÉGÉ

Malgré que le comportement de la neige soit bien documenté en milieu rural grâce à des réseaux de mesure en place depuis longtemps, la complexité des milieux urbains fait en sorte que le transfert de données acquises dans une ville à une autre n'est pas justifiable. Dans le but de la recherche présentée dans cette thèse, des mesures de la couverture neigeuse ont été effectuées dans un quartier résidentiel de la ville de Montréal, Québec, Canada et dans une de ses banlieues au cours de la saison hivernale 2007-2008. Les tendances générales se comportent similairement à celles observées en milieu rural à l'exception que les valeurs de densités se rapprochaient plus de valeurs observées au cours d'autres études urbaines. Les propriétés de la neige ont alors été mises à l'échelle de la zone source convective d'équipements de mesure de flux énergétiques. Les flux convectifs n'ont pas montrés de signe d'une dépendance aux conditions de neige. La base de données de l'évolution des propriétés de la neige a également servi dans la validation d'une version autonome du modéle de neige faisant partie du modéle d'échange de surface ISBA. Les meilleurs résultats ont étés obtenus pour des endroits subissant le minimum de perturbations humaines. Les pires résultats découlent de la simulation d'endroits très dérangés.

ACKNOWLEDGEMENTS

I would like to extend my sincerest thanks to my supervisor, Dr. Ian Strachan for the expert guidance and support he provided throughout my studies as well as the occasional non-work related conversation to lighten the mood. I am also very grateful for the help provided by Dr. Onil Bergeron, who designed the snow protocol, produced the necessary subroutines to access any energy flux data and who was my hotel-roommate when it came the time to travel somewhere.

I would like to thank the laboratory technicians we had over the course of the project: Pierre-Luc Lizotte, Jean-François Aublet and Kenton Ollivierre who assisted in the snow measurement process and who gave up many of their weekends to be on call for the "weekend weather watch". They each made the work more efficient and more enjoyable in their own special way.

Thanks to the many people at environment Canada: Dr. Frédéric Chagnon who shared his previous experience in measuring snow properties and who came out often to assist in snow measurements, Dr. Stéphane Bélair who provided me with a copy of the standalone version of the snow model and some tips on how to get it running as well as some tips on model validation and the occasional (but very appreciated) career advice and Dr. Jocelyn Mailhot who also gave feedback and advice on model validation procedures.

I would like to thank the homeowners that allowed us to access their property to perform snow and energy flux measurement operations. A special mention goes to Mr. Jacques Vanier who was almost always around to offer a helping hand, some words of wisdom, the right tool for the job or a suitable combination of these three for the situation at hand without there ever being any kind of obligation for him to do so.

Thanks to my housemates, Maryse and Jenna, for tolerating and being nice to me, introducing me to their friends and sharing the occasional delicious meal with me. And last but not least, I would like to thank the folks at home: my parents, my brother and grandmother who offered their encouragements, gave me outdoor work to do on the farm so that I'd get lots of fresh air and fed me exceptionally well when I would pay them a visit.

CONTRIBUTION OF AUTHORS

"As an alternative to the traditional thesis format, the thesis can consist of a collection of papers of which the student is an author or co-author. These papers must have a cohesive, unitary character making them a report of a single program of research."

This thesis consists of two manuscripts.

SNOWPACK EVOLUTION IN URBAN AND SUBURBAN MONTREAL, CANADA

Eric Christensen[1], Ian B. Strachan[1], Onil Bergeron[1]

[1]Dept. of Natural Resource Sciences, McGill University, Montreal, Quebec.

This manuscript is the original work of Eric Christensen with the following exceptions: Dr. Onil Bergeron elaborated the snow measurement protocol and performed post-processing and cleaning on energy flux data. Dr. Ian Strachan provided expert advice, financial support and editing of this document.

VALIDATION OF THE ISBA SNOW MODEL IN THE CONTEXT OF MONTREAL URBAN AND SUBURBAN SNOW

Eric Christensen[1], Ian Strachan[1], Stéphane Bélair[2]

[1]Dept. of Natural Resource Sciences, McGill University, Montreal, Quebec.

[2]Recherche en Prévision Numérique, Environment Canada, Dorval, Quebec.

This manuscript is the original work of Eric Christensen with the following exceptions: Dr. Stéphane Bélair provided the author with the standalone snow model and expert advice on getting it to run. Dr. Ian B. Strachan provided analytical insight, financial support and editing of this document.

TABLE OF CONTENTS

ABSTRACT ii

ABRÉGÉ iii

ACKNOWLEDGEMENTS iv

CONTRIBUTION OF AUTHORS vi

LIST OF FIGURES ix

LIST OF TABLES xi

1 Introduction 1

2 Literature review 4

2.1 Surface radiation and energy budget 4
2.1.1 Net Radiation 6
2.1.2 Ground heat flux 7
2.1.3 Convective fluxes 7
2.1.4 Snow's effect on the surface energy budget 8
2.1.5 Energy budget measurement 11
2.1.6 Instrument source area or field of view 14
2.2 Snow measurements 21
2.2.1 Snow Water Equivalent 22
2.2.2 Depth 23
2.2.3 Density 24
2.2.4 Areal Coverage 25
2.2.5 Albedo 26
2.2.6 Temporal vs. Spatial studies 27
2.3 Simulating snow 31
2.3.1 "Old-school" snow models 32
2.3.2 "Next-generation" snow-climate models 34
2.3.3 Urban snow simulations 38

3 Snowpack evolution in urban and suburban Montreal, Canada 41

3.1 Introduction 41
3.2 Theory 42
3.2.1 Snow's effect on the energy budget 42

3.2.2 Snow properties . . . 44
3.3 Materials and Methods . . . 45
3.3.1 Site description . . . 45
3.3.2 Snowcover measurements . . . 48
3.3.3 Convective energy flux calculations . . . 54
3.3.4 Convective source area estimations . . . 55
3.4 Results . . . 56
3.4.1 Snow property evolution . . . 56
3.4.2 Snow and the urban energy budget . . . 64
3.5 Discussion . . . 72
3.5.1 Snowcover evolution . . . 72
3.5.2 Energy fluxes and snow properties . . . 76
3.6 Summary and conclusions . . . 79

Preface to Chapter 4 . . . 82

4 Validation of the ISBA snow model in the context of Montreal urban and suburban snow . . . 83

4.1 Introduction . . . 83
4.2 Model description . . . 86
4.2.1 Model physics . . . 86
4.2.2 Model inputs and outputs . . . 91
4.2.3 Model execution . . . 92
4.3 Snow validation dataset . . . 94
4.4 Results . . . 95
4.4.1 Overall trends . . . 95
4.4.2 Best model run performance . . . 97
4.4.3 Worst model run performance . . . 104
4.5 Discussion . . . 106
4.5.1 Highlights . . . 106
4.5.2 Low and medium distubance snow types . . . 107
4.5.3 Roadside snowbanks and alley shoulders . . . 108
4.5.4 Urban undisturbed snowcover type . . . 110
4.5.5 Model bias . . . 111
4.6 Summary and Conclusions . . . 112

5 Summary and Conclusion . . . 114

References . . . 116

LIST OF FIGURES

Figure page

2–1 Absorption coefficient of snow as a function of wavelength. . . 9

2–2 Source weight function as defined in Schmid (1994). 16

2–3 Geometrical derivation of the radiation source area. 21

3–1 Sampling sites for snow measurements. 46

3–2 Snow types encountered during snow measurements at the suburban site. 49

3–3 Snow types encountered during snow measurements at the urban site. 50

3–4 Spatial arrangement of transects at the urban and suburban sites. 51

3–5 depth measurements 52

3–6 density measurements 53

3–7 albedo measurements 54

3–8 Measured snow depth for the different snow cover types at the suburban site. 57

3–9 Measured snow depth for the different snow cover types at the urban site. 58

3–10 Measured snow density for the different snow cover types at the suburban site. 59

3–11 Measured snow density for the different snow cover types at the urban site. 60

3–12 Measured snow albedo for the different snow cover types at the suburban site. 61

3–13 Measured snow albedo for the different snow cover types at the urban site. 62

3–14 Estimation of snow cover proportions in suburban convective source area 65

3–15 Estimation of snow cover proportions in urban convective source area 66

3–16 Proportions of prevalence of snow cover types at the suburban site. 67

3–17 Proportions of prevalence of snow cover types at the urban site. 67

3–18 Weighted snow depth at the urban and suburban sites. 68

3–19 Weighted snow density at the urban and suburban sites. . . . 68

3–20 Daytime averaged energy fluxes and Bowen ratio at both sites. 69

3–21 Informative ratios of daytime averaged fluxes. 70

3–22 Sequential digital photographs of a suburban backyard. 78

3–23 Sequential digital photographs of a urban backyard. 78

4–1 SWE model output for all 9 snow cover types. 98

4–2 Depth model output for all 9 snow cover types. 99

4–3 Density model output for all 9 snow cover types. 100

4–4 Scatter-plots of SWE output for all snow cover types. 101

4–5 Scatter-plots of depth output for all snow cover types. 102

4–6 Scatter-plots of density output for all snow cover types. 103

4–7 Density output for medium and minimal disturbance snow types. 109

LIST OF TABLES

Table		page
2–1	Names and common SI units of symbols used in the energy budget section.	5
2–2	Names and common SI units of symbols used in the source area modelling section.	16
3–1	Height in meters of temperature and humidity sensors at the urban and suburban stations.	47
3–2	Length of snow measurement transects and the distance between snow depth point measurements.	50
4–1	Names and common SI units of symbols used in the model description section.	87
4–2	Forcing variables input to the snow model.	92
4–3	Model outputs and prognostic variables of the snow model	93
4–4	Key model validation statistics describing the agreement between simulated and observed snow properties	96
4–5	Average of normalized goodness of fit statistics (d, slope and r^2).	97
4–6	Index of agreement (d) for best fitting snow types concerning snow depth and water equivalent.	97
4–7	Root mean squared error (RMSE) for best fitting snow types concerning snow depth and water equivalent.	97

CHAPTER 1
Introduction

Weather forecasting is an important activity in today's society both in terms of ensuring public safety and for event planning. For example, municipal workers can be better prepared on mornings of severe snowfall, local authorities can alert concerned populations of incoming ice storms in an attempt to mitigate their effects and farmers depend on weather forecasts in the summer months as they try to dry and harvest forage for the coming winter.

The operational weather forecasting systems that perform this task are typically made up of two parts: a general circulation model (GCM) to simulate the large-scale movement of air masses and a land surface model (LSM) to model the energy and mass exchanges between the surface and the planetary boundary layer of the atmosphere. The latter is highly dependent on local surface conditions. Both components are coupled for constant feedback between one another.

Current versions are optimized for rural areas and provide reasonably accurate predictions ($\geq 60\%$ accuracy) (Ripley and Archibold, 2002). However, with an ever increasing proportion of the population now residing in cities, it is becoming imperative to be able to simulate weather in urban areas as well as the effects that these may have on meteorological patterns downstream (Bornstein and Lin, 2000). To achieve this effectively, a different land surface scheme must be adopted; one that accounts for additional energy exchanges unique to the urban environment.

The Environmental Prediction in Canadian Cities (EPiCC) Research Network aims to meet this requirement by developing an urban-atmosphere modeling system evaluated for Canadian urban climates (EPiCC, 2010). This is done through a coordinated effort of ground based energy flux observations, computer modelling and remote sensing. Ground based observations are carried out in two contrasting cities: Montreal, with a continental climate and abundant winter snowfall, and Vancouver, which has a maritime climate, mild winters and where much summer irrigation of residential lawns occurs.

Snow occupies an important place in the urban energy balance, significantly increasing surface albedo and providing the system with a new medium for heat storage both in the form of a potential increase in snow temperature and in the production of liquid water that remains within the snow. In the case where melting exceeds the water retention capacity of the snowpack and produces runoff, the latter can constitute a form of energy dissipation (Oke, 1997). These modifications to the energy budget are quite well quantified in a rural context and the relationships between snow properties and atmospheric exchanges apply equally well to other environments (i.e. the city). What changes is how the snow properties themselves evolve in those environments. In the case of the city, for example, direct human intervention such as snowplowing and spreading of abrasives as well as more indirect influences such as splashing of contaminants by automobile traffic and the melting of snow near buildings complicate the processes of snowpack accumulation, densification and discoloration (Semádeni-Davies and Bengtsson, 1998; Semádeni-Davies, 1999). What is left to do, then, is to work to gain a better understanding of the evolution of snow properties in the city for which simulation of winter energy fluxes is required.

This thesis has three objectives:

1. To collect, using physical observations, a dataset of snow property evolution in urban and suburban Montréal.
2. To scale up the snow properties to the convective source area of a flux tower and attempt to infer links between changes in the snowpack and the measured energy fluxes.
3. To use the observational data in the validation of the snow submodel of the ISBA land surface scheme in order to qualify the ability of this rural model to simulate snow in urban conditions.

Following this introduction is a review of the prominent literature on the subjects of the surface energy budget, snow measurements and the simulation of snow properties. In the context of this research, a snow observations campaign was undertaken in the city of Montreal over the course of the winter of 2007-2008. Several snow properties were measured during the entire winter from the time of the first snowfall until complete ablation of the snowpack. The results from this campaign (Objective 1) as well as a comparison between snow properties and measured energy flux data (objective 2) are presented in chapter 3. A standalone version of the (rural) snow submodel contained within ISBA was initialized and validated using the Montreal snow dataset. This process and the results (objective 3) are presented in detail in chapter 4.

CHAPTER 2
Literature review

For most of the Canadian winter, snow covers the ground, altering human activity in sectors such as land transportation, agriculture and winter recreation. It also acts to create a store of water made available to fauna and flora that is released upon melting and profound modifications in the energy budget and reductions in ecosystem productivity (Pomeroy and Goodison, 1997) are documented in the literature.

2.1 Surface radiation and energy budget

The collection of energy inputs and outputs to an ecosystem is often referred to as the surface *energy budget* although, the term *energy balance* is often employed interchangeably. These exchanges of heat obey the conservation of energy and, in the case of a natural surface, can be expressed as in equation 2.1, below. Therein, Q^* is the net radiation input to the system, Q_G is the ground storage flux, Q_H is the convective sensible heat flux, Q_E is the convective latent heat flux, Q_P is the photosynthetic energy uptake, Q_B is the energy stored in the air and Q_A is the horizontal energy flux associated with advection Oke (1997). By convention, the net radiation is positive when directed toward the surface and all-non radiative fluxes are positive when directed away from the surface. Names and SI units of all variables used in this section are shown in table 2–1.

$$Q^* = Q_G + Q_H + Q_E + Q_P + Q_B + Q_A \tag{2.1}$$

Table 2–1: Names and common SI units of symbols used in the energy budget section in order of appearance

Symbol	Variable Name	SI Units
Q^*	Net radiation	W m^{-2}
Q_G	Ground heat storage flux density	W m^{-2}
Q_H	Sensible heat flux density	W m^{-2}
Q_E	Latent heat flux density	W m^{-2}
Q_P	Photosynthetic energy uptake	W m^{-2}
Q_B	Air energy storage	W m^{-2}
Q_A	Horizontal energy advection	W m^{-2}
$K_\downarrow$	Downwelling shortwave radiation	W m^{-2}
$K_\uparrow$	Upwelling shortwave radiation	W m^{-2}
$L_\downarrow$	Downwelling longwave radiation	W m^{-2}
$L_\uparrow$	Upwelling longwave radiation	W m^{-2}
α	Albedo (shortwave radiation reflection coefficient)	(no units)
ϵ	Thermal emissivity	(no units)
σ	Stefann-Boltzmann constant	W m^{-2} K^{-4}
k_s	Soil thermal conductivity	W $m^{-1}K^{-1}$
T_s	Soil temperature	K
K_H	Eddy diffusivity coefficient of heat transport	m^2s^{-1}
K_V	Eddy diffusivity coefficient of vapour transport	m^2s^{-1}
C_a	Heat capactiy of air	J m^{-3} K^{-1}
L_v	Latent heat of vaporisation	J kg^{-1}
$\overline{\theta}$	Potential Temperature	K
$\overline{\rho}_v$	Vapour Density	kg m^{-3}
Q_R	Rainfall heat flux density	W m^{-2}
ΔQ_S	Snowpack heat storage flux density	W m^{-2}
ΔQ_M	Latent heat due to melting	W m^{-2}
ζ	Shortwave radiation absorption coefficient	(no units)
Ψ	Shortwave radiation transmission coefficient	(no units)
k_λ	Wavelength dependent extinction coefficient	m^{-1}
k_{plate}	Thermal conductivity of the heat flux plate	W $m^{-1}K^{-1}$
ρ_a	Air density	kg m^{-3}
C_p	Heat capacity of air at constant pressure	J m^{-3} K^{-1}
T	Air temperature	K
q	Specific humidity	$\frac{kg_{(WaterVapour)}}{kg_{(Moistair)}}$

In most common cases, Q_A, Q_B and Q_P are negligible compared to the other terms of eq. 2.1. Thus, it can be simplified to

$$Q^* = Q_G + Q_H + Q_E \tag{2.2}$$

2.1.1 Net Radiation

The first term in the surface energy budget (equation 2.2) refers to the net radiation at the surface under study. It is defined as the difference between incoming and outgoing shortwave and longwave radiation (eq. 2.3).

$$Q^* = K_\downarrow - K_\uparrow + L_\downarrow - L_\uparrow \tag{2.3}$$

where $K_\downarrow$ corresponds to incoming global solar radiation, $K_\uparrow$ is the portion of $K_\downarrow$ reflected back upward from the surface and is a function of the latter's albedo (α; dimensionless) (eq. 2.4), $L_\uparrow$ is the longwave radiation emitted upward from the surface , and $L_\downarrow$ is the longwave radiation emitted from the atmosphere that is received at the surface .

$$\alpha = \frac{K_\uparrow}{K_\downarrow} \tag{2.4}$$

The longwave terms are a function of the respective emitting temperature (T; K) and emissivity (ϵ; dimensionless) and can be expressed as:

$$L_\uparrow = \varepsilon_{surf.}\sigma T^4_{surf.} \tag{2.5}$$

$$L_\downarrow = \varepsilon_{atmos.}\sigma T^4_{atmos.} \tag{2.6}$$

where σ is the Stefan-Boltzmann constant. Inserting eqs. 2.4 and 2.5 back into the radiation budget (eq. 2.3), a new form of the latter is obtained that better expresses the surface's control through reflection and emission of radiation (eq. 2.7) (Stull, 1989).

$$Q^* = K_{\downarrow}(1-\alpha) + \sigma\left(\epsilon_{surf.}T_{surf.}^4 + \epsilon_{atmos.}T_{atmos.}^4\right) \tag{2.7}$$

2.1.2 Ground heat flux

The soil heat flux is the vertical conduction of heat between the different contacting soil layers. Therefore it is expressed in equation 2.8 as the product of a soil thermal conductivity (k_s) and the vertical gradient of soil temperature ($\partial T_s/\partial z$) (Oke, 1997). When the soil surface is warmed during the day by positive net incoming radiation, a temperature gradient is introduced between the upper and lower soil layers. This induces conduction downward, transporting heat away from the surface, into the ground (positive soil heat flux). Conversely, in the case of soil surface cooling, the temperature gradient would be reversed and heat would be transported upwards, toward the surface from deeper in the ground (negative soil heat flux).

$$Q_G = -k_s\frac{\partial\overline{T_s}}{\partial z} \tag{2.8}$$

2.1.3 Convective fluxes

During the daytime, the net radiation is typically positive indicating an energy surplus. The principal means for the the surface to remove this excess energy is through the exchange of sensible (Q_H) and latent heat (Q_E). Together, these are termed *convective fluxes* because their vertical exchange relies on atmospheric turbulent mixing.

These fluxes are typically expressed using a gradient-diffusion relationship where in the fully turbulent case, an eddy diffusivity (K_H and K_V), is multiplied by an appropriate gradient to result in:

$$Q_H = -C_a K_H \frac{\partial \overline{\theta}}{\partial z}$$
$$Q_E = -L_v K_V \frac{\partial \overline{\rho}_v}{\partial z} \tag{2.9}$$

2.1.4 Snow's effect on the surface energy budget

The surface energy budget changes substantially with the presence of a snowpack. Comparing equation 2.2 and equation 2.10, the most notable differences are that a previously ignored driver, Q_R, the heat supplied by rainfall and from the freezing of liquid precipitation inside the snowpack becomes significant enough to be considered; and two new outputs are included: the net heat storage, ΔQ_S, corresponding to the heat involved in warming the snowpack without incurring a change of phase and ΔQ_M, the storage of energy in the snowpack in the form of latent heat due to melting. The latter can also count toward a loss of energy if the melt water leaves the area as runoff.

$$Q^* + Q_R = Q_E + Q_H + Q_G + \Delta Q_S + \Delta Q_M \tag{2.10}$$

More subtly, incoming radiation is no longer only either absorbed, (ζ), or reflected, (α), right at the surface but also possibly transmitted (Ψ) to deeper within the bulk of the snowpack (possibly even to the underlying soil) because the active surface is no longer opaque (Oke, 1987).

$$\Psi + \alpha + \zeta = 1 \tag{2.11}$$

Absorption of solar radiation is described by Beer-Bouguer-Lambert's law (eq. 2.12) where $F_{\downarrow}$ is the incoming solar radiation flux for a given depth, z,

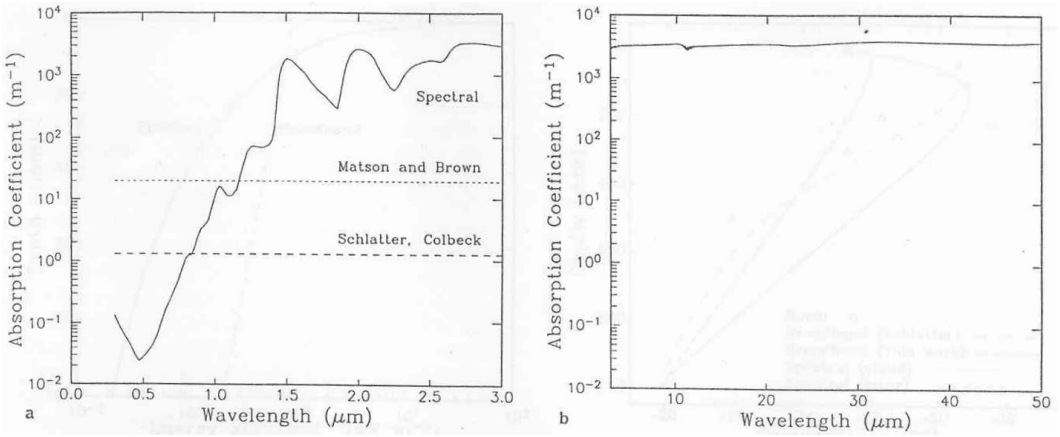

Figure 2–1: Absorption coefficient of snow as a function of wavelength, for snow-grain radius 100 μm and density 400 kg m^{-3} (Brandt, 1993).

and wavelength, λ (related to $K_\downarrow$ through eq. 2.13). k_λ is the wavelength dependent extinction coefficient. As shown in figure 2–1, k_λ has a minimum value around $\lambda = 0.47\mu m$ (blue) and increases rapidly with increasing wavelengths. This has inspired prior hypotheses concerning the formation of a subsurface maximum in the temperature profile because of the ability of shortwave radiation to penetrate the snowpack whereas longwave radiation emission can only occur at the surface. This *solid-state greenhouse effect* has been recreated in models (Colbeck, 1989) using wavelength averaged values for the absorption coefficient. A later study, considering wavelength dependent properties (Brandt, 1993) refuted these findings, attributing experimental evidence of this phenomenon to radiative heating of buried temperature sensors.

$$F_\downarrow(z + \Delta z, \lambda) = F_\downarrow(z, \lambda)\, e^{-k_\lambda \Delta z} \tag{2.12}$$

$$\int_{-\infty}^{\infty} F_\downarrow(\lambda, z = 0)\, d\lambda = K_\downarrow + L_\downarrow \tag{2.13}$$

Another important modification to the energy balance is the proportionally large increase in the value of the albedo (α) which in turn greatly decreases the value of the net radiation Q^* input to the system (eq. 2.3).

The convective terms, Q_E and Q_H find their equations (eq. 2.9) intact, however the temperature and water vapour gradients can see their behaviour changed by snow (Oke, 1987). Likewise, for conduction (eq. 2.8), snow improves the insulating abilities of the ground, decreasing the thermal conductivity (k_S) rendering Q_G insignificant except for cases with thin snowcover. Further analysis of the effect of snow on the energy balance requires seperating the problem into the case of a cold winter-time snowpack and that of a ripe melting snowpack.

Cold snowpack case

When the snow temperature is well below 0°C, no melting occurs in its bulk and only a small amount of evaporation can take place at the surface if enough incident radiation is received. Therefore, the 'melt' energy flux, Q_M, and the latent heat flux, Q_E, in eq. 2.10 become negligible. The likelihood of receiving rain in a cold period of winter is quite small, so the energy input from rainfall, Q_R, can be set aside as well. This leaves a much simplified energy budget over snow shown in equation 2.14 in the case of a cold snowpack (Oke, 1987).

$$Q^* = Q_H + Q_G + \Delta Q_S \tag{2.14}$$

Ripe snowpack case

As the temperature approaches the melting point, the snowpack is said to ripen as temperatures equalize throughout by way of rapid redistribution of heat from the top down brought on by snow at the surface melting, percolating through the snowpack and refreezing, releasing energy (Male and Gray, 1981). The snowpack being isothermal, temperature gradients are eliminated and heat transfer within the pack (Q_G) goes to zero.

Considering that melting generally occurs when air temperatures are warmer than 0°C and that the vapour pressure immediately over melting snow is, at most, the saturation vapour pressure value for 0°C , convective fluxes (Q_H and Q_E) are expected to be directed toward the snow surface (unless if the air is particularly dry, then Q_E will be upward); thus adding to the energy inputs and helping to melt the snowpack further. Since the snow temperature cannot rise any more, melting of the snowpack (ΔQ_M) is the means by which all of this incoming energy is stored and eventually expelled from the snowpack if melting lasts long enough to produce runoff. This yields the following energy budget for the case of a ripe snowpack:

$$Q^* + Q_R = Q_E + Q_H + \Delta Q_M \tag{2.15}$$

2.1.5 Energy budget measurement

Although the above mentioned relationships between the different energy budget components are deduced from fundamental principles, they are examined experimentally in order to verify their accuracy as well as to provide micrometeorologists with a sense of the proportions each term takes depending on the conditions. Often, the only approach is to proceed using ground based measurements.

Conductive exchange

The most common method for measuring soil heat flux is the *combination method* where heat flux at a known depth is measured using soil heat flux plates and the heat storage in the layer above the plates is derived by calorimetry (Cobos and Baker, 2003). Soil heat flux plates are usually constructed of a ceramic or resin disk of a known thermal conductivity into which is embedded a thermopile that measures the temperature difference between the 2 faces of the plate. From this temperature difference, Q_G at the reference depth is

deduced using Fourier's heat transfer law (eq. 2.16) where k_{plate} is the thermal conductivity of the heat flux plate and Δz is its thickness.

$$Q_G(z) = -k_{plate}\frac{dT}{dz} \approx -k_{plate}\frac{\Delta T}{\Delta z} \tag{2.16}$$

Calorimetry is implemented by measuring the soil temperature and heat capacity at different depths for a period of time. This serves to calculate the heat storage flux above the heat flux plate. Once the heat flux at the reference depth and the storage flux between the surface and the flux plate are known, their sum is the heat flux through the surface (Fuchs and Tanner, 1968).

Convective Exchange

The most reliable and direct approach for measuring the convective component of the energy balance is the eddy covariance technique (Arya, 2001). This method requires simultaneous high frequency measurements of 3-dimensional wind speed and of the scalar to be tracked; measurement frequency is crucial to resolving the turbulent eddies as they move past the sensor.

In the case of sensible and latent heat flux, the scalar properties to be tracked are the temperature and water vapour concentration of the air respectively. Fine wire thermocouples are employed for air temperature because of their smaller thermal inertia than conventional thermocouples. Water vapour concentration is most often measured using infra-red gas analyzers.

Knowing the vertical wind speed within a high degree of precision and the air temperature as well as the water vapour pressure contained in the passing eddies, one can calculate the latent and sensible heat fluxes using equation 2.17 (Stull, 1989) where ρ_a is the density of air; C_p, the volumetric heat capacity of air at constant pressure; T, the air temperature; L_v, the latent heat of vaporisation and q, the specific humidity. Primed variables denote fluctuation about the mean quantity and variables with an overbar

denote the time-average of that quantity. The fluxes calculated with eq. 2.17 quantify "how much" of the target quantity has gone past the experimental setup per unit time and area and in which direction.

$$Q_H = \overline{\rho_a}\overline{w' \left(C_p T\right)'}$$
$$Q_E = \overline{\rho_a} L_v \overline{w'q'} \tag{2.17}$$

Radiative exchange

The net radiation (Q^*) can be measured using two pyrradiometers, installing one facing up and the other facing down. These measure total radiation incident on the instrument using a thermopile to measure the temperature difference between the shaded and insolated face of a blackened plate (Oke, 1987). This combination of instruments makes a net radiometer, providing as its sole output, the net incoming radiation. Some research applications require more detailed knowledge of each of the individual radiative fluxes (eq. 2.3). In this case, two pyranometers and two pyrgeometers are installed. These work similarly to pyrradiometers, however they are equipped with a dome made of a material selected to filter the admitted radiation for only shortwave or longwave radiation fluxes. One of each is positioned facing down to measure the upwelling radiation. The signals from each device are logged separately and the net radiation is calculated afterwards.

Other fluxes

The remainder of the energy budget components showcased in equation 2.10 are obtained through different means. The rainfall over snow term, Q_R, can be approximated knowing the amount of precipitation and the air temperature. The net heat storage flux term, ΔQ_S, that comes into play when a volume is considered (not necessarily snow) is obtained by calorimetry much

in the same way as the change of storage calculated in soil heat flux studies as mentioned earlier. Some terms in the energy budget cannot be so easily resolved experimentally. For example, the latent heat of melting, ΔQ_M, would require detailed knowledge of changes in liquid water content in the snowpack and of the amount expelled by runoff. Estimates of these can be reached through modeling approaches.

2.1.6 Instrument source area or field of view

The techniques just described to resolve components of the surface energy budget, by their very nature, have a limited scope. That is to say that they only detect energy or mass fluxes within a limited *source area* or *field of view*. Depending on the variable in question, determining the spatial extent of that source area or field of view is not a trivial matter.

Soil heat flux

The area "seen" by soil heat flux Q_G measurements can be assimilated as a single point in space: any detection of thermal exchanges occur at that point. Any changes in heat storage above the plate determined via calorimetry are, again, confined to a narrow column of soil. The associated disadvantage with using a method that is so spatially restricted (and consequently well defined) is the difficulty with which obtained energy flux information can be scaled up to the full scope of the experiment. This can be overcome by sampling the soil heat flux at multiple locations representative of different conditions occuring within the site of interest.

Convective fluxes

By definition, the values obtained by the eddy covariance technique for the convective fluxes, Q_H and Q_E, are associated to the individual packets of air that flow by the sensor and are detected. The provenance of these packets is dictated by many atmospheric variables and cannot be resolved intuitively.

This does not prove to be a problem when measurements are performed in areas of ideal homogeneous fetch (e.g. flat agricultural land covered in identical monoculture plots); but when those conditions are not met, the question of representativeness of flux measurements arises. To deal with this, the *footprint* or *source weight function* is used. Regardless of the means of calculating it, it is defined as the transfer function between the measured value and the set of forcings at the surface (Schmid, 2002). In equation 2.18 below, $\mathbf{r}$ is the position vector of the sensor, $\mathbf{r}'$ is the vector separating source and sensor (meaning $(\mathbf{r}+\mathbf{r}')$ is the position of the source), $\eta(\mathbf{r})$ is the value measured at the instrument, $Q_\eta(\mathbf{r}+\mathbf{r}')$ is the source or sink strength distribution and $f(\mathbf{r},\mathbf{r}')$ is the transfer function. The integration is performed over all real space.

$$\eta(\mathbf{r}) = \int_{\Re} Q_\eta(\mathbf{r}+\mathbf{r}')\, f(\mathbf{r},\mathbf{r}')\; dr' \tag{2.18}$$

Based on the intensity of the source weight function, contours encompassing the fraction of the total volume under the footprint function, P, are defined as isopleths (f_P). The source area (Ω_P) corresponds to the "area bounded by the normal projection of the isopleth [of level P] (f_P) on the x-y-plane" (see figure 2–2) (Schmid, 1994). Foken and Leclerc (2004) reminds the unseasoned experimentalist about this important detail: Ω_P does not encompass the entirety of the area sensed by the instrument.

The main methods for calculating the source area are the analytical Eulerian approach and the lagrangian stochastic approach, including both forward and backward calculation schemes (Schmid, 2002). Eulerian analytical footprint and source area studies look to get as close as possible to an anlytical solution of the advection diffusion equation in order to maximise mathematical simplicity and reduce computational expense at runtime. Schmid (2002)

Table 2–2: Names and common SI units of symbols used in the source area modelling section in order of appearance.

Symbol	Variable Name
$\mathbf{r}$	Position vector of the sensor
$\mathbf{r}$'	Vector separating source and sensor
$\eta(\mathbf{r})$	Value measured at the instrument
Q_η	Source or sink distribution
f	Transfer (footprint) function
P	Given fraction of total volume under footprint function
f_P	Isopleth of level P
Ω_P	Area bounded by f_P projected onto x-y-plane
z_m	Measurement (sensor) height
z_s	Source height
N	Number of particles released over a time increment
δa	Elemental source area
w	Vertical velocity of a fluid element
r	Radius of radiometric footprint isopleth

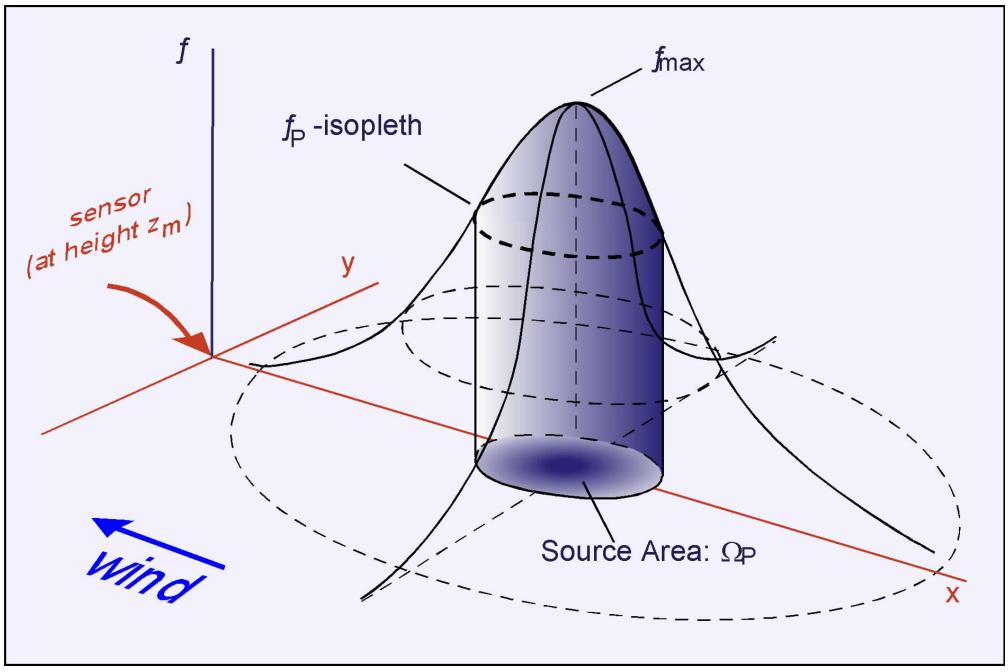

Figure 2–2: Source weight function as defined in Schmid (1994).

suggests that the analytical approach began in earnest with the differential footprint model presented in Schuepp et al. (1990) and that development continued from there, involving successive refinements presented in Horst (1999), Haenel and Grünhage (1999) and Kormann and Meixner (2001) to name a few. It should be noted that the main focus of the latter two was to further simplify mathematical operations. This was done at the cost of physical reality. With today's readily available and inexpensive computing power, some authors prefer to refer to the Horst and Weil method because of it's higher degree of exactitude. Other authors (Leclerc et al., 2003; Foken and Leclerc, 2004) also include the FSAM showcased in Schmid and Oke (1990) and Schmid (1994) in this analytical approach.

An important assumption used in this technique, as well as by others, is that of the inverted gaussian plume. This states that the source weight function "is only dependent on the separation vector between source and sensor, $\mathbf{r}'$, not on the location itself, $\mathbf{r}$"(eq. 2.19) (Schmid, 2002); implying that the surface roughness and stability are uniform in the region. Further, it requires a transfer function, $f(\mathbf{r}')$, that is independent of the source distribution, Q_η. Consequently, if the source has an effect on atmospheric turbulence, for example, in a momentum source or sink, the approach is fundamentally flawed unless the experimental design prescribes a sensor height much greater than the length scale of the individual surface elements; allowing the assumption that turbulent mixing can cancel individual spatial perturbations in the footprint.

$$f(\mathbf{r}, \mathbf{r}') \approx f(\mathbf{r}') \tag{2.19}$$

Lagrangian stochastic models work by assimilating the atmospheric diffusion from a surface to the dispersion of particles that impact the surface within

an expected source area and then move independently of each other carried along by advection and dispersed by turbulence. The position, $\mathbf{x}$, and velocity, $\mathbf{u}$, of each of these particles is described by the stochastic differential equation below where $u^i\,(i = 1, 2, 3)$ are the components of particle velocity, a_i is a function expressing the deterministic component of acceleration in direction i due to turbulence over time, b^{ij} is a function expressing the component of acceleration in direction i due to random fluctuations and $d\xi^j$ is the increment for the random acceleration component, taken from a gaussian distribution with zero mean and variance dt (Kljun et al., 2002; Thomson, 1987). Please note the repeated j index in the second term, denoting a scalar product via the Einstein convention.

$$du^i = a^i\left(\mathbf{x}, \mathbf{u}, t\right) + b^{ij}\left(\mathbf{x}, \mathbf{u}, t\right) d\xi^j \tag{2.20}$$

$$d\mathbf{x} = \mathbf{u}\, dt \tag{2.21}$$

Forward Lagragian models "simulate the release of a large number of particles from a point source [...]. The forward in time integration of eq. 2.20[...] provides a modeled distribution of positions and velocities." (Schmid, 2002) This distribution is then related to a vertical flux of material or energy by assuming that the latter is represented by the joint distributions of vertical velocity and position of the particles. The source weight function is then deduced from a discrete number of simulated particles by constructing a probability density function (PDF) that expresses the probability of a particle released from the source at time t' will be found in the elemental volume of the sensor at time t with a vertical velocity of $w \pm dw/2$. (eq. 2.22) (Schmid, 2002). in eq. 2.22, z_s is the source height, z_m the measurement height, p the PDF and f is the footprint function.

$$f\left(x,y,z_m\right)=\int_0^t\int_{-\infty}^{\infty}wp\left(0,0,z_m,w,t|x,y,z_s,t'\right)\,dw\,dt' \tag{2.22}$$

Combining eqs. 2.20, 2.22 and the inverted plume assumption, one can estimate $f\left(x,y,z_m\right)$ as in equation 2.23 below (Schmid, 2002). Notable models using this approach include Leclerc and Thurtell (1990) and Hsieh et al. (2000).

$$f\left(x,y,z_m\right)\approx\frac{1}{N}\frac{d^2}{dxdy}\left[n_{\uparrow}\left(x,y,z_m\right)-n_{\downarrow}\left(x,y,z_m\right)\right] \tag{2.23}$$

Backward Lagrangian models work on the same basic principles as forward models but with time evolution reversed. This is achieved through a linear coordinate system transformation of the time axis: $t\rightarrow t'=T_0-t$ where T_0 is an arbitrary constant, most likely the time for which a source area calculation is required. What this means from a practical point of view is that focus is shifted from simulating trajectories of particles emitted from a point source at a pre-defined location and rejecting all but those passing through the sensor volume to starting with only those trajectories that interact with measurement equipment and following them back to whichever potential source they may have come from. An important advantage of this method is the footprint distribution is obtained directly (eq. 2.24) without having to depend on the inverted plume assumption; thus remaining valid in horizontally heterogeneous flow (Schmid, 2002). Here, $\mathbf{x}$ is the position of an elemental source, N is the number of particles released over a time increment, δa is an elemental source area, w is the vertical velocity of a fluid element, $\mathbf{r}$ is the sensor location and the indices j and i represent the individual fluid elements and touchdowns within the source respectively.

$$f(\mathbf{x}) = \frac{2}{N\delta a} \sum_{j=1}^{N} \sum_{i=1}^{N_{Td}^{j}} \frac{w_j(\mathbf{r})}{\left|w_{j,i}^{T}\right|} \tag{2.24}$$

Another advantage is that different source geometries or reference surfaces above the ground can be considered in post-processing for a same model-run. Conversely, a move of the sensor position requires re-running the model whereas this was not an issue in the forward approach. Backward Lagrangian models have been decribed and applied in Rotach et al. (1996) and Kljun et al. (2002) to name a few.

Net radiation

The area probed by radiometry is defined as a function of the surface geometry and the field of view and height of the sensor. Due to the generality of equation 2.18 it can still be used in this case, requiring only a different form for the transfer function, f. A simple example is the study of a flat area (see figure 2–3); Schmid (1997) calculates a source weight function and accompanying source area, of the form shown in eq. 2.25.

$$f_R = \left(z_m + \frac{r^2}{z_m}\right)^{-2} \tag{2.25}$$

Given the absence of angular terms in eq. 2.25, the footprint function possesses cylindrical symmetry making its isopleths form concentric circles with the nadir axis at their center. The radii of these isopleths as a function of the P level (see section 2.1.6) is expressed as:

$$\frac{r(\Omega_{P,R})}{z_m} = \left(\frac{1}{P_R} - 1\right)^{-1/2} \tag{2.26}$$

More complex environments such as cities or forests require insight into the surface geometry in order to cope with the intrinsic anisotropy of the surface. Soux et al. (2004) present the SUM model which can be used to

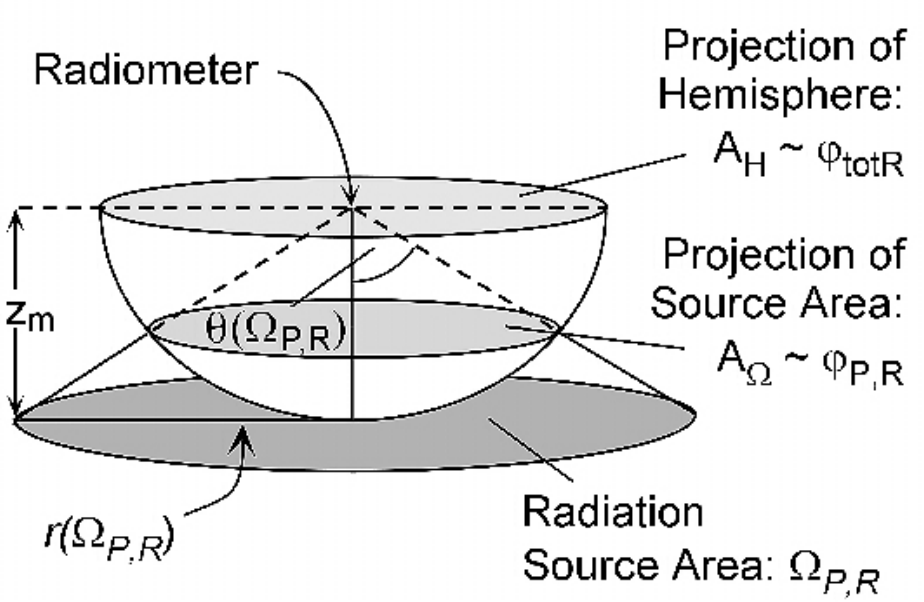

Figure 2–3: The Geometrical derivation of the radiation source area. The source area level P is the ratio of the projection of the source area onto the lower hemisphere and then onto the radiometer plane, A_Ω, to the projection of the entire hemisphere onto the radiometer plane, A_H (Schmid, 1997)

calculate the proportions of facets "seen" by instrumentation in an urban environment as well as provides ample explanation to the reasoning for such a model.

2.2 Snow measurements

Snow measurement campaigns can take on many forms depending on the properties one wishes to study, the resources at hand, the terrain upon which the study is to take place and the processes of interest. The properties chosen govern the experimental requirements in terms of instrumentation, personnel training and site selection. The snowpack characteristics to be tracked are, themselves, heavily influenced by the purpose of the study. Pomeroy and Gray (1995) states that three of the most important physical properties of a snowcover are depth, density and water equivalent. These three along with snow albedo and areal coverage are the focus of the current section.

2.2.1 Snow Water Equivalent

The snow water equivalent (SWE) is the most important variable from a hydrological perspective (Semádeni-Davies, 2000). It corresponds to the amount of water stored in the snowpack that is released by melting it (Goodison et al., 1981). This volume of water, resulting from the accumulation of precipitation over an entire winter, is quickly released during the spring melt period; providing abundant water for plant growth but also possibly causing flooding in urban areas with inadequate drainage (Ho and Valeo, 2005).

The SWE of a snowpack can be measured by multiple means. Gravimetric measurements consist of using a snow tube to obtain a vertical core of snow which can then be weighed to determine the mass of water contained therein (Pomeroy and Gray, 1995). The inherent portability of this method makes it very attractive for spatial studies as the same instrument can be used in many different locations and is easily carried by the operator. The personnel-intense character of the operation, however, can limit the number of samples taken in a given time interval; limiting the temporal resolution of the study.

Snow pillows allow for automated measurements, permitting much better temporal resolution of the SWE in a given location. These consist of large (surface areas ranging from 3.7m^2 to 11.2m^2) flat, bag-like structures filled with an antifreeze fluid and connected to a manometer; installed on level ground, under the snow. As the weight of snow on the pillow builds up, pressure is increased at the gauge and the snow water equivalent is inferred from these pressure readings. The permanence of the installation implies that only one location can be measured throughout the entire winter by each instrument (Goodison et al., 1981).

Snow and ice's ability to attenuate the earth's natural gamma radiation provide another means to measure the SWE. This is done by measuring a

background value when the snowcover is absent and then determining the difference in the presence of a snowpack. This can be done in fixed installations (Goodison et al., 1981) allowing for good time resolution or it can be mounted on an aircraft (Pomeroy and Gray, 1995) in order to cover a large area or terrain that is otherwise inaccessible. Similar experiments can be conducted using microwave sensing equipment. These can be mounted on satellites, permitting regular monitoring of the snow water equivalent (Pomeroy and Gray, 1995).

2.2.2 Depth

Researchers from a variety of fields view snow depth as a fundamental property which must be tracked in any study involving a snow covered surface. Bergeron et al. (2008) highlight the dependence of the regional carbon balance of black spruce forests on winter snow pack depths and Messier (1995) postulates hypotheses on the effects of snow on deer and moose demography to name a few. Beyond these examples, knowledge of the snow depth is important in the practice of a variety of specialized activities: municipal workers need to decide when snow clearing operations have to be undertaken, ski resorts manage their trails based on the snow depth and farmers may wish to judge if their crops will be provided with a sufficient insulating blanket to survive through the cold of winter or if their grazing livestock will need to be fed (Steppuhn, 1981).

Depth measurements can be performed manually using graduated probes inserted into the snowpack along a snowcourse (Pomeroy and Gray, 1995). As is the case with the snow tube for snow water equivalent, this method is very portable and allows the operator and instrument to visit many locations in a

single campaign; thus sampling a large area. Personnel-fatigue and arduousness of terrain, however, can limit the frequency of visits to a particular site, making for coarse temporal resolution.

A fix for these difficulties consists of using permanent markers installed in the snow that can be read from afar on the ground or from an aircraft using binoculars. Although this method is somewhat less labour-intensive, the precision on the depth measurements can be significantly lower and melting can occur around the permanent markers in regions undergoing intense solar radiation (Pomeroy and Gray, 1995). Typical values for depth and snow water equivalent are extremely dependent on location as they are heavily influenced by precipitation and wind relocation patterns.

Automated snow depth measurements can be performed by installing ultrasonic snow depth sensors at the location of interest. These emit high frequency sound pulses and calculate the depth of the snowpack from the return-time. The use of such sonar equipment has advantages such as integrating over the entire interaction surface (circles up to 2m in diameter), high time resolution and non-disturbance of the snow (Pomeroy and Gray, 1995).

2.2.3 Density

Snow density is related to Depth and SWE information for a particular location through:

$$\mathrm{SWE} = 0.001\, d_S\, \rho_S \tag{2.27}$$

where d_S is the depth of the snowpack in the same units as SWE (generally cm) and ρ_S is the density in kg m^{-3} (Pomeroy and Gray, 1995). Thus, this property does not reveal any new information about the snowpack. However, once calculated, it gives access to a wide variety of thermal, mechanical and electromagnetic snow properties such as specific heat, latent heat and thermal diffusivity; Young's modulus, compactive viscosity and shear strength; and

electrical conductivity and the dielectric constant, respectively are functions of snow density(Langham, 1981).

Having an effect over such an array of fundamental properties means that changes in snow density affect a wide range of human activities from winter-road building to the use of snow as a seasonal insulating material. Common snow densities observed in rural areas range between 10 kg m^{-3} for wild snow (Very dry, freshly fallen snow) up to 350 kg m^{-3} for hard wind slab (snow having undergone major compaction under the action of the wind and surface melting due to solar radiation but without having experienced bulk melting) and to extreme values of 600 to 700 kg m^{-3} for glacial firn (McKay and Gray, 1981) (snow partly consolidated into ice through a process involving a single or multiple melt-refreeze cycles (Langham, 1981)). Higher densities, on average, can be found in urban environments where displaced snow has been observed to exhibit densities between 200 kg m^{-3} for piles in residential suburbs (Semádeni-Davies, 1999) to over 700 kg m^{-3} for particularly "compacted, blended, and contaminated urban snow" (Sundin et al., 1999).

2.2.4 Areal Coverage

The proportion of the ground covered by snow has an effect on the regional albedo (see below) as well as on determining the amount of water contained within the snow pack for mass balance studies. Due to variations in topography, vegetation, wind patterns and human intervention, snow is not deposited evenly across the landscape. Snow areal coverage can be calculated using complex considerations of the physical processes at work (Tarboton et al., 2001) or it can be measured. Measurements can be performed visually from the ground (Ueno et al., 2007; Lemonsu et al., 2008) or using aerial photography (Semádeni-Davies, 1999; Tarboton et al., 2001). It could also potentially be

inferred from snow surveys (Goodison et al., 1981). Ueno et al. (2007) employs a snow coverage proportion factor to combine with the point snow water equivalent measurements to obtain what they call the "spatial equivalent snow water quantity".

2.2.5 Albedo

As shown in eq. (2.7), an increase in α brought on by the presence of snow can greatly diminish the net shortwave input to the system under study. It therefore becomes paramount to understand how the albedo of snow varies over time in order to properly model it and include it in considerations of feedback between climate and snow cover (Warren and Wiscombe, 1980; Wuttke et al., 2006). The study by Wuttke et al. (2006) concentrates entirely on the spectral albedo and on albedo as a function of time and solar zenith angle. These were measured using both a broadband, commercially available, albedometer and a spectral albedometer equipped with a dual monochromator. The authors report values ranging between 0.88 and 0.99 for broadband albedo. Such energy resolved studies are very important for the interpretation of albedo measurements by remote sensing (Grenfell et al., 1994) as the latter rely on only a few discrete bands and not the entire shortwave spectrum.

Urban hydrology specialists also undertake albedo measurements (Ho and Valeo, 2005; Semádeni-Davies and Bengtsson, 1998), concerned with the effect that the ability of snow to absorb (reflect) solar radiation has on the rate of snowmelt (Semádeni-Davies and Bengtsson, 1998). Snow albedos have been reported to vary from under 0.3 (Semádeni-Davies, 1999) up to nearly 0.9 (Ho and Valeo, 2005) demonstrating high variability for this property in the city. Ho and Valeo (2005) also report on the evolution of albedo on different urban snow cover types, finding exponential decay for the more disturbed snow that is found in snow piles and roadside snowbanks and a linear decay for cleaner

snow such as the sidewalk edge and open areas. Both trends were identified on datasets of 25 days or less.

Conway et al. (1996) reports results for albedo decay, this time, over a short period in more controlled plots. The context of that experiment involved small particles of soot embedded in the snow and it was shown that migration of these soot particles away from the surface was occurring, contributing to brighten the snow and increase the albedo over time. Another use for albedo data is to be able to identify snowfall events at automated stations by looking for sudden increases in the snow's shortwave reflectivity (Ueno et al., 2007). Thus, small amounts of precipitation that may go unnoticed by automated depth sensors are recorded and accounted for. Indeed, Kung et al. (1964), using airborne measurement techniques and climatological data, found a dependency between surface albedo and snow depth for depths below 5 inches on a variety of land use types. The resulting relationship is of great importance for estimating snow depth by way of remote sensing techniques.

2.2.6 Temporal vs. Spatial studies

Another paramount decision in the design of snow measuring experiments involves whether the focus of the measuring campaigns will be spatial or temporal in nature. Both approaches are well represented in the literature.

Spatial studies take place over extended areas, attempting to discern trends in snow properties as a function of position and to link these trends to local environmental factors. Knowledge of snowpack heterogeneity goes a long way for refining the design of snow models by justifying or invalidating important assumptions used therein for upscaling. It can also assist later measurement campaigns by providing observation teams with a means to "fill-in" data of less often measured properties by using empirical correlations between these and other, more easily measured ones.

In more "down-to-earth" applications, the spatial information acquired in these types of experiments can aid in decision making in subject matters as far reaching as construction, drainage and the flow of snowborne pollutants. Kung et al. (1964) (section 2.2.5) is a prime example of a spatial study. The airborne measurements they performed, combined with local climatological and land use data, allowed them to infer albedo maps for the North American continent as well as to find a link between the snow depth and the surface albedo. Degunther et al. (1998) modelled changing spatial conditions, considering different wavelengths to predict the behaviour of albedo over snowpacks of different shapes. Although not an experimental study, it soundly relies on basic physical principles to draw conclusions on a snow property in different environmental circumstances. Blöschl et al. (1991) performed an extensive field campaign to measure several snow properties (e.g. areal coverage, snow water equivalent, albedo, etc.) in an alpine catchment. This data was then used to construct spatial relationships forming the basis of a snowmelt model, linking processes occuring in one model gridsquare to those in adjacent ones.

Research performed over extended periods of time and whose objective is to discern the evolution of the properties of interest are considered to be temporal in nature. Such measurements are often performed at short time intervals to provide a high resolution view into processes occurring in the snowpack. This data is valuable for the creation of empirical simulations or the validation of physically based point snow models. These can then serve, for example, to estimate values for snow properties or the start and end times of snow coverage under specific sets of initial conditions and climatological inputs. Due to the heterogeneity of study sites and in the interest of thoroughness, observations often need to be performed in several locations with

different characteristics in order to adequately represent each of these measurement locations. This gives a "semi-spatial" aspect to such studies but it is to be noted that they remain temporal in nature because the goal is to track evolution through time of snow exhibiting significantly different properties separately and not interaction through space between them. Most experiments readily available in the literature are of this kind. Investigations like these can involve large areas encompassing many different land use classifications such as remote sensing studies (Brest, 1987) and ground based operations using large, established climatological networks (Ueno et al., 2007).

The urban case

Performing snow measurements in a rural setting often involves setting and following a snow survey course chosen to best represent the local snow and meteorological conditions and topography. Such snow courses are generally 120 to 270 m long with measurements spaced at 30 m for hilly terrain and much longer on flat lands; involving spacings of sometimes up to 500 m between measurements (Goodison et al., 1981). This is to limit the bias in the measurements from any one point by taking several. In natural areas, undisturbed snow is the norm and individual measurement points are selected to reflect this.

Areas in which basic snow characteristics and evolution processes vary greatly within a small spatial scale such as urban areas, however, offer a special challenge: much of the snow has been disturbed and relocated by human activities, but not at all in a uniform manner. This forms a tight patchwork of large variations within small distances in the city.

These "snow cover types" are defined here as the snow typically found on a given land-use category (e.g. front lawns, sidewalk shoulders, back alley shoulders, etc.) and exhibiting a consistent set of characteristics that are

generally attributed to the management practices undergone by the snow in question. Semádeni-Davies (1999) points out, in the context of an urban snow study in Luleå Sweden, that "Snow is ploughed from streets [...] and car-parks and is piled [...] or is removed to snow dumps". "Snow accumulation patterns are tempered by buildings and snow-handling measures [and] buildings, roads and private property act as barriers to regular sampling intervals" making it very difficult, if not impossible, to apply the traditional rural sampling tactics of snow courses to get a complete picture of the properties of urban snow. Ho and Valeo (2005) also mentions that the spatial variability of urban snow "[hinders] the use of [the rural snow course] method".

A common solution proposed by previous authors dealing with this highly variable environment is to define measurement locations that adequately represent each one of the different snow cover types and to visit these during each snow measurement operation. This practice can vary substantially in its final form as snow cover types can be defined differently, depending on the extent of the study. Ho and Valeo (2005) chose to use four snow cover types: snow piles, referring to the large piles of snow resulting from the mechanical removal of snow from parking lots and other such impervious surfaces; snow on road shoulders, being the snow displaced by snowplows during road clearing activities; snow on sidewalk edges, referring to snow shoveled from the sidewalk and undisturbed snow, the natural and undisturbed snow found in city parks and recreational fields. Valeo and Ho (2004) expand on this previous catalog in order to consider eight different types of snow: the previous four as well as some examples of bare ground and an additional type of undisturbed snow; rooftops. Conversely, other authors choose to restrict their snow measurements to where snow accumulation is sufficient, generally corresponding to front lawns and the snowbanks in alleyways (Lemonsu et al., 2008). This is

a practical approach as it ensures that certain properties such as density are more likely to be defined. Albedo measurements, which vary greatly in the absence of snow, were also taken on bare surfaces such as plowed sidewalks and streets as additional data.

Through special care in the experimental design, this semi-spatial aspect can be limited, allowing effort and resources to better be concentrated on studying the temporal evolution of a particular snow type. For example, the study of suburban hydrology performed in Buttle and Xu (1988) showcases results from a small catchment with reasonably homogeneous properties. Therein, only two snow cover classes are identified and studied: front and back yards. The author remarks that "snow that falls on roofs often melts relatively quickly as a result of increased exposure to solar radiation and [anthropogenic] heat flux from the roofs themselves" and that street clearing operations remove snow from roadways, justifying the simple classification adopted for identifying snow types. The trade off is that less information is collected that can lead to a comparison between snow undergoing different environmental factors.

2.3 Simulating snow

Time-evolution of snowpack properties as well as feedback relationships between it and atmospheric conditions are well described by differential equations that are best treated iteratively. Numerical modelling thus lends itself well to solving the problem of snow simulation. Only a select few of the interactions between the snowpack and the surrounding environment are understood and can be expressed at a fundamental level, the rest are described empirically. Empiricism does not restrict the construction of a model of whichever level of complexity desired, but it does limit its *generality*; meaning that caution is required when attempting to simulate the given phenomena in a different environment or with "special snow conditions" that are previously untested.

2.3.1 "Old-school" snow models

Due to the above mentioned feedback relationship between snow cover conditions and atmospheric processes, it can be expected that snow behaviour is of great interest to meteorologists and climatologists. Thus, many early atmospheric and climate models contained snow "packages"that set snow properties (e.g. areal coverage and albedo) as a function of other known, measurable or simulated parameters such as time of year, latitude or air temperature (Bélair et al., 2003b; Marshall et al., 1994). Some examples of this type of model include Manabe (1969), North and Coakley (1979) and Barnett et al. (1989).

Concurrently, other disciplines (e.g. hydrology, engineering, avalanche control, etc.) required different information about the snowpack such as snow water equivalent, depth and density. Such data is not as reliably generated from "tables" such as those put to use in the above mentioned atmospheric models. Also, scientists concerned (almost) only with snow have more available computing power at their disposal to devote to the problem than did climatologists running GCMs. Thus, these researchers produced more detailed models that were based more heavily on physical principles of snow and empirical relationships between the snow, the atmosphere and the soil that aimed to reproduce the evolution of snow properties over time. Obled and Rosse (1977) is a good early example: the authors constructed a specialized model of the snowpack that allowed them to calculate temperatures at different depths and to predict the amount of runoff produced by melt. Concentrated on the shortwave radiative properties of snow, Wiscombe and Warren (1980) describes a very detailed analytical model to calculate the spectral albedo of snow as a function of grain radius, the proportion of diffuse to direct illumination, solar zenith angle and snowpack thickness and density. Such information is

very valuable for GCM builders but it was some time before it or anything of similar complexity could be integrated into large-scale climate models due to the aforementioned restriction on computing resources. Kondo and Yamazaki (1990) reworked the snow melt problem, using energy budget considerations to keep track of melting and refreezing in the snowpack. Aside from modifying the properties of under-the-snow soil and producing runoff, this also directly impacts the density of the overlying snow pack.

That same year of 1989 saw the creation of CROCUS (Brun et al., 1989) for operationnal avalanche forecasting. This model uses as many as 50 "numerical layers" to represent the mechanical properties of the natural layers of the snow pack. Some other particularities of this snow model was its "per-band" values for shortwave albedo and absorption coefficient and it's ability to calculate the settling of the snow pack to name a few. Brun et al. (1989) also describes some testing undergone by the CROCUS model. The first campaign was performed at a well-instrumented site at Col de Porte in the French Alps in order to maximise inputs to the model and to ensure the most accurate parameterization possible. The authors report that "the model is efficient for simulating the different phenomena affecting the snowcover and its stability." To further assess the acuracy of the model in conditions more representative of where it is put to use, further campaigns were conducted at two sites used for operational avalanche forecasting: Alpe d'Huez, Isère and Le Monestier, Hautes-Alpes. Meteorological data is only collected twice daily at these locations so empirical functions for variables such as air temperature and incoming shortwave radiation were used in order to interpolate hourly values from the available observations to serve as inputs to the model. It is reported that the model was able to simulate the snow profiles without major losses in quality

even when poor meteorological data was available but that performance could be improved through better modelling of snow metamorphism in each layer.

2.3.2 "Next-generation" snow-climate models

With greater computing power becoming more widely available, meteorologists and climatologists sought to refine their general circulation models by including more complex snow packages in their land surface schemes; resembling those used in the "snow-only" models of other disciplines. Thereafter, by simulating snowpack evolution, it was possible for such models to make valid predictions in the advent of a "climatologically abnormal" season. Due to the complexity that land surface schemes exhibit in their own right, these can be, and have been, for the most part, developed independently from general circulation models (Yang et al., 1997).

The Biosphere-Atmosphere Transfer Scheme (BATS) by Dickinson et al. was one of the earlier widely used land surface modules with a complex snow component (Yang et al., 1997, 1999). BATS tracks the snow surface density and albedo as well as the bulk snow water equivalent, areal coverage and snow melt. It concentrates on the snow's surface layer, merging the lower layers with the ground in terms of temperature calculations. The model considers processes initiated below the surface only if these trigger an effect on the surface (e.g. upward conduction from the ground that warms the snow surface). They are otherwise ignored. Yang et al. (1997) describes a validation experiment in which BATS is compared to snow measurements performed at six locations in Russia over the course of several years. They found reasonable agreement between predicted and observed values for snow water equivalent, surface temperature, time of accumulation, end of ablation (The net volumetric decrease in the snow water equivalent of a snowpack (Male and Gray, 1981)) and the alteration due to ageing. Modifications that would improve

model predictions of snow cover fraction, depth and albedo have been tested, however such changes reduce the accuracy of the model in terms of SWE and snow surface temperature so a compromise was made to optimize the use of the BATS (Yang et al., 1997).

A few years after BATS's inception came the development of the Interactions between Sol Biosphere Atmosphere (ISBA) scheme (Noilhan and Planton, 1989). It was soon after implemented in Météo-France's climate model, Action de Recherche Petite Échelle Grande Échelle (ARPEGE) and at the Canadian Meteorological Center (CMC) in 2001. This first version of ISBA contained a snow model but it was rather similar to that of Manabe (Douville et al., 1995) (addressed in section 2.3.1). The high level of success of ISBA as a land surface module in the absence of snow motivated improvement of the scheme's on-snow performance. Douville et al. (1995) developed a snow package destined to replace the original one in ISBA. New considerations involved the addition of calculations of the snow density, of the heat transfer coefficient, of the snow albedo and snow melt and included 2 layers in the snowpack for temperature computations. Bélair et al. (2003a) implements additional improvements to Douville's snow package: adding a new reservoir for liquid water in the snowpack, considering melting due to rainfall incident on the snowpack and changing the representation of snow density in the model. These principal changes addressed certain "over-simplifications" in Douville's version. Douville et al. (1995) performed validation runs of their version of the ISBA snow model using meteorological forcing and hydrological data from Le Col de Porte, France; Yershov, Russia and Mount Iwate, Japan. Overall good performance of their improvements to the Manabe-type snow module were observed. However, a few weak points remain: mainly an overestimation of the rate of depth decrease during snowmelt, run-off rates that increase too

early and the appearance of a spike in springtime soil moisture. Results from the model validation performed in Bélair et al. (2003a) indicate that version of the ISBA snow model overcomes the aforementioned problem of the snowpack depth decreasing too quickly during melt but that runoff and surface temperature predictions are not improved. High dependence on atmospheric forcing and too great a degree of model simplicity, respectively, are given as possible causes for the lack of increase in performance.

The Canadian Land Surface Scheme (CLASS) was developed in 1991 by Verseghy and published in 2 tomes (Verseghy, 1991; Verseghy et al., 1993). The first of these focused on modeling the energy balance of bare and snow covered soils whereas the second treated vegetation, with and without ground snow cover and intercepted snowfall. In the cases where vegetation is absent, CLASS considers the snow cover as an extra, variable-depth, soil layer with it's own specific thermal, radiative and hydrological properties.When vegetation is introduced, the preceding considerations are kept for snow on the ground between the trees, shrubs or crops but additional calculations are required to determine the effects of intercepted snow resting on the surface of the vegetation. Neither Verseghy (1991) nor Verseghy et al. (1993) report the use of any observational data to validate CLASS. Comparisons performed therein between the Canadian Land Surface Scheme and what is referred to as the old scheme in the Canadian Climate Center's (CCC) GCM (McFarlane et al., 1992) for conditions associated with fresh snow on unfrozen ground and melting snow on frozen ground reveal significant discrepancies in terms of snow cover, depth, density, underlying soil moisture, snow surface temperature and evaporation. It is noted that the CCC GCM run with CLASS produces fewer temperature and precipitation anomalies than the older force-restore-bucket model of McFarlane. Suggestions are made that comparisons of model output

to field data "would be helpful in order to verify some aspects of the model formulation." Boone et al. (2004) report results from a large scale runoff project showing that the best agreement with experimental values was obtained with models using an *explicit* approach to snow. CLASS was grouped into this category for that experiment. The snow model intercomparison project (Brown et al., 2006) showed that newer versions of CLASS "provided realistic simulations of snowcover" but that a number of aspects still needed further attention such as the albedo of deep snowpacks, melting during major mid-winter thaws and shallow snow cover depletion.

Two other snow models that appear frequently in the literature are Loth et al. (1993) and Lynch-Stieglitz (1994). The former presents a very detailed snow cover package suitable for use in GCMs. The model consists of a multi-layer approach in which interactions are based on the system's mass and energy balances. Each of the layers are created with the arrival of a new snowfall and are merged in with adjacent layers when their properties become similar within a preset threshold. Validation revealed excellent model performance in the prediction of the times of accumulation and the end of ablation as well as "good correspondence between the observations and the simulated values of snow depth and water equivalent" in a wide variety of snow conditions. This level of quality of prediction was obtained without locally parameterizing the model, reinforcing the authors' argument that it would work well in a GCM context.

Lynch-Stieglitz (1994) uses 3 layers to represent the snow cover in which "heat and mass flow within the snowpack are physically modeled". Energy transport is modeled as linear diffusion with the atmospheric temperature setting one of the boundary conditions. Mass (water) flows downward through the layers under the effect of gravity. If a given layer is cold enough to refreeze

the water or it has enough capacity to hold it as a liquid, the downward progression of the mass is stopped at that layer, similar to the CROCUS model (Brun et al., 1989). When tested against observational data, the model was found to effectively predict behaviour for snowpack growth/ablation and densification as well as the timing of melting events and snowpack collapse. Good agreement also occured between simulated and observed surface energy fluxes. Sub-surface soil temperatures predicted by the model corresponded well with data from a similar site. Snow depth and water equivalent were reported to be over-estimated during winters with numerous warm-rain-on-snow events, perhaps caused by the lack of provisions in the model for such events. Subsequent papers (Marshall et al., 1994; Yang et al., 1997; Bélair et al., 2003a) dispute the relevance of using these more complex snow models in GCMs, implying that it hasn't been shown that these more computationally expensive packages that emphasize improving the representation of vertical processes produce more accurate or precise climate predictions than those of "intermediate complexity" with reasonable horizontal representation like the snow subroutines in BATS, ISBA or CLASS.

2.3.3 Urban snow simulations

Due to the urban nature of the research showcased in this document, the following urban models, that could otherwise be lumped in with the previously discussed simulators, have been given their own section.

The Town Energy Budget (TEB) model by Masson (2000) is a complete land surface scheme developed to simulate energy exchanges in urban landscapes, complete with canyon geometry and impermeable surfaces. Snow property evolution was included to extend the model to the case of mid and high latitude cities that experience snowfall. These appear as factors in the equations governing "the energy budget of the surfaces [. . .], the heat flux from the

road [to] the canyon or from the roof [to] the atmosphere and the radiative [properties of] the canyon surfaces" (Masson, 2000). However, actual evolution of these snow properties in the model is determined by a snow scheme of the implementer's choosing such as the package developped by Bélair (Bélair et al., 2003a) or Loth (Loth et al., 1993) (described in 2.3.2). A few extra implementations are suggested to *urbanize* the chosen snow subprogram such as a faster rate of decrease and a lower minimum value for snow albedo as well as a snow removal mechanism.

Important contributions to modelling urban snow/climate phenomena have also been submitted by hydrologists interested in predicting runoff from mostly impervious urban catchments at the time of snowmelt. The results can be used for stormwater drainage system design (Ho and Valeo, 2005) and the understanding of pollution runoff from the urban snow pack (Buttle and Xu, 1988). In order to properly understand the production of runoff, urban hydrology models attempt to track the evolution and redistribution of snow in the city. Valeo's model (Valeo and Ho, 2004) uses an energy budget approach to predict snow melt. Snow properties such as albedo and the liquid water contained in the snow pack in 8 different snow cover types found in the city (i.e. parking lots, roads, driveways and sidewalks, around parking lots, road shoulders, driveway edges, rooftops and parks) are simulated. The snow water equivalent is set at initialisation time under the assumption that snow removal crews only leave behind a given amount of snow. The "start-time" of the model is immediately after snow-plowing. Model validation revealed the Urban Snow Model to be effective at predicting snow runoff peak intensities and the time to peak. Only in extreme cases of very high peak flowrate does the model tend to underestimate the outflow from the snowpack.

In contrast to Valeo and Ho (2004) highlighted above, which follows the energy budget method, three urban hydrology snow models based on the degree-day approach are reviewed in Semádeni-Davies (2000): MouseNAM, SWMM and HBV. The degree-day technique relies on a temperature index to calculate the rate of meltwater production. Thus, when the daily average temperature is greater than a set "melt threshold" (often 0 °C) the daily snow melt would be written as in equation 2.28 for a daily average temperature of T_a, a melt threshold of T_m and a melt rate factor of C. Otherwise, no melt occurs. As can be inferred from the very nature of the input data, this approach does not permit a temporal resolution shorter than one day. This makes it easier on computing power but can't capture the finer details of snowmelt arising from hourly temperature and illumination effects.

$$M = C\,(T_a - T_m) \tag{2.28}$$

The many different approaches to the modelling of snow properties showcased in this section allow the simulation and prediction of how snow conditions evolve in different environments and under the influence of different drivers. Given that snow is just one part of a greater system, it is advantageous to integrate snow models within land surface models in order to account for various processes involving the finer details of the surface energy budget. This land surface model is then coupled to general circulation models to account for larger scale atmospheric activity and precipitation.

CHAPTER 3
Snowpack evolution in urban and suburban Montreal, Canada

3.1 Introduction

Snow covers the ground for a substantial portion of the year. Its effects on the surface energy balance, local ecology as well as the level to which it can bring change to human activities, are considerable. Given this, it becomes desirable to measure and characterize the snowpack in the hopes of using that information to eventually predict snow behaviour. Existing snow measurement networks collect data on some or all of a set of recognized snow properties at regular intervals in locations across North America.

The records from these stations have permitted the elaboration, parameterization and validation of sophisticated models to simulate the evolution of snow properties (Yang et al., 1997; Bélair et al., 2003a; Verseghy, 1991; Verseghy et al., 1993). These networks, however, operate primarily in rural areas, resulting in very good knowledge and prediction capability for rural snow but a relative lack of information when it comes to snow that is subject to human perturbations. More recent campaigns have sought to collect data on the evolution of snow properties in cities around the world such as Calgary (Ho and Valeo, 2005), Montreal (Lemonsu et al., 2008) and Peterborough (Buttle and Xu, 1988), Canada and Luleå, Sweden (Semádeni-Davies, 1999; Sundin et al., 1999) to name a few.

Such projects have provided the necessary data to test the performance of existing models in the context of snow in an urban environment and to construct new models more appropriate for application in such highly disturbed

environments. Traditionally, this task has mostly been undertaken by hydrologists, interested in the production of runoff at the end of the winter season. More recently, however, the land surface modeling community is expressing interest in urban snow as well because of the high proportion of people living in cities and the consequent importance to accurately forecast weather there.

This Study is part of the framework of the Environmental Prediction in Canadian Cities (EPiCC) network. The goal of EPiCC is to gain a better understanding of energy exchanges occuring in Canadian cities in order to improve the accuracy and precision of weather forecasting in urban environments. This endeavour involves scientists from Environment Canada and three Canadian universities (McGill University, University of British Columbia and University of Western Ontario) working on energy flux measurements, remote sensing and model simulations. The current study describes the urban snow observations campaign that was conducted in Montreal over the course of the winter of 2007-2008. Measurements of snow depth, snow water equivalent, albedo and aerial coverage were conducted over several different snow management types at an urban and a suburban location. Snow properties were scaled up to the convective source area of energy flux measurement instrumentation located at each of the sites to allow comparisons between weighted snow properties and convective energy fluxes.

3.2 Theory

3.2.1 Snow's effect on the energy budget

The presence of snowcover has dramatic effects on the local surface energy budget. The radiation balance of a surface can be written as

$$Q^* = K_\downarrow (1 - \alpha) + L_\downarrow - L_\uparrow. \tag{3.1}$$

where $L_{\uparrow}$ and $L_{\downarrow}$ are the longwave radiation emitted upward from the surface and downward from the atmosphere, respectively. $K_{\downarrow}$ is the incident shortwave radiation and Q^* is the net radiation. The high albedo of snow (α) decreases the net radiation input to the system (Pomeroy and Goodison, 1997). This energy is dissipated as expressed in the energy budget equation (equation 3.2) below where Q_E is the latent heat flux density, Q_H is the sensible heat flux density, Q_G is the conductive soil heat flux density at the soil-snow interface, ΔQ_M is the energy used to melt the snow and ΔQ_S is the heat storage in the snowpack through an increase in temperature without a phase change.

$$Q^* = Q_E + Q_H + Q_G + \Delta Q_S + \Delta Q_M \tag{3.2}$$

ΔQ_M stems from the high latent heat of fusion of the snowpack. As the notation suggests, this energy flux constitutes a change in storage as long as the resulting melt water remains within the snowpack. If enough melt occurs to cause saturation of the snowpack with water and subsequent runoff, then ΔQ_M acts as a mechanism of energy loss. In cold conditions, values of ΔQ_M are very small due to insufficient energy input to melt snow.

The smaller input of energy into the system due to the smaller Q^* means less energy is available to be dissipated via Q_H and Q_E. In cold winter conditions, very little liquid water is available to evaporate, contributing to reduce Q_E to almost negligible values in comparison with Q_H. During the melt, snow and atmospheric conditions are often such that sensible and latent heat fluxes are directed downwards toward the snowpack, the majority of the available energy in the system going towards melting snow into liquid water, ΔQ_M. Only in the cases of very dry atmospheric conditions will Q_E be directed upwards (Oke, 1987).

3.2.2 Snow properties

Properties used to characterize snowcover are selected based on the importance of their impact on the local environment and the ease with which they can be measured. The snow water equivalent (SWE) is the most important from a hydrological perspective (Semádeni-Davies, 2000) as it corresponds to the depth of water obtained by melting the snowpack over the same area (Goodison et al., 1981). SWE can be measured gravimetrically using a snow tube or by installing a snow pillow. Gamma ray attenuation and microwave reflection are other methods employed for probing the snow water equivalent. They have the advantage of being non-intrusive (Pomeroy and Gray, 1995).

Snow depth is viewed by many (Bergeron et al., 2008; Messier, 1995) as a fundamental property in the understanding of related processes. Except for cases of extreme low density (i.e."wild snow" (McKay and Gray, 1981)), deeper snow can also mean reduced mobility for both people and animals. The depth of the snowpack also influences how it buffers temperature gradients between the atmosphere above and the soil below, significantly reducing heat loss to the atmosphere and conductive heat fluxes (Q_G). Depth can be measured using probes manually inserted into the snowpack, using permanent markers installed in a set number of locations or using automated ultrasonic snow depth sensors (Pomeroy and Gray, 1995).

Snow density ρ_S is linked to the snow depth and the snow water equivalent through

$$\rho_s = 1000 \times \frac{SWE}{depth_{snow}}. \tag{3.3}$$

A wide variety of thermal, mechanical and electromagnetic properties of snow are functions of density: specific heat, latent heat of fusion; Young's modulus, compactive viscosity; electrical conductivity and the dielectric constant (Langham, 1981). These properties, in turn have an impact on an array of

human activities from winter-road building to the use of snow as a seasonal insulating material.

Albedo is another common variable to study due to its strong effect on the surface energy budget and some empirical relationships that tie it to snow depth (Kung et al., 1964) and density (Warren and Wiscombe, 1980) making it useful to the remote sensing community. It can also be used as an indicator of fresh snowfall events at automated stations where the accumulation is too small to be detected by automated snow depth sensors (Ueno et al., 2007).

3.3 Materials and Methods

3.3.1 Site description

The urban location for this study is Montreal (45°30′N 73°40′W) located at the confluence of the St-Lawrence and Outaouais rivers in the southern portion of the province of Québec, Canada. Montreal features a densely urbanised portion concentrated on the middle-third of the island, around Mount Royal with large portions immediately adjacent built up for residential or industrial uses. Areas further to the north and west are covered with sparser and more recent suburban developments (Maxwell, 1971; Ville de Montréal, 2010). The population, according to the 2006 census, of the city of Montreal was 1.6 million and the census metropolitain area was home to 3.6 million people in 2006 (Canada, 2007).

Snow measurements were performed around two sites where energy flux data was collected as part of the EPiCC Network; one in the suburb of Pierrefonds in the western portion of the island and another in the urban residential burough of Rosemont Petite-Patrie (figure 3–1 a); to the north of Mount Royal and the downtown core.

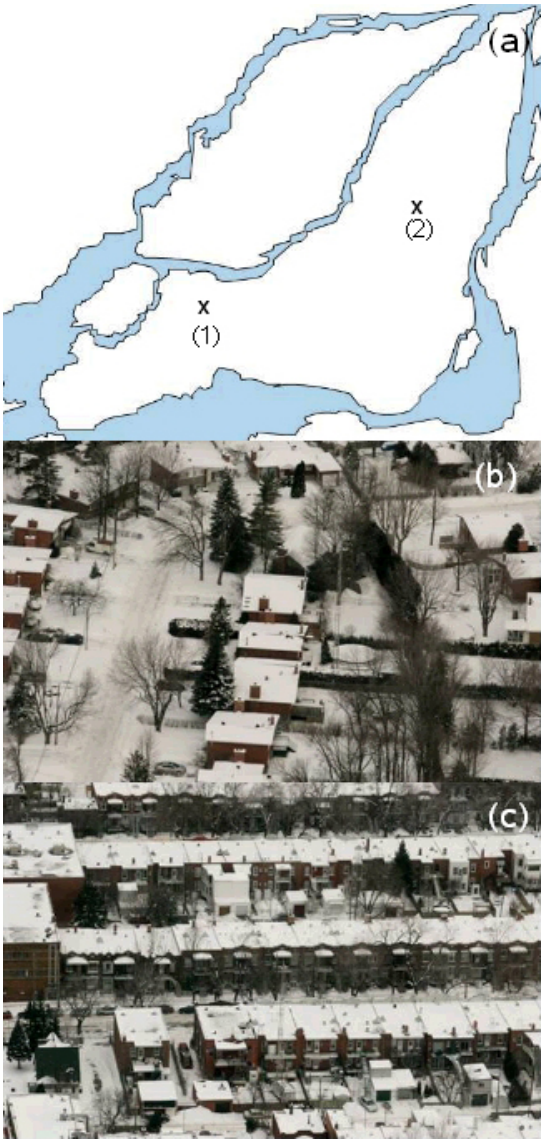

Figure 3–1: Sampling sites for snow measurements. (a) Overall map showing relative location of sites on the island of Montreal: (1) is suburban site and (2) is urban site. (b) Aerial photograph of suburban site (Nanni, 2008a). (c) Aerial photograph of urban site (Nanni, 2008b).

Table 3–1: Height in meters of temperature and humidity sensors at the urban and suburban stations.

Site	Tower	Street canyon	Alley canyon
Urban	25.5	4.5	4.5
Suburban	25.5	2	2

The suburban site is mainly comprised of single family dwellings with peaked roofs and large front and back lawns. Buildings, vegetation and impervious surfaces in a 9 hectare area surrounding the measurement site are found at a ratio of 20:65:15 respectively, showing a large prevalence of vegetative cover (Christen, 2009). The low amount of vehicular traffic is not sufficient to completely melt snow left on the road surface after any plowing operations are complete (figure 3–1 b).

The urban site is covered with flat-roofed two to three story buildings containing two or more apartments. The spacing between buildings is smaller due to much smaller front lawns and backyards (figure 3–1 c). This results in land cover proportions of 32:30:38 for buildings, vegetation and impervious surfaces, respectively in a similar 9 ha area (Christen, 2009).

Standard meteorological measurements

Both of these stations were equipped with standard meteorological equipment. Temperature and relative humidity data at three heights (table 3–1) were acquired using temperature and humidity probes (HMP45C-212 for the urban site and HMP45C for the suburban site, Vaisala). Wind speed and direction was measured at 26m with a propellor vane wind monitor (05103-10, RM Young Co. Traverse City, MI, USA). Snow depth was measured using an acoustic snow ranging sensor (SR50, Campbell Scientific, Logan, Utah). Soil volumetric water content integrated from the surface to a depth of 15 cm was measured at the suburban site using a soil moisture probe (CS616, Campbell Scientific, Logan, Utah) and soil temperatures at 5 and 15 cm were measured

using thermocouples (Type T, Omega, Laval, Qc, Canada) implanted in the ground. Besides standard meteorological information, both stations were also equipped to measure surface temperatures using Infra-red thermometers (MI, Raytek Corporation, Santa Cruz, CA, USA; MI-N510, Mikron Infrared Inc., Oakland, NJ, USA). Data from each of these sensors were collected at a frequency of 0.5 Hz, averaged over 5 minutes and logged on a CR23X datalogger (CSC).

Energy budget measurement

The energy flux measurement equipment at the sites encompasses an eddy covariance system to resolve the convective fluxes, a net radiometer (CNR1, Kipp & Zonen, Delft, The Netherlands) for the incoming and outgoing shortwave and longwave radiative fluxes and a soil heat flux plate (HFT3, Campbell Scientific,Logan, Utah) for conductive fluxes into the ground. Convective energy fluxes derived using eddy covariance were calculated from three dimensional wind speed measured using a sonic anemometer (CSAT3, Campbell Scientific, Logan, Utah), water vapour and CO_2 concentrations measured using an open path infra-red gas analyzer (LI-7500, Li-COR Biosciences, Lincoln, NE, USA) and air temperature in the anemometer path measured by way of a fine wire thermocouple (FW3, Campbell Scientific, Logan, Utah). Data from these sensors was collected at a frequency of 20Hz, logged to a datalogger (CR5000, Campbell Scientific, Logan, Utah) and averaged over 30-minute periods .

3.3.2 Snowcover measurements

Similarly to the study described in Valeo and Ho (2004), ten snow cover types were identified at the study sites based on the land use and the different snow management practices carried out on each of these land use categories: nine of these are shown in Figures 3–2 and 3–3 when they are present for either

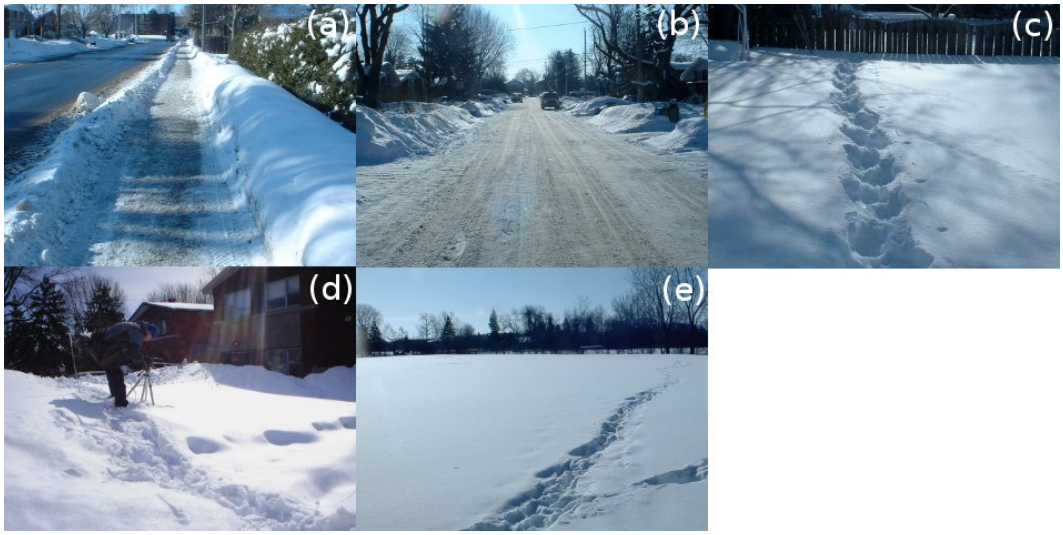

Figure 3–2: Snow types encountered during snow measurements at the suburban site. (a) Sidewalks. (b) Street and street shoulders. (c) Backyards. (d) Front lawns. (e) Undisturbed.

site: undisturbed snow, as can be found in parks and recreational fields; the walking surface of sidewalks; sidewalk shoulders, characterized by a snowbank between the sidewalk and the street and formed by the shoveling of snow from the sidewalk to the side; the driving surface of alleyways; alley shoulders, produced by the passage of snowplows to clear the alley's driving surface; the driving surface of the street; the street shoulder, consisting of the snow left behind by municipal snow clearing operations due to the presence of parked cars; front lawns and backyards. The tenth snow cover type is rooftops to which no access was granted to snow measurement crews for safety reasons.

Sampling was performed along transects established within each of these snow cover types (fig. 3–4). These transects were positioned within each snow type in such a way as to maximise the number of measurement points for any single visit to the transect. This study focused on four snow properties at the study sites: the snowpack depth, snow water equivalent (SWE), the effective albedo of the snowpack and the areal coverage by snow.

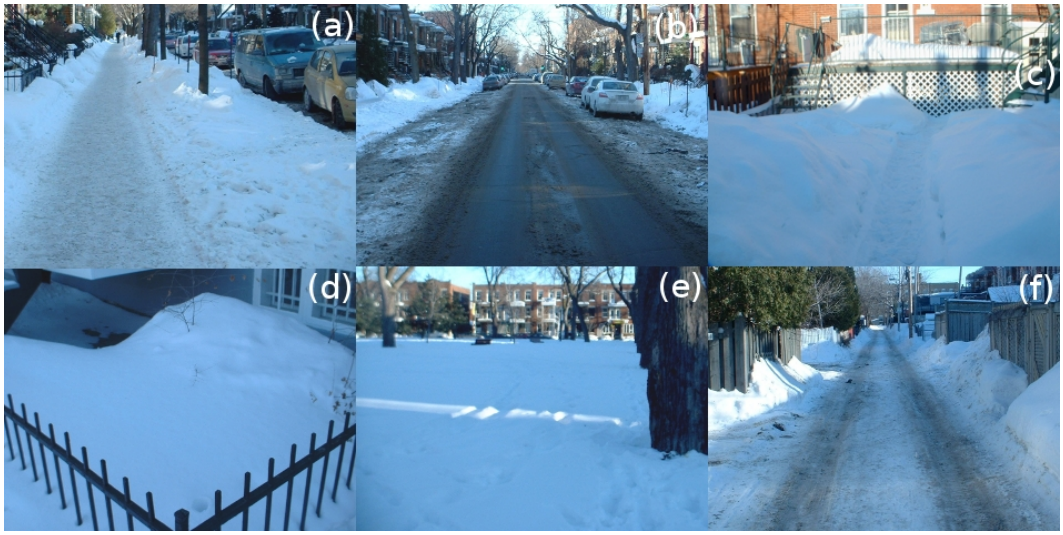

Figure 3–3: Snow types encountered during snow measurements at the urban site. (a) Sidewalks and sidewalk shoulders. (b) Street and street shoulders. (c) Backyards. (d) Front lawns. (e) Undisturbed. (f) Alley and alley shoulders.

Table 3–2: Length of snow measurement transects and the distance between snow depth point measurements.

Snow cover type	Distance between points (m)	Number of points
Undisturbed snow	5	15
Sidewalk shoulder	5	15
Alley shoulder	5	15
Street shoulder	5	15
Front lawn (urban)	0.5	Entire width
Front lawn (suburban)	1	Entire width
Backyard	1	Entire width

Depth measurements were performed using graduated wooden sticks for the first part of the winter and a laser-etched aluminum avalanche probe (Avalanche Tech speed probe 240cm, Genuine Guide Gear) for the remainder (fig. 3–5). These tools were inserted into the snow pack until the operator felt the tip make contact with the underlying soil. The intervals between depth measurements in different snow cover types are presented in table 3–2.

A mount rose type snow sampler was used to measure SWE (fig. 3–6). Snow cores were taken at each end of the transect. Density was then inferred from the SWE and the depth at the end points. The average snow water

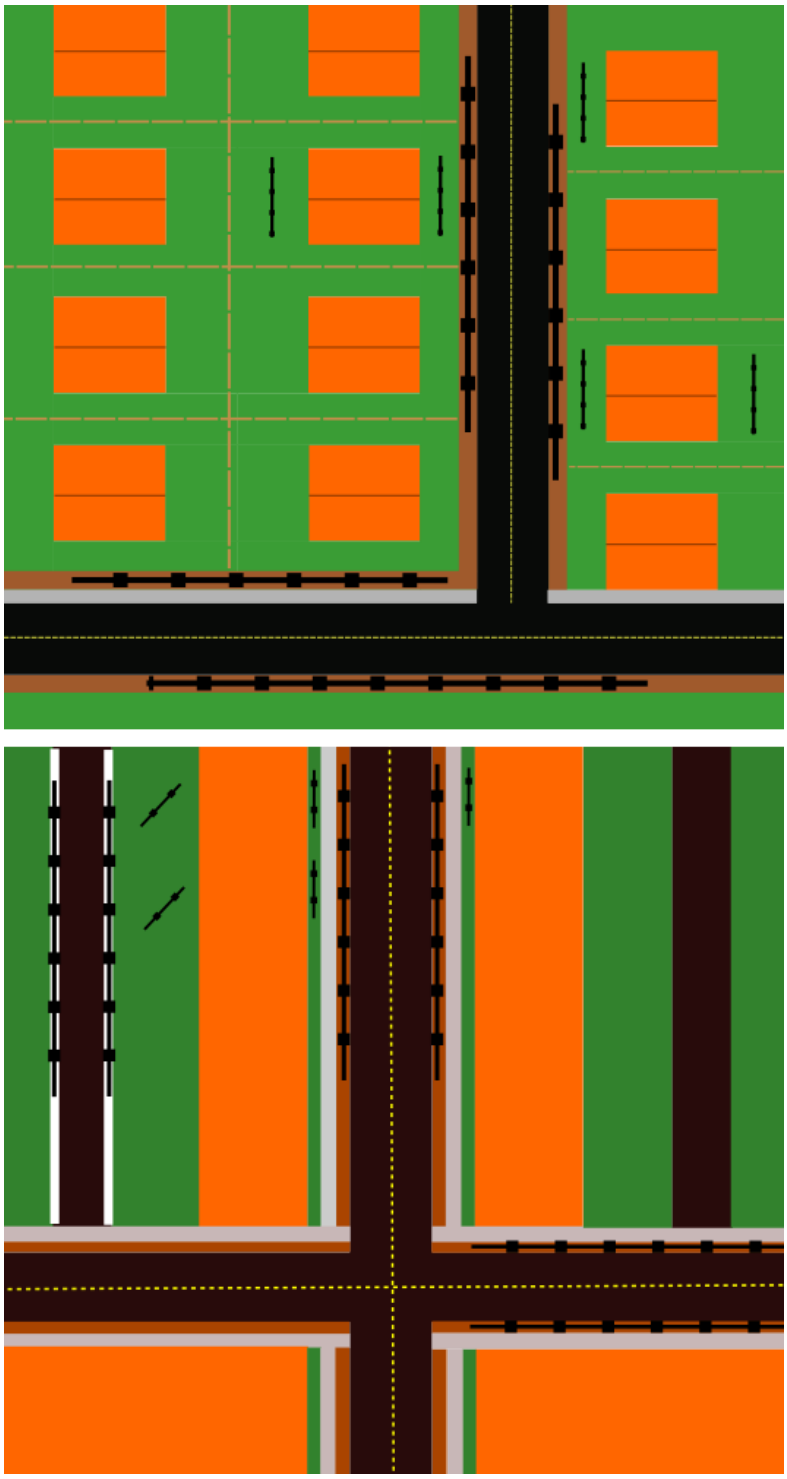

Figure 3–4: Arrangement of transects at the suburban (top) and urban (bottom) sites. Buildings are represented in orange, front and backyards in green, pavement in black, sidewalks in grey, sidewalk shoulders in brown and the alley shoulders in white. Undisturbed locations are not shown. Diagram is not to scale and number of transect points for each snow type is indicated in table 3–2.

Figure 3–5: depth measurements

equivalent for the transect can then be estimated from the average depth of the transect and the average density of the end points assuming density along the length of the transect to be adequately represented by the end points.

Snow albedo measurements were taken at one point along each transect where the illumination was the most consistent and the snow appeared to be the most representative of the rest of the transect. Additional measurements were taken in areas with very thin or no snow cover where there weren't any depth transects established such as the driving surfaces of roadways and sidewalks. To avoid effects from solar zenith angle and variability in cloud cover, albedo data was acquired between 10:30 and 13:30 LST on clear, sunny days. The instruments used were two Yankee TSP-400 solar pyranometers with a nominal view angle of 180°, one installed facing upwards to measure the incoming solar radiation and the other positioned facing downwards to measure reflected solar radiation. These were mounted on the end of a meter long segment of aluminum tubing, secured to a tripod to facilitate levelling of the

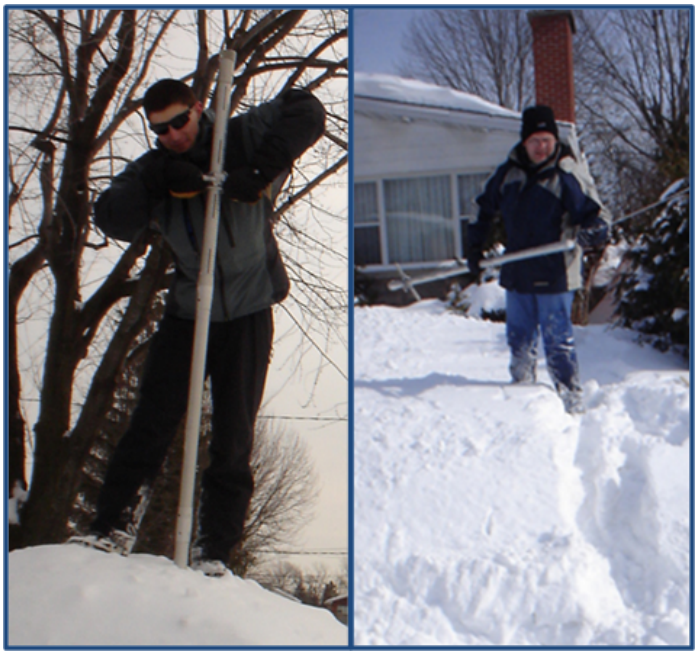

Figure 3–6: density measurements

device and to limit the effect of the operator on the value of the measurement (fig. 3–7). Albedo measurements at each site were alternated between the morning and the afternoon in order to limit any bias in the results that could have been caused by superficial melting of the snowpack over the course of the noon-hour.

Areal coverage information was acquired by way of digital photography at each of the measurement locations. Pictures were taken from the end of each transect facing towards the center. Additional photographs were taken in the streets and the alleyway. The main purpose of these records is for quality control during the analysis of the data of the above-mentioned snow cover properties.

Figure 3–7: albedo measurements

3.3.3 Convective energy flux calculations

The eddy covariance data was provided through the EPiCC project. A number of processing and quality assurance steps are required prior to covariance calculations being made. These have been standardized in the micrometeorological community through international flux network programs. Briefly, wind speeds were rotated to set, first, the mean lateral then mean vertical wind velocities to zero (Tanner and Thurtell, 1969). Data were then subjected to a despiking algorithm that identified and removed spikes (three or fewer consecutive points that are at least the lesser of 3.5 standard deviations or a pre-defined variable dependent absolute value away from a running mean). Variables are detrended based on the block average approach (Baldocchi, 2003) and WPL density corrections are applied (Webb et al., 1980). Convective energy fluxes were then calculated as the covariance of fluctuations

about the mean of vertical wind speed and of the scalar quantities of interest: temperature and specific humidity.

Quality control procedures were then implemented to remove problematic data. Data are rejected if they exceed certain thresholds of mean, maximum, minimum or standard deviation; if they were acquired during periods for which the instrumentation was known to be malfunctioning or undergoing maintenance; if unfavourable weather was affecting instrument performance; if an insufficient number of values were collected or too many spikes were identified in a given averaging period; if the application of a block average detrending scheme yielded sufficiently different values than the application of linear detrending and the variable in question has a small enough value or, finally, if the wind is from a direction that would imply flow disruption from the sonic anemometer.

3.3.4 Convective source area estimations

The Flux Source Area Model (FSAM) (Schmid and Oke, 1990; Schmid, 1994) was used to estimate the source area of convective energy flux measurements. An automated procedure was implemented to prepare inputs to FSAM and calculate coordinates of points around isopleth lines. Inputs from each day were averaged over the daytime period (1000 to 1530 EST). When daytime averaged inputs were not within model parameters, shorter periods within the day for which acceptable averages could be calculated were sought (minimum duration of 90 minutes). If no such periods could be found, the day was discarded. Model output was imported into a geographic information system (ArcGIS 9.2, ESRI, Redlands CA, USA) to allow comparison operations between snow cover type distributions around the sites and the calculated source areas. Vector layers of snow cover type distribution were drawn using available aerial photos based on assumptions linking snow types to the underlying

land use (eg. sidewalks, backyards, etc.). Proportions of snow cover types measured on a given day by eddy covariance equipment were then calculated.

Using these proportions of snowcover types, snow depth and density are scaled up to the source-area by areally weighting the properties of each of the snow types investigated in this study. This is not performed for albedo for two reasons: the source area for net radiation is not the same as for convective energy fluxes (Schmid, 1997) and spatially averaging albedo does not take into account larger scale geometrical factors that significantly alter the albedo measured at tower height, particularly in urban environments.

3.4 Results

3.4.1 Snow property evolution

General trends in observed snow depth are similar to those expected in a typical rural setting: gradually increasing throughout the winter season, interrupted by the mid-winter melt in January, and experiencing a peak in late March just before the spring melt occurs and complete ablation of the snowpack takes place (Figs. 3–8 and 3–9). At both sites, undisturbed snow types exhibit the overall smallest depths, with maximum values of 68 cm and 47 cm for suburban and urban sites, respectively, whereas the deepest snow is found at the urban site in backyards ($\text{Depth}_{\text{max}} = 118$ cm) and, at the suburban site on front lawns ($\text{Depth}_{\text{max}} = 103$ cm) and in roadside snowbanks ($\text{Depth}_{\text{max}} = 101$ cm). The latter two snow cover types do not experience their maximum depth simultaneously.

At the suburban site, roadside snowbanks and undisturbed snow both show a sudden increase in snow density occuring in late December - early January followed by oscillations around a generally increasing trend (Figs. 3–10 and 3–11). Fluctuations are of greater amplitude for the undisturbed sites than for the snowbanks. Snowbanks are the only snow cover type at either

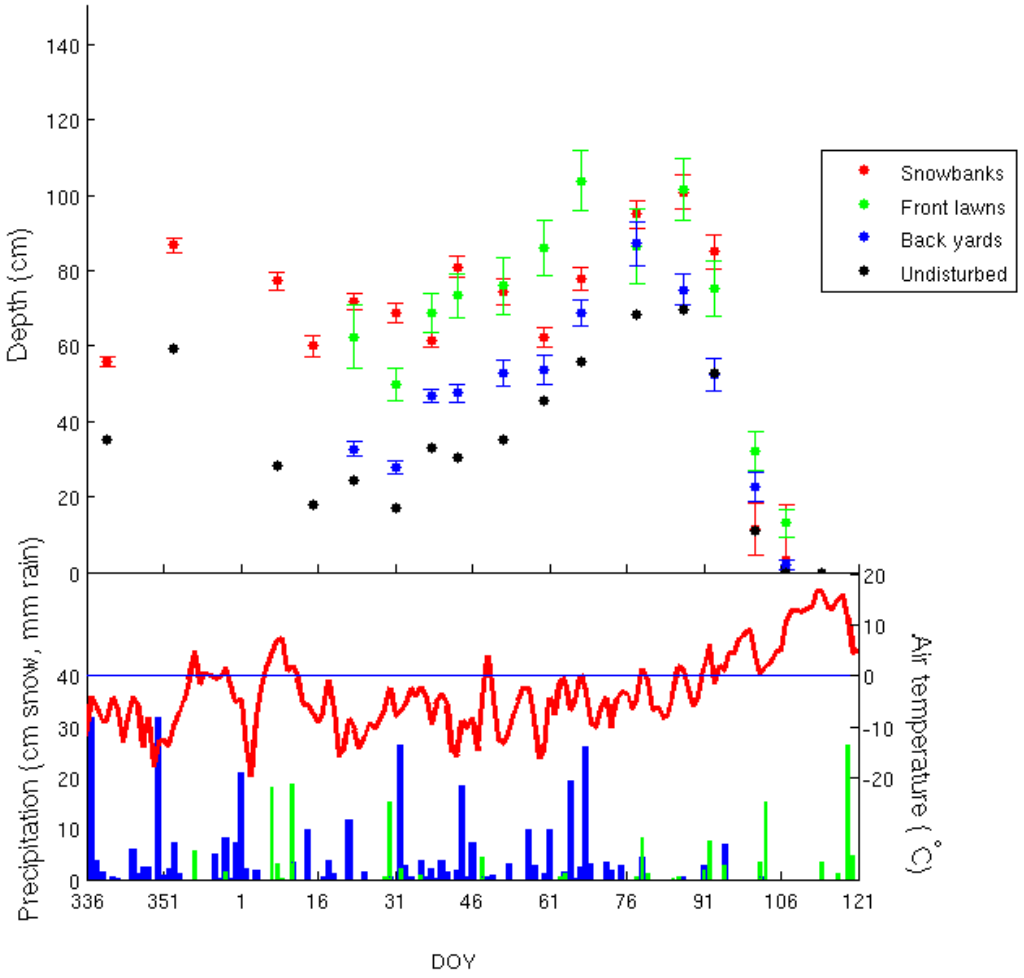

Figure 3–8: Top plot is measured snow depth for the different snow cover types at the suburban site. Error bars correspond to 95% confidence intervals calculated from the data averaged to produce each point. Bottom plot is cumulated precipitation and daytime average air temperature values measured at Dorval international airport. Blue and green bars represent snow in cm and rain in mm respectively. The red line is air temperature in °C.

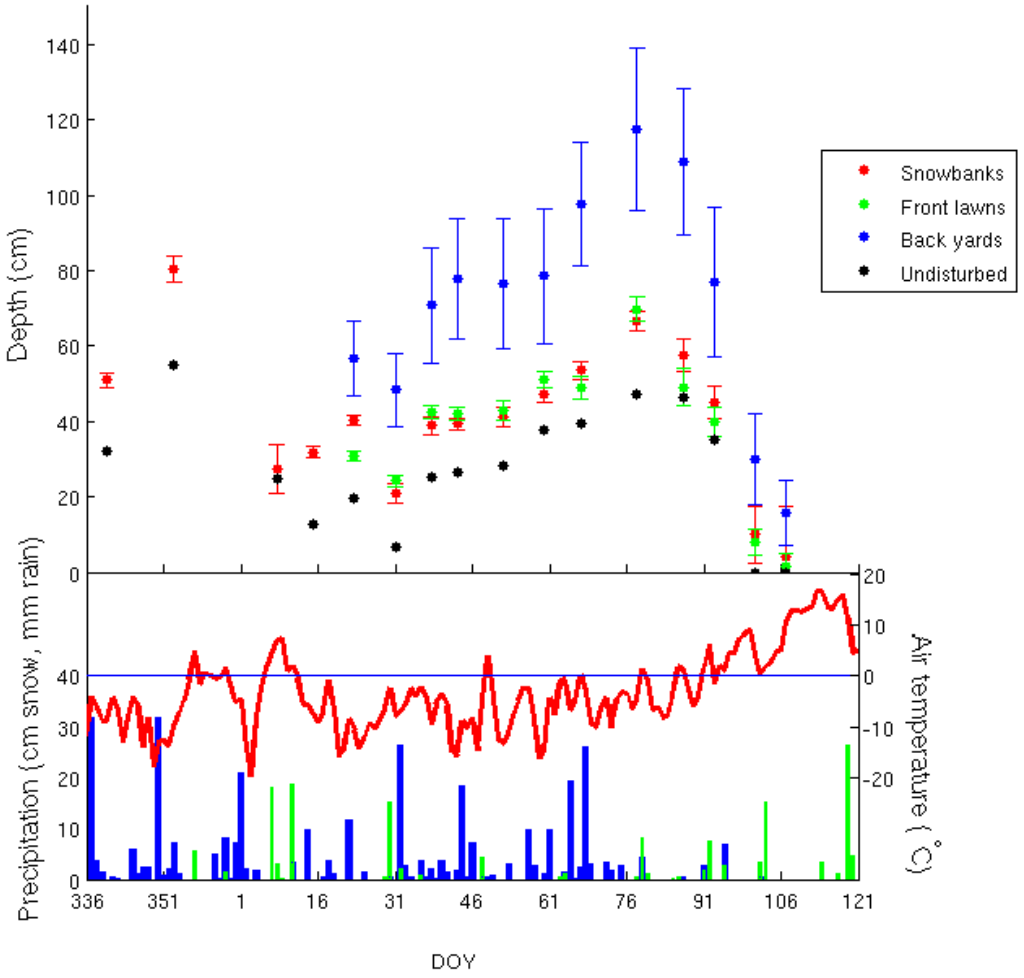

Figure 3–9: Top plot is measured snow depth for the different snow cover types at the urban site. Error bars correspond to 95% confidence intervals calculated from the data averaged to produce each point. Bottom plot is cumulated precipitation and daytime average air temperature values measured at Dorval international airport. Blue and green bars represent snow in cm and rain in mm respectively. The red line is air temperature in °C.

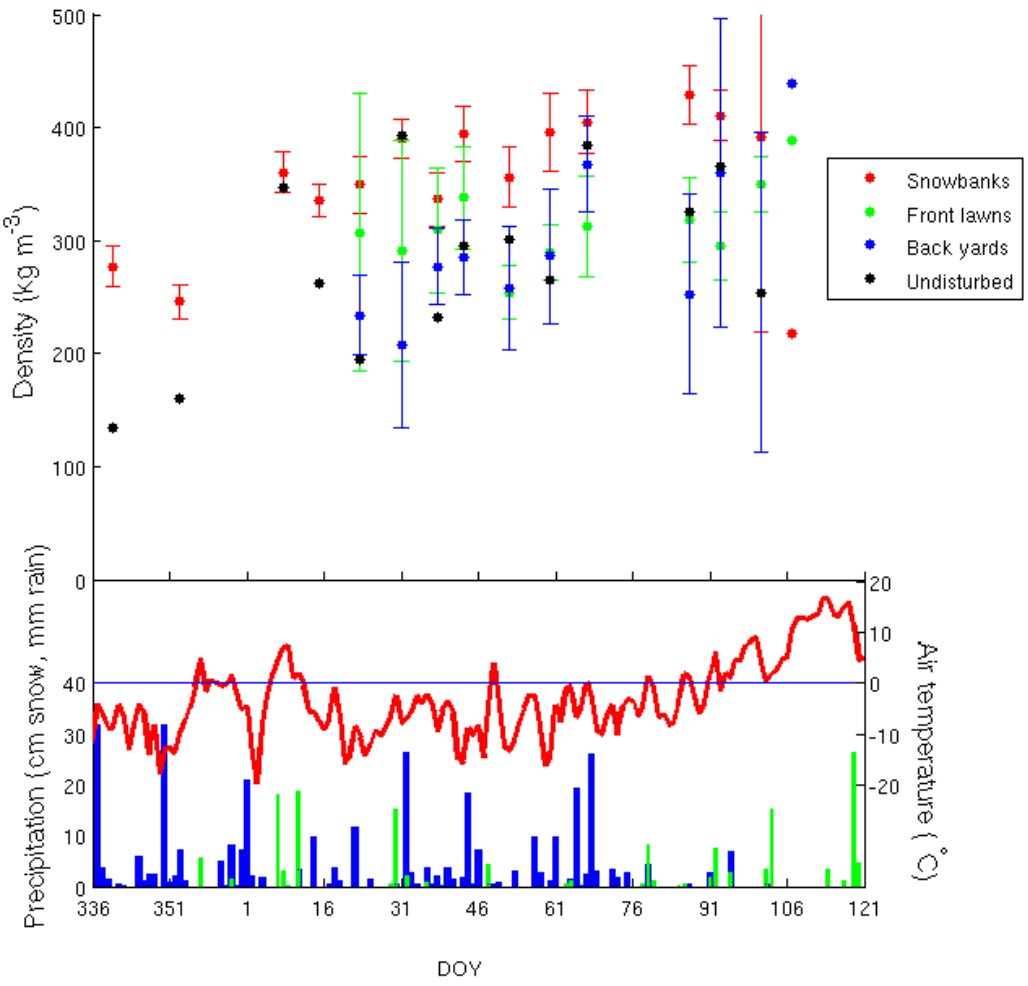

Figure 3–10: Top plot is measured snow density for the different snow cover types at the suburban site. Error bars correspond to 95% confidence intervals calculated from the data averaged to produce each point. Omitted error bars indicate insufficient data to calculate uncertainty. Bottom plot is cumulated precipitation and daytime average air temperature values measured at Dorval international airport. Blue and green bars represent snow in cm and rain in mm respectively. The red line is air temperature in °C.

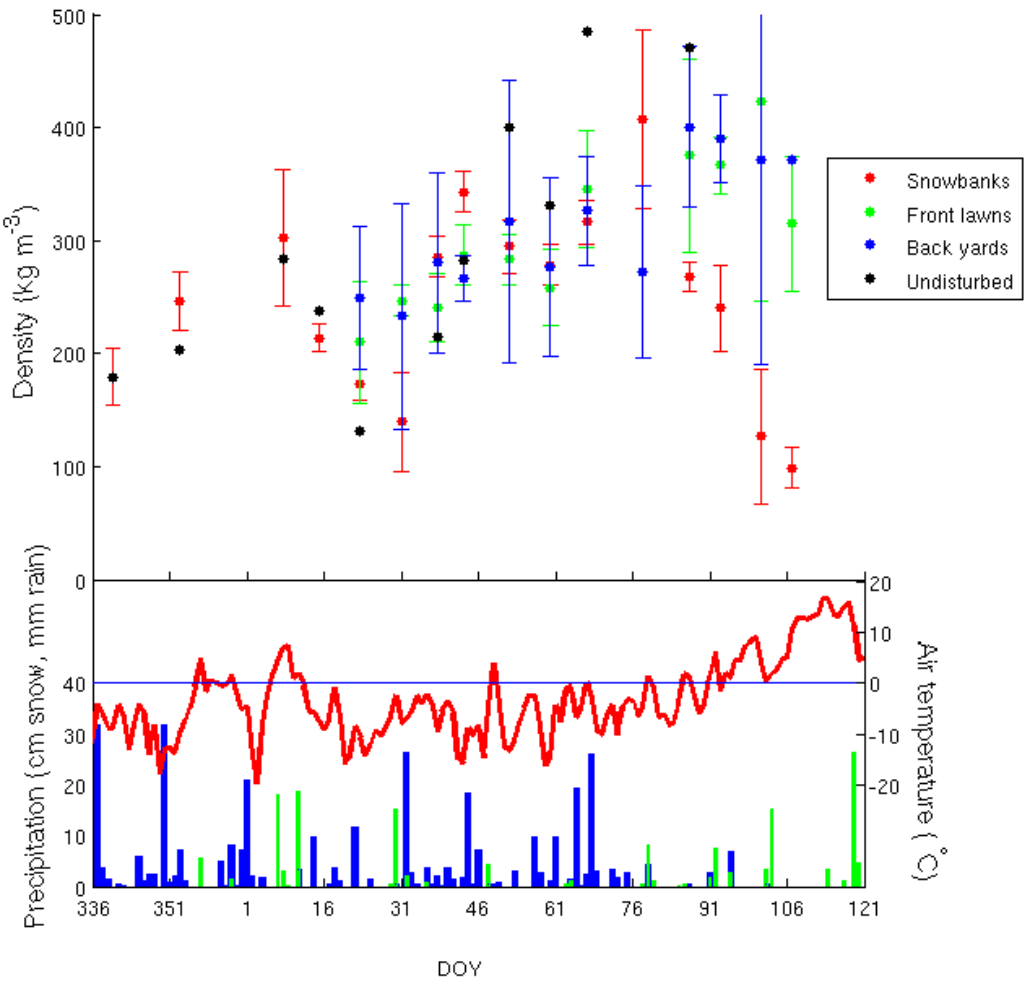

Figure 3–11: Top plot is measured snow density for the different snow cover types at the urban site. Error bars correspond to 95% confidence intervals calculated from the data averaged to produce each point. Omitted error bars indicate insufficient data to calculate uncertainty. Bottom plot is cumulated precipitation and daytime average air temperature values measured at Dorval international airport. Blue and green bars represent snow in cm and rain in mm respectively. The red line is air temperature in °C.

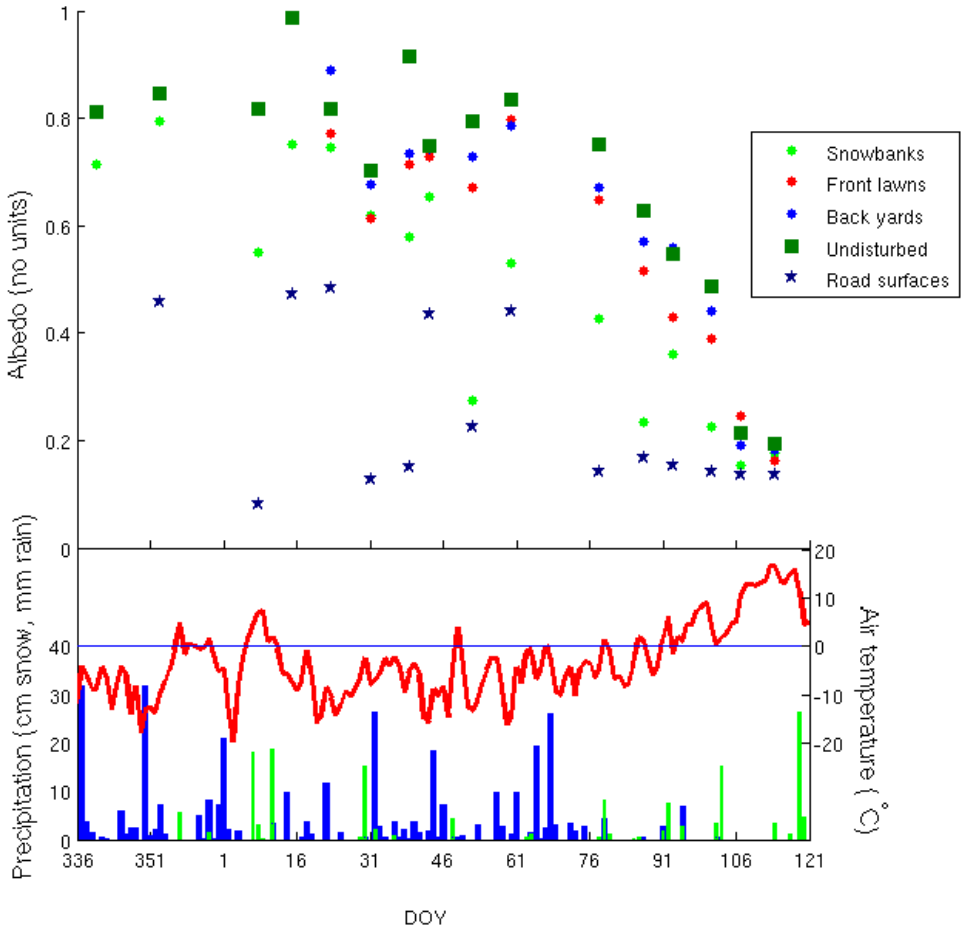

Figure 3–12: Top plot is measured snow albedo for the different snow cover types at the suburban site. Bottom plot is cumulated precipitation and daytime average air temperature values measured at Dorval international airport. Blue and green bars represent snow in cm and rain in mm respectively. The red line is air temperature in °C.

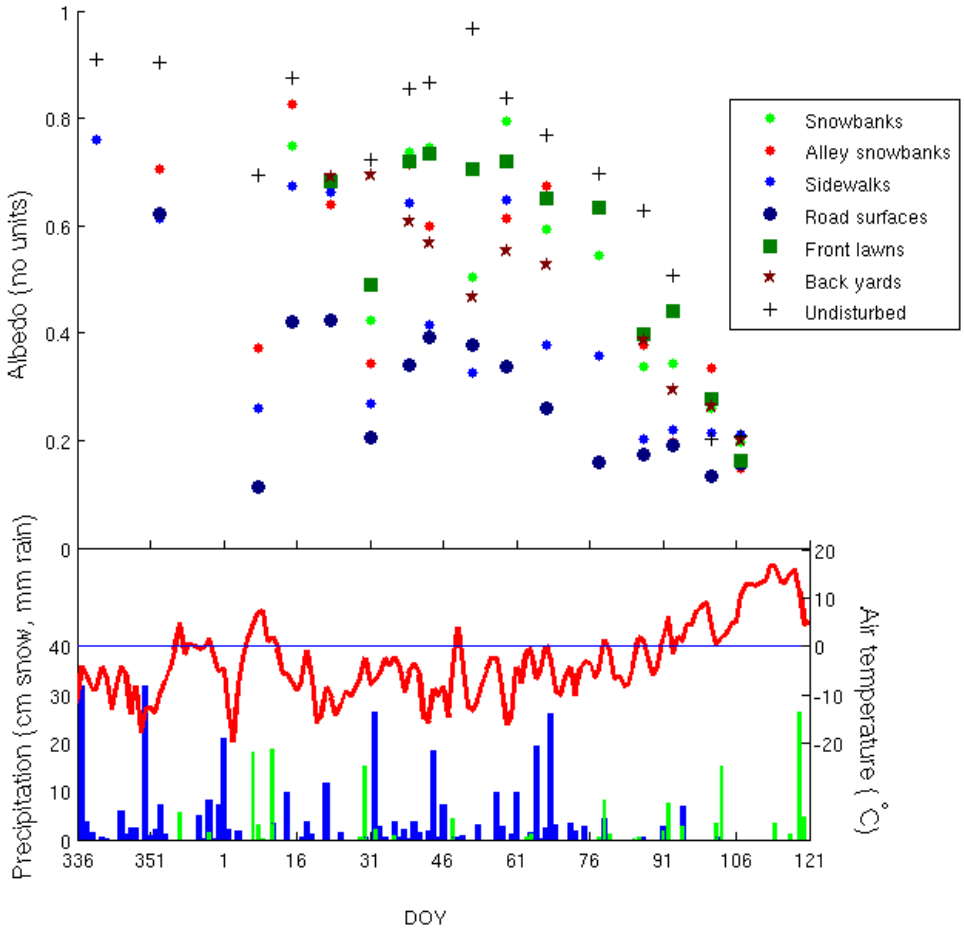

Figure 3–13: Top plot is measured snow albedo for the different snow cover types at the urban site. Bottom plot is cumulated precipitation and daytime average air temperature values measured at Dorval international airport. Blue and green bars represent snow in cm and rain in mm respectively. The red line is air temperature in °C.

site to exhibit a "real" decrease in density during the spring melt. The sudden increase at the start of the season is not detectable for other cover types because measurements only commenced in January, 2008. However, the same non-monotonic increase is present. The greatest densities were observed in backyards ($\rho_{\max} = 439$ kg m^{-3}), and roadside snowbanks($\rho_{\max} = 428$ kg m^{-3}) while front lawns had the lowest maximum value for density ($\rho_{\max} = 389$ kg m^{-3}).

At the urban site, densities display a variety of trends depending on the snow cover type in question. Undisturbed snow in parc Molson and snowbanks exhibit an initial increase from December to early January followed by an equal decrease throughout January before adopting a similar trend to that observed at the suburban site: oscillations around a generally increasing trend; increasing until complete ablation of the snowpack. The snow density on front lawns and backyards displayed the same trends from late January. The largest value encountered for maximum density was in undisturbed snow ($\rho_{\max} = 484$ kg m^{-3}) and the smallest was in backyards ($\rho_{\max} = 326$ kg m^{-3}).

For albedo, less disturbed snow types such as the soccer field, front lawns and backyards at the suburban site and the undisturbed snow (park), front lawns, backyards and roadside snowbanks at the urban site, exhibit behaviour similar to that expected from snow in a typical rural setting (Figs. 3–12 and 3–13). Consistently high albedo values were observed throughout the winter period until the spring melt, at which point there was a rapid and steady decrease towards the albedo of the underlying ground or vegetation. Snow types that experience snow removal (street and sidewalk surfaces at both sites), have generally lower values of albedo corresponding to that of the underlying impermeable surface. Occasional sudden increases are seen throughout the year, coinciding with site visits occuring soon after snowfalls, before snow removal crews reached the area.

3.4.2 Snow and the urban energy budget

The different land uses as well as the proportion of each snow cover type in the tower source area were derived using an overlay of the modelled source area, aerial photographs and a map of snow cover types (Figures 3–16 and 3–17). Source areas were modelled for each of the days of snow observations that had tower-flux measurements that passed quality criteria resulting in fifteen days at the suburban site and ten days at the urban site. At the suburban site, seven of the days had source areas that were located to the west-south-west of the tower with three located to the north-east and the remaining five distributed in other directions. At the urban site, source areas for five days were located to the west-south-west of the tower with the remaining five distributed in other directions.

Weighted snow properties

The relative proportions of each of the snowcover types contained within the tower flux source area at the suburban site are shown in Figure 3–16. Impervious surfaces occupy the greatest proportion of source areas on average (31.8%), followed by backyards (24.3%) then by front lawns and roofs (≈17.4% each), undisturbed / recreational areas (5.3%) and roadside snowbanks (3.3%). Urban snow coverage is similarly represented in figure 3–17. In Rosemont, rooftops represent the largest surface (38.4%) with impervious surfaces occupying 28.2%, followed by backyards (13.9%), front lawns (8.0%), sidewalk shoulders (5.1%), street shoulders (4.8%), alley-side snowbanks (0.9%) and undisturbed / recreational areas (0.4%).

The snow depth weighted by proportion of cover type for both sites is shown in figure 3–18. At the suburban site, larger fluctuations around the perceivable general trend and a greater maximum value ($\text{Depth}_{\text{max-sub}} = 50$ cm) than the urban site ($\text{Depth}_{\text{max-urb}} = 34$ cm) is seen. Both maxima occur on

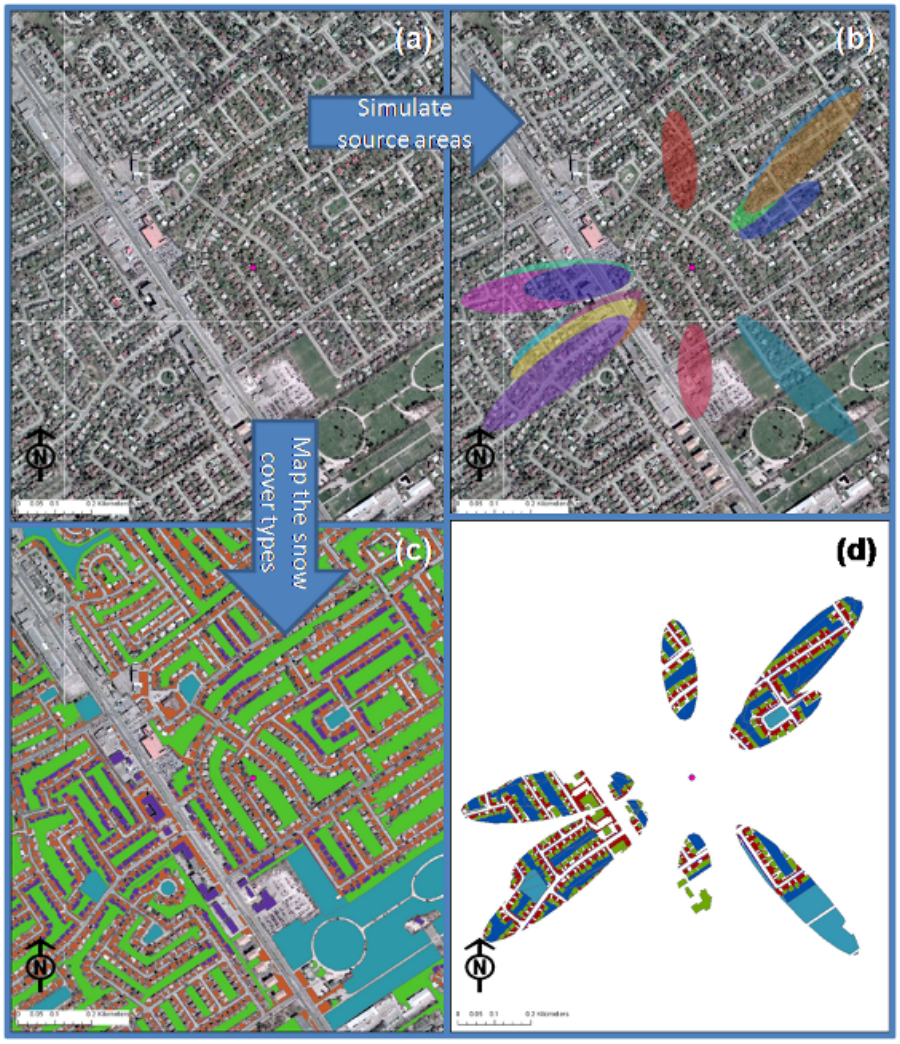

Figure 3–14: (a)Aerial photo of the suburban site and surrounding area. Position of the micromet tower is represented by a pink dot. (b) Superposition of calculated flux source areas onto aerial photo. (c) Map of different snow cover types deduced from land use seen in aerial photo. Green is backyards, blue is undisturbed snow, orange is front lawns and dark red is roadside snowbanks. (d) Snow cover types within the tower flux source area obtained by overlaying (c) with (b).

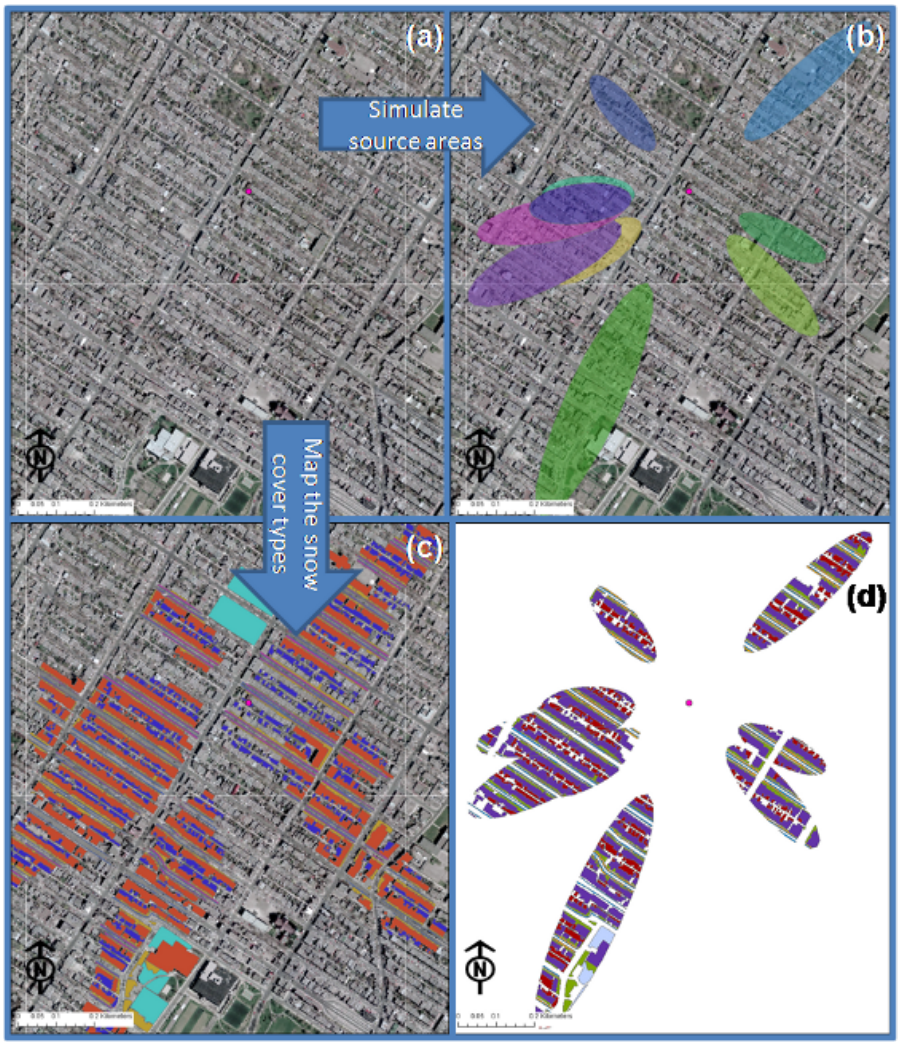

Figure 3–15: (a)Aerial photo of the urban site and surrounding area. Position of the micromet tower is represented by a pink dot. (b) Superposition of calculated flux source areas onto aerial photo. (c) Map of different snow cover types deduced from land use seen in aerial photo. Orange is rooftops, light blue is undisturbed / recreationnal areas, dark blue is backyards, yellow is front lawns, middle blue is street shoulders, purple is sidewalk shoulders and green is alley shoulders. (d) Snow cover types within the tower flux source area obtained by overlaying (c) with (b).

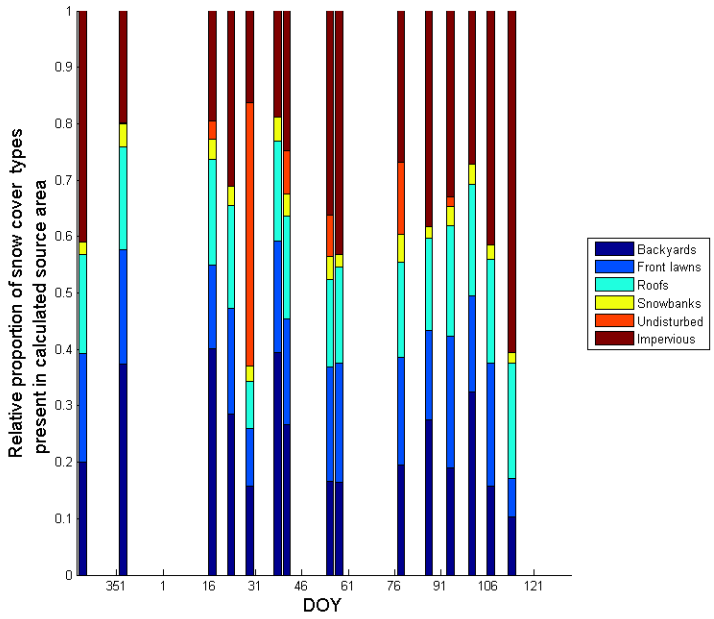

Figure 3–16: Proportions of prevalence of snow cover types at the suburban site.

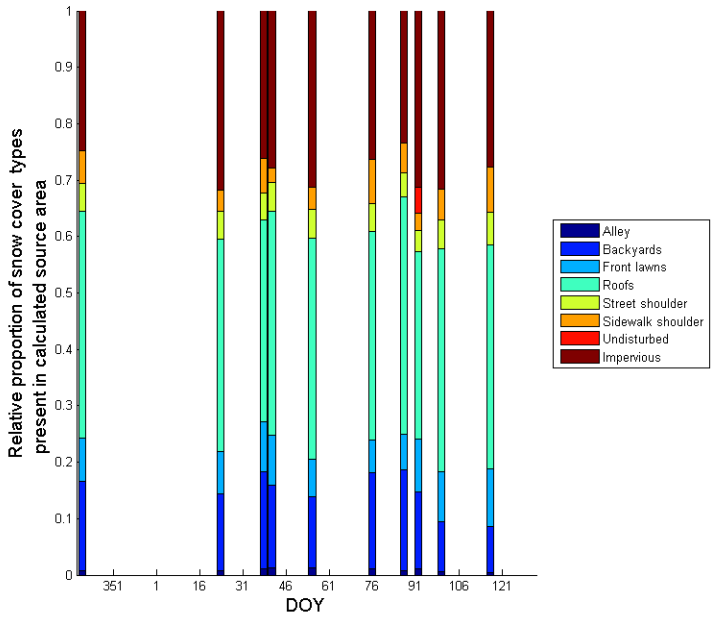

Figure 3–17: Proportions of prevalence of snow cover types at the urban site.

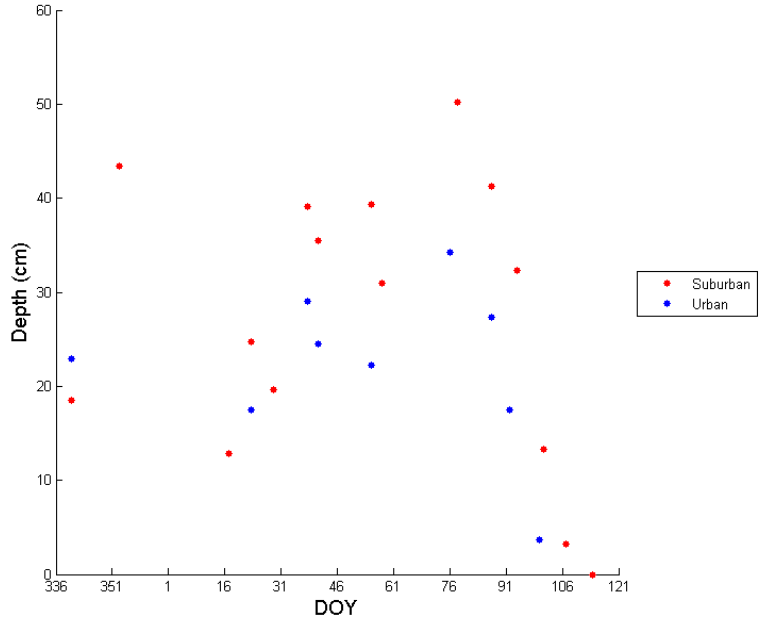

Figure 3–18: Weighted snow depth at the urban (blue) and suburban (red) sites.

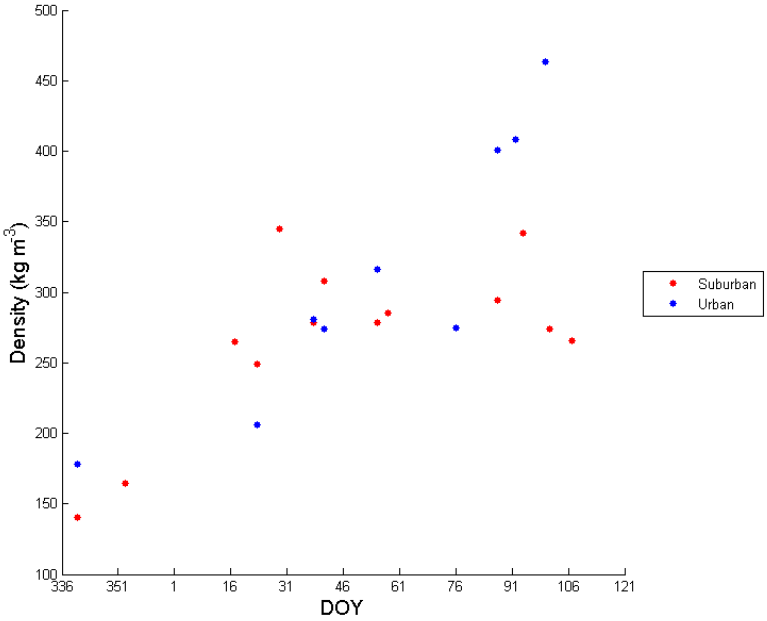

Figure 3–19: Weighted snow density at the urban (blue) and suburban sites (red).

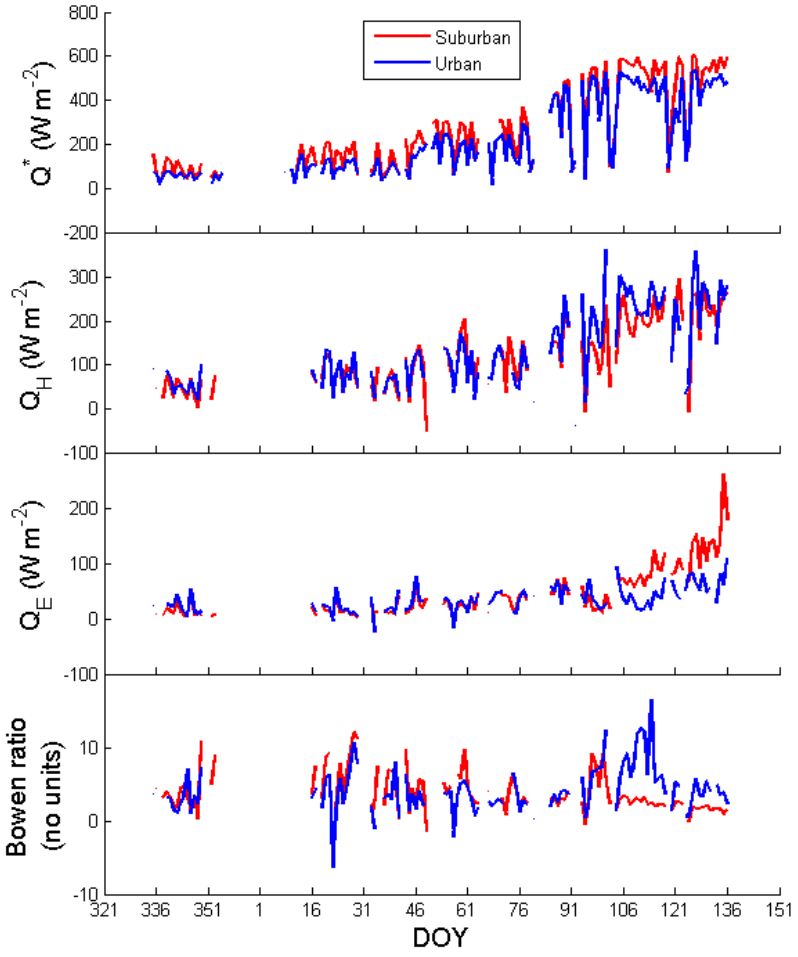

Figure 3–20: Daytime averaged energy fluxes and Bowen ratio for days for which convective source areas could be calculated. for the suburban site (red) and the urban site (blue). The gap from DOY 353 to 15 corresponds to a period during which flux measurements were suspended.

the same day and sudden increases at either site resulting from snowfall occur at the same measurement date.

Up until the end of February, area-weighted densities (Fig 3–19) at the sites behave similarly, following a generally linear increase. In March, they diverge; the urban site showing increasingly greater and faster growing densities whilst the suburban site exhibits a leveling off around a value of ≈ 287 kg m^{-3}.

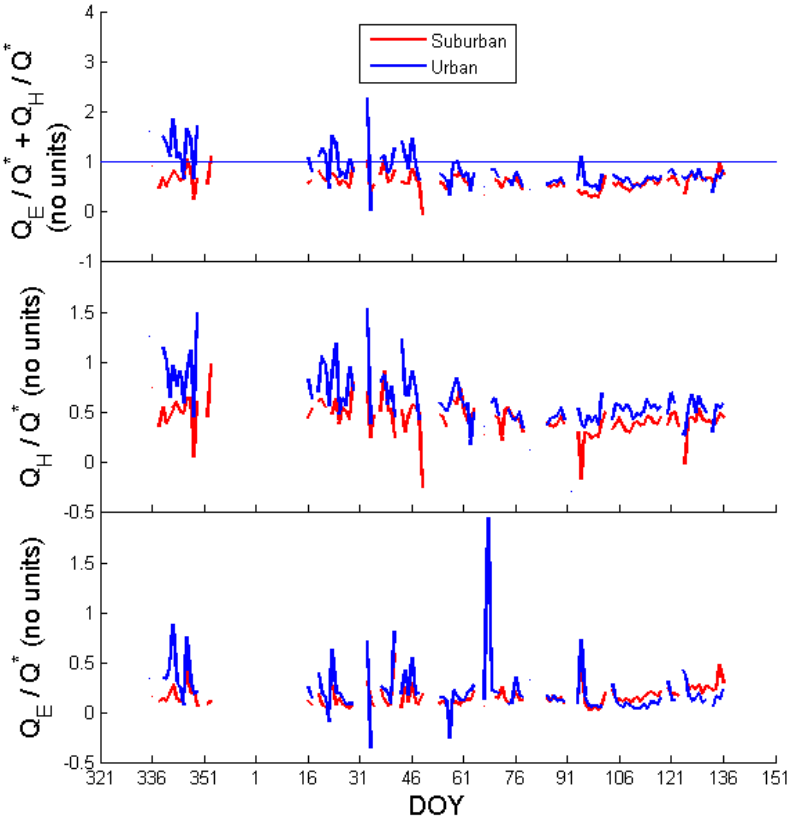

Figure 3–21: Ratio of daytime averaged sensible heat flux,Q_H, and latent heat flux, Q_E, to the net radiation, $Q^*$for the suburban (red) and urban (blue) sites.

Daytime averaged energy fluxes

Net radiation, Q^*, starts out the winter season very small ($\approx$ 100 W m^{-2}) and remains at low values up until mid February (DOY 40) after which it shows an increasingly rapid increase over the course of the winter (Figure 3–20). A "levelling-off" takes place as of the 10^{th} of April (DOY 100) and radiative flux values tend toward a more constant behaviour ($Q^*_{sub} \approx$ 570 W m^{-2} and $Q^*_{urb} \approx$ 420 W m^{-2}) for the rest of the period examined.

Sensible heat flux density, Q_H, behaves similarly to net radiation: remaining fairly constant until early February (DOY 40) and then increasing almost linearly through to mid-April and levelling off (Figure 3–20). The early winter minimum is $Q_H \approx$ 75W m^{-2} and the final equilibrium tends toward $Q_H \approx$ 235W m^{-2} at both sites. Day to day variations introduce "spikes" into the data. These increase the range of Q_H values; ranging between -15 and 400 W m^{-2} at the urban site and between -40 and 320 W m^{-2} at the suburban site.

Latent heat flux density, Q_E, is very small, showing almost zero values for both sites right up until the end of the melt in mid-April ($\approx$DOY 100) at the suburban site and late April ($\approx$ DOY 110) at the urban site (figure 3–20). Afterwards, there is a sudden increase at the suburban site that offsets it from urban values for the remainder of the period. Both seem to increase at the same rate. This offset is reflected in the Bowen ratio, β, as well (Figure 3–20). Caution must be used in approaching β earlier in the year due to the very small values of Q_E that make it quite sensitive to any fluctuation in Q_H.

The evaporative fraction, Q_E/Q^* (bottom panel, figure 3–21) shows very little long-term variation over time. However, a very broad and flat "bump" is detectable from DOY 50-100 as well as a very gradual increase beginning on DOY 100 that continues beyond the timeframe of the experiment. This

places a local minimum between these two features at DOY 100. Otherwise, daily variations show sometimes very large spikes occuring on days of low net radiation values.

The Q_H/Q^* is noticeably noisier. Particularly for the urban site and especially before DOY 70, when Q_H and Q^* are starting to increase significantly. Days before mid-February (DOY < 40) show a greater fraction for the urban site. Despite the high level of noise, it is possible to detect a very gradual decrease from DOY 15 to 85, after which it stabilizes and remains constant apart from daily fluctuations through to the end of the winter.

The sum of these two fractions, $\frac{Q_E+Q_H}{Q^*}$, exhibits similar characteristics as Q_H/Q^* but with a positive offset of ≈ 0.3 that corresponds to the contribution of the evaporative fraction. Urban data is seen to be greater than unity for a number of days before DOY 60, however this happens very rarely for suburban values. Ignoring daily variations, the general trend of both sites shows a very shallow minimum near DOY 95. It is more appreciable for the suburban site.

3.5 Discussion

3.5.1 Snowcover evolution

The deepest snow cover at the urban site was observed in backyards. This is due to intensive manual relocation of snow from the alleyway by the homeowners coupled with a lack of mechanical snow removal by the municipality akin to what takes place along roadways. Protection from wind compaction and direct sunlight is also provided by adjacent trees, fences and buildings. These features additionally contribute to snow trapping much like snow fences and wind breaks (Pomeroy and Gray, 1995). Front lawns at the suburban site receive a similar additional input of snow through the shoveling of driveways by homeowners and regularly spaced cedar hedges play the role of snow traps. Potential "roll-over" of roadside snowbanks onto front lawns could also

be ocurring; contributing to further snow accumulation. In contrast, the shallowest snowpack is recorded in undisturbed areas at both sites. These are generally more exposed to the elements and do not receive snow relocated from elsewhere.

The deepest snow cover types at each site also exhibit the largest uncertainties. For example, urban backyards generally have one corner occupied by a large snow pile, while the remainder of the surface may consist of more natural snow accumulation or a cleared pathway. This introduces quite a bit of variability within each transect despite the similarity between different backyards. Suburban front lawns, meanwhile, are reasonably uniform and most variability is introduced by differences between different front lawns as they may be subjected to different "micro-environments" based on the side of the street and the tree cover.

All locations where density was measured (figs. 3–10 and 3–11) experience a "bump" that builds up over the course of late December, reaches a maximum in early January (DOY 7) and then quickly decreases to a local minimum in mid-January ($\approx$ DOY 22). The initial rise is brought on by natural cold-weather ageing of the snowpack as well as two warm periods taking place from DOY 355 to 363 and DOY 5 to 11 during which several *rain-on-snow* events occured, further accelerating the increase in density through repeated melt-refreezing of the snowpack. After the peak is reached on DOY 7, continued ablation of the old snow throughout its volume (see depth, figs. 3–8 and 3–9) as well as the addition of fresh new snow through several snowfall events work to reduce the snow density to a local minimum. After this, temperatures remained well below freezing and the cold weather regime took over again.

The observed non-monotonic increase in the density of all snow cover types throughout the winter season can be resolved into two separate behaviours: a general, almost linearly increasing trend corresponding to the ageing of the snow pack through settling and progressive "growth" of the snow crystals through repeated melt-refreeze cycles as well as "high-frequency" ($\approx$ 2 weeks) fluctuations around that trend. The latter is driven by frequent snowfall events and occasional rainfall events accompanied by warm periods. The effects of these processes are somewhat buffered in the cases of certain snow types such as suburban snowbanks and front lawns as well as urban front lawns and back yards. This may be due to shelterng of suburban front lawns by surrounding buildings and manual and mechanical snow relocation operations taking place on the other snow types that can compact the newly added snow, artificially increasing its density more quickly. The reported range of density values at both sites ($\rho_{\text{sub}} = [134, 439]$ kg m^{-3} and $\rho_{\text{urb}} = [132, 484]$ kg m^{-3}) is higher than that usually reported for natural snow found under normal conditions ($\rho_{\text{natural}} = [10, 350]$ kg m^{-3}) (McKay and Gray, 1981). The densities measured in the course of this study are consitent with those found in other urban studies ($\rho_{\text{typical}} = [200, > 700]$ kg m^{-3}) (Semádeni-Davies, 1999; Sundin et al., 1999); indicating that similar densification processes are at work in different cities around the world. Densities in suburban backyards and in the urban undisturbed snow types show remarkably high values and variability. The latter location is where both the lowest and highest density were measured at the urban site and the former is the densest snow at the suburban site. This is unexpected for two snow cover types that undergo little to no intentional human intervention. Urban backyards, which are the recipients of large amounts of displaced snow, exhibit the smallest value for a maximum density. This may be because the snow is hand-shoveled, which doesn't compact the

snow or "drag it on the dirty ground", through which denser contaminants would be introduced, as much as removal using machinery.

Albedo data shows two different behaviours depending on the snow cover type in question. Surfaces that do not experience regular and complete snow removal such as recreational fields or front lawns, for example, exhibit a relatively high albedo with only small fluctuations for most of the winter (up until DOY 77) followed by a rapid decrease to the albedo of the underlying surface during the spring melt period. This is consistent with the oft-documented evolution of albedo over rural snow. Measured albedo during the "stable winter period" varies between ≈ 0.4 for urban backyards and suburban snowbanks and ≈ 0.9 for the undisturbed snow types at both sites. Bare surfaces, such as streets, sidewalks and the alley, on the other hand, generally exhibit much lower albedo values and greater variability ($\alpha_{\text{bare}} \approx [0.1, 0.6]$). The lower albedo is influenced by the underlying surface, which shows through between fresh snowfalls. The periodic removal of snow causes high variation; sometimes snow measurement days coincided with the period during which snow remained on the road surface between clearing operations.

Weighted snow properties

Area weighted averages of snow depth (figure 3–18) and density (figure 3–19) based on the prevalence of each snow type within the convective source area show similar behaviour to what is observed in the individual snow cover types examined above. Snow depth exhibits a peak on DOY 77 for both sites, there being more snow at the suburban site, followed by a rapid decline in the snowpack depth during the melt period. Weighted values of depth at the suburban site are always less than the least deep suburban snow type for the same day (usually undisturbed). This is probably due to the generally high prevalence of impervious / cleared surfaces in the convective source area

(figure 3–16); an absence of snowcover being assumed over that area, it greatly contributes to lowering the average value.

In the case of the urban site, where roofs dominate the source area, weighted values are no longer always smaller than any of the depths of individual snow types. However, the maximum ($\text{Depth}_{\text{max-weighted-urb}} = 34$ cm) is still much less deep than those found in specific snow covers. Sudden increases in snow depth occur simultaneously at both sites and coincide with large snowfall events.

The behaviour of area-weighted snow density is quite similar between sites up until the end of February (DOY 57): a non-monotonic increase resolvable into a nearly linear trend and rapid oscillations around this trend. Afterwards, the behaviour of snow densities at both sites diverges: the urban site continues to increase toward a value of 360 kg m^{-3} and the suburban site increases progressively more slowly and eventually decreases toward a value of 287 kg m^{-3}. The latter behaviour of the suburban site density takes place regardless of ever increasing density for all but the roadside snowbank snow type and is attributable to a repartitioning of the snow cover types within the estimated convective source area (figure 3–16). Later in the season, a larger portion of the area is occupied by impervious surfaces (which are not involved in averaging of density because they are snow free) and there is a smaller prevalence of front lawns and backyards, making rooftops count for a successively greater weight over the last few days of the winter. The weighted density of urban snow does not experience this same final decrease in density due to the greater isotropy of the site.

3.5.2 Energy fluxes and snow properties

Daytime averaged energy fluxes

The observed behaviour of Q^* is as expected throughout the experiment; the increasingly rapid increase coincides well with the rapid decrease in albedo due to melt and soiling of the snowpack (Figs. 3–12 and 3–13).

The behaviour of sensible heat flux density mirrors that of net radiation as expected. This is confirmed in the flat behaviour of Q_H/Q^* (fig. 3–21), particularly near the end of the winter. Latent heat flux density evolves quite differently; showing an increase at the end of the melt period after which suburban Q_E differs noticeably from urban Q_E. This is caused by the removal of the snowpack and its homogenizing effect, revealing the respective substrates with their different moisture properties. As pointed out in the site description (section 3.3.1), the suburban site is covered in 65% permeable surface whereas the urban site has 30% indicating that water produced by the recent melt is not removed by drainage systems to the same degree at the suburban site and can remain available in the soil for evaporation.

The broad maximum occuring in the Bowen ratio at the urban site from DOY 86 to 117 with values exceeding unity, begins with the melt period at that site and then continues several days after it ends, suggesting a very dry environment. (fig. 3–18). This may indicate that a significant portion of the energy input remaining after dissipation through Q_H is being used to melt the snowpack but that the runoff is removed immediately from the system by drainage before it can be evaporated and detected by the tower's eddy covariance instruments. The same phenomenon is not noted at the suburban site.

Figure 3–22: Sequential digital photographs of a suburban backyard to illustrate the rapidity with which snowcover becomes patchy then melts completely.

Figure 3–23: Sequential digital photographs of a urban backyard to illustrate the rapidity with which snowcover becomes patchy then melts completely.

Flux ratios

The local minimum in the evaporative fraction precedes an increase that extends beyond the plot for both measurement sites. Thus, starting from when the snow coverage becomes patchy (figs. 3–22 and 3–23), there is increasingly more of the available energy being used to evaporate water.

The high degree of noise observed in Q_E/Q^* and more so in Q_H/Q^* up until $\approx$ DOY 50 is mostly caused by small values for net radiation that amplify any fluctuation in latent or sensible heat flux. The noisier nature of these ratios for the urban site than for the suburban is because of the smaller and smoother values of Q^* at the former compared to the latter.

Whereas Q_E/Q^* shows very little noticeable difference between the sites, Q_H/Q^* has significantly higher values for the urban site up until DOY 40. A likely explanation is that energy inputs to the system in the form of anthropogenic heat fluxes, Q_F, are larger at the urban site where building and population density is far greater.

These higher values observed for the urban site are carried over to the sum of these two fractions, $\frac{Q_E+Q_H}{Q^*}$, where many urban but few suburban datapoints are greater than unity. Thus, there must be an additional energy input to the system at the urban site whose intensity is smaller at the suburban site its effect either ceasing or being negated as of early March. A likely candidate is space heating in buildings: the general trend of daily mean temperatures begins to increase as of DOY 60 after having remained rather low until then, daily fluctuations aside.

3.6 Summary and conclusions

This study sought to gather a complete dataset of snowcover evolution over a winter season in urban and suburban Montreal. A winter measurement campaign identified and targeted the different snow cover types arising from

various degrees of human intervention at different locations in the city. Results were then scaled up to the convective source area of a flux tower in order to discern patterns in energy fluxes and attempt to associate them to changes in areally weighted snow conditions.

In general, the examined snow properties in the urban and suburban environments behave in the same manner as snow subjected to rural conditions as described in the literature (McKay and Gray, 1981). Snow depth experiences a gradual increase throughout the cold part of the winter as snow accumulates and a rapid decrease during the spring melt. Snow density undergoes a gentle increase throughout the course of the observed period. Values of density are much higher than those normally seen in nature and are more consistent with previous urban studies. The albedo of non-snowplowed surfaces remains high during the cold part of the winter and decreases rapidly at melt.

Weighted snowcover properties (particularly depth) are heavily influenced by bare surfaces in the source area. Thus, weighted-average snow depth is considerably smaller than what is measured in almost any given location in the area near the tower.

Net radiation measured on site is seen to react to the rapid decrease in albedo at melt time by undergoing a sudden increase. Sensible heat flux shows no signs of being influenced by snow properties, any seasonal variation being entirely driven by changes in net radiation. Latent heat flux shows a comparative deficit during the melt of the snowpack followed by a return to normal.

Future work to be performed consists of a multi-year comparison using snow data collected during the second winter of the EPiCC campaign. This would increase the available data on snow evolution in urban Montreal and reduce the possibility of coincidental links between snow and fluxes being

detected. Secondly, another snow-flux comparison study similar to the one described here should be attempted in a more homogenous environment such as a forest or agricultural area to eliminate some of the uncertainties introduced by the inherent imprecision of convective flux source area modelling. The results could be useful in land surface modelling efforts. Finally, the study of runoff production and the store of liquid water within the snow would be very useful in quantifying the snow melt flux ΔQ_M thus providing a more complete understanding of the energy budget than what is currently available.

Preface to Chapter 4

In the preceeding chapter, the measurement of properties of the snowcover throughout the winter in urban and suburban Montreal was documented. The overall trend of snow property evolution was found to be similar to that expected in a typical rural snowpack. On average, higher density and lower albedo were reported. Measurements were scaled up to the convective source area of a flux tower. Radiative fluxes showed a dependence on the presence of snowcover and it's effect on the surface albedo but no association was found between convective fluxes and snowpack properties.

Similarities between general trends in the behaviour of urban snow properties and that of natural snow open the possibility of using this dataset to analyze the performance of a snow model designed for rural snow at simulating urban snow properties. In the next chapter, snow data output from the ISBA land surface model are compared to the urban snowcover evolution dataset.

CHAPTER 4

Validation of the ISBA snow model in the context of Montreal urban and suburban snow

4.1 Introduction

Numerical weather forecasting systems simulate the displacement of air masses and their interaction with the underlying surfaces over time in order to provide predictions of the weather occurring at a given time and place. This complex task is often subdivided into at least two parts: general circulation modeling, which deals with movement of weather patterns and land surface modeling which handles energy and mass exchanges between the surface and the atmosphere above. Whereas the former relies on well developed and universal principals of hydrodynamics, the latter is highly dependent on conditions at the surface and is still the target of much research; both on the part of the observational and the modelling communities.

Surface fluxes bring important modifications to the overlying weather patterns: intensity of convective activity as well as changes to the diurnal evolution of the boundary layer lead to different precipitation patterns and low-level temperature and humidity conditions (Bélair et al., 2003b). Coupled with the realisation that these fluxes cannot be experimentally resolved for all points in space nor can such campaigns provide data for times in the future, it's obvious that these energy and mass exchanges need to be represented numerically. This is performed using models that were designed, parameterized and validated using observations taken over as wide of a range as possible of different surfaces (land, sea, ice, ...) under different conditions (moist, dry, hot, cold, ...).

One of these surfaces deserving special attention is snow. The reason for this is that snow covers most of the Canadian landscape for a significant period of the year, replacing the properties of the underlying ground with it's own (Pomeroy and Goodison, 1997). Simpler "snow packages" contained in certain atmospheric and climate models proceed by setting snow properties (e.g. areal coverage and albedo) as a function of other known, measurable or simulated parameters such as time of year, latitude or air temperature (Manabe, 1969; North and Coakley, 1979; Barnett et al., 1989). This was more commonplace when computer resources were at a premium and remains sufficient in the context of certain long range climate simulation projects. Unfortunately, such a snow modelling package doesn't simulate 2-way feedback occuring between snow and atmospheric conditions, potentially introducing a bias toward more "climatically normal" conditions.

Traditionally, it has been in the domain of other disciplines (e.g. hydrology, engineering, avalanche control, ...) to produce more detailed snow models that track properties of the snowpack that are not as directly accessible such as the snow water equivalent, depth, density and temperature (Obled and Rosse, 1977; Wiscombe and Warren, 1980; Kondo and Yamazaki, 1990; Brun et al., 1989). As computing power became more available, techniques used in the design of those models were integrated into land surface schemes; thus offering better simulation of feedback effects and overall performance in years that differ significantly from those seen before. Such "Next-Generation" snow-climate models include the Biosphere-Atmosphere Transfer Scheme (BATS) (Yang et al., 1997, 1999), the Interactions between Soil Biosphere and Atmosphere (ISBA) model (Noilhan and Planton, 1989; Douville et al., 1995; Bélair et al., 2003a) and the Canadian Land Surface Scheme (CLASS) (Verseghy,

1991; Verseghy et al., 1993; Boone et al., 2004; Brown et al., 2006) to name a few.

Although the above mentioned land surface schemes have shown good performance in the simulation of snowcover in rural areas (Essery et al., 1999; Brown et al., 2006), they are not tested to handle snow in the city. Whereas a typical rural snowpack is subject to primarily natural agents such as insolation, precipitation and relocation by wind (influenced by topography and vegetation), urban snow also undergoes anthropogenic influences such as relocation by snowplowing, ablation through application of salt, complete removal from the area by mechanical means and "darkening" through abrasive spreading and being in a dirty environment. These processes (along with many other non-snow-related urban-specific processes) are not included in typical land surface models due to the relatively small proportion of area occuppied by cities. However, due to the ever growing urban proportion of the population in Canada (80%) and worldwide (50%) and to the increasing amount of evidence of the effect of cities on weather downstream (Bornstein and Lin, 2000), more effort is being committed to simulating energy exchanges and the evolution of surface properties (including snow) in an urban environment (Masson, 2000). Concurrently, the most important contributions to modelling urban snow have been submitted by hydrologists interested in runoff from snowpack ablation (Buttle and Xu, 1988; Valeo and Ho, 2004; Ho and Valeo, 2005; Semádeni-Davies, 2000).

This study focuses on the validation of the snow scheme used in the current implementation of ISBA at the Canadian Meteorological Center for operational forecasting (Bélair et al., 2003a) in the context of urban snowcover. The following aims to describe, firstly, the basic operating principles of the snow model used; secondly, the observation data that was used for model

validation and, finally, the details of the execution and validation of the snow model.

4.2 Model description

Simulations were performed using a standalone version of the snow model usually included in the Interactions between Soil Biosphere and Atmosphere (ISBA) land surface scheme and modified by the Meteorological Service of Canada (Bélair et al., 2003b,a). A brief description follows. A more complete description of the snow model can be found in Bélair et al. (2003b,a).

4.2.1 Model physics

ISBA calculates a single energy budget over the land portion of a model grid area. Thus, surface properties such as the thermal coefficient (eq. 4.4) are weighted averages (by proportion of surface coverage) of the soil, vegetation and snow contained within the grid square. This study which focuses solely on the snow submodel run in an offline mode, sets the proportion of surface covered by snow to 100%.

The snow submodel works by considering two reservoirs in the snowpack: the mass of liquid water, W_L, and the mass of snow, W_S. Through different interactions with the environment, each of these can grow, shrink or have one change into the other. Through the processes of accretion, ablation and phase change, some snow properties (e.g. density) or energy fluxes (e.g. latent heat flux) are affected. The temporal evolution of other snow properties, such as albedo is calculated using empirical functions derived from prior experimental campaigns. The evolution of snow depth, h_S, on the other hand, is not directly tracked, but is instead inferred from the snow density, ρ_S, and the mass of snow contained within the snow pack, W_S. Names and SI units of all variables used in this section are shown in table 4–1.

Table 4–1: Names and common SI units of symbols used in the model description section in order of appearance.

Symbol	Variable Name (value if a constant)	SI Units
t	Model time	s
W_S	Solid snow mass	kg
W_L	Mass of liquid water in snowpack	kg
P_S	Solid precipitation	kg s^{-1}
E_S	Surface sublimation	kg s^{-1}
$freez_s$	Freezing of liquid water in the snowpack	kg s^{-1}
$melt_s$	Melting of snow into liquid water	kg s^{-1}
T_0	Fusion temperature of water (273.16)	K
T_S	Snow surface temperature	K
C_S	Thermal Coefficient	K $m^{1/2}$ J^{-1}
L_f	Latent heat of fusion for water	J kg^{-1}
Δt	Model timestep	s
λ_s	Thermal conductivity of snow	W K^{-1} m^{-1}
c_s	Heat capacity of snow	J K^{-1}
τ	Time constant	s
$melt_{rain}$	Melting due to incident rainfall	kg s^{-1}
T_{rain}	Temperature of incident rainfall	K
P_r	Liquid precipitation	kg s^{-1}
R_{snow}	Runoff from snowpack	kg s^{-1}
Q^*	Net radiation	W m^{-2}
Q_H	Sensible heat flux	W m^{-2}
Q_E	Latent heat flux	W m^{-2}
$freez_g$	Mass of ground undergoing freezing	kg s^{-1}
$melt_g$	Mass of ground undergoing melting	kg s^{-1}
T_2	Snowpack bulk temperature	K
α_s	Snow albedo	(No units)
W_{cm}	Mass of 1cm of water over a unit surface (10)	kg
ρ_s	Relative snow density	(No units)
ρ_{Snew}	Relative density of freshly fallen snow	(No units)
ρ_i	Relative density of ice (0.9)	(No units)

Snowpack solid mass

Evolution of the snow mass, W_S, is governed by solid precipitation, P_S, surface sublimation, E_S, freezing of liquid water within the snowpack, $freez_S$, and the melting of snow into water, $melt_S$ such that:

$$\frac{\partial W_S}{\partial t} = P_S - E_S + freez_S - melt_S \tag{4.1}$$

The freezing and melting of liquid water and snow within the snowpack are expressed as

$$freez_S = \frac{T_0 - T_S}{C_S L_f \Delta t} \qquad \text{with } 0 \leq freez_S \leq \frac{W_L}{\Delta t} \tag{4.2}$$

$$melt_S = \frac{T_S - T_0}{C_S L_f \Delta t} + melt_{rain} \qquad \text{with } 0 \leq melt_S \leq \frac{W_S}{\Delta t} \tag{4.3}$$

where T_0 is the freezing/melting temperature of snow ($T_0 = 273.16K$), C_S is a thermal coefficient for snow (eq. 4.4), L_f is the latent heat of freezing, T_S is the snow surface temperature and Δt is the model timestep. The thermal coefficient for snow is calculated from its thermal conductivity, λ_S, it's heat capacity, c_S and the time constant, τ.

$$C_S = 2\left(\frac{\pi}{\lambda_S c_S \tau}\right)^{1/2} \tag{4.4}$$

In the event of rainfall occurring on the snowpack, the solid mass reservoir experiences melting due to the heat brought in by the rain:

$$melt_{rain} = \frac{T_{rain} - T_0}{2 C_S L_f \Delta t} \qquad \text{with } melt_{rain} \geq 0 \tag{4.5}$$

where T_{rain} is the temperature of incident rainfall.

Snowpack liquid mass

The liquid water content in the snowpack changes with time as a function of the total amount of rainfall reaching the ground, P_R, the runoff from the snowpack, R_{snow}, the melt rate, $melt_s$, and the freeze rate, $freez_s$.

$$\frac{\partial W_L}{\partial t} = P_r - R_{snow} + melt_s - freez_s \tag{4.6}$$

The liquid water discharged as runoff R_{snow} behaves as a function of the current water storage in the snowpack relative to a threshold value W_{Lmax}. This function differs depending on whether the snowpack contains more or less than the threshold value. W_{Lmax}, itself depends on the solid mass of snow and the density.

Temperature of the snowpack

The ISBA snow model employs a *force-restore* (Deardorff, 1978) method to simulate temperature interactions between the snow surface and the underlying bulk volume as

$$\begin{aligned}\frac{\partial T_S}{\partial t} &= C_S \left(Q^* - Q_H - Q_E\right) + \\ &\quad C_S L_f \left(freez_g - melt_g + freez_s - melt_s\right) - \frac{2\pi}{\tau}\left(T_S - T_2\right) \qquad (4.7)\\ \frac{\partial T_2}{\partial t} &= \frac{1}{\tau}\left(T_S - T_2\right) \qquad (4.8)\end{aligned}$$

Here, Q^*, Q_H and Q_E are the net radiation, sensible heat and latent heat fluxes respectively; L_f is the latent heat of fusion, $freez_g$ and $melt_g$ are the masses of ground undergoing freezing and melting, respectively; τ is a one day time constant and T_2 is the bulk temperature of the snowpack.

In the event of rainfall on the snowpack, the increase in snow temperature due to the addition of water that is warmer than the snow is already accounted for in equation 4.5 which, itself, is incorporated in the $melt_s$ term in eq. 4.7.

Snow albedo

The model handles the albedo of snow as an empirical function of time separating the problem into two cases: one for a cold snowpack (eq. 4.9) and another for a melting one (eq. 4.10). The last term in the RHS of both of these equations is the increase in albedo attributable to new snowfall. It is considered to increase linearly with a slope dictated by the rate of precipitation. Other parameters and time-constants, $\alpha_{Smin} = 0.5$, $\alpha_{Smax} = 0.8$, $\tau = 1$ day, $\tau_f = 0.24$ and $\tau_a = 0.008$ are defined to set the limits for observed albedo in rural settings and to ensure proper evolution over time. Note how the decrease in albedo for cold snow is linear but that for melting snow is exponential, trending asymptotically toward the minimum allowable value, α_{Smin}.

$$\alpha_S(t) = \alpha_S(t - \Delta t) - \tau_a \frac{\Delta t}{\tau} + \frac{P_S \Delta t}{W_{cm}} (\alpha_{Smax} - \alpha_{Smin}) \qquad \text{for a cold snowpack} \tag{4.9}$$

$$\alpha_S(t) = \alpha_{Smin} + [\alpha_S(t - \Delta t) - \alpha_{Smin}] e^{\left(-\tau_f \frac{\Delta t}{\tau}\right)} + \frac{P_S \Delta t}{W_{cm}} (\alpha_{Smax} - \alpha_{Smin}) \qquad \text{for a melting snowpack} \tag{4.10}$$

Snow density

The evolution of snow density is calculated in three steps, the first considering the gradual increase due to gravitational settling of the snowpack (eq. 4.11). Note the asymptotic behaviour towards the maximum relative snow density, ρ_{Smax}, which is a function of snow depth and of whether or not melting is occurring. Time constants τ and τ_f are the same as those used to

calculate the evolution of albedo in eqs. 4.9 and 4.10.

$$\begin{aligned}\rho'_s =& \rho_{Smax} - \left[\rho_{Smax} - \rho_s\left(t-\Delta t\right)\right] e^{\left(-\tau_f \frac{\Delta t}{\tau}\right)} \quad \text{if } \rho_s\left(t-\Delta t\right) < \rho_{Smax} \\ \rho'_s =& \rho_s\left(t-\Delta t\right) \quad \text{if } \rho_s\left(t-\Delta t\right) \geq \rho_{Smax}\end{aligned} \tag{4.11}$$

Secondly, the result of the ageing process above is reused for calculating the density after it is decreased by a fresh snowfall (eq. 4.12). The relative density of freshly fallen snow, ρ_{Snew}, is a function of air temperature and wind speed modulus. W_S^i is the largest amplitude term between the snowpack's current solid mass, W_S, and the mass of falling snow that has accumulated during the latest model timestep, $P_S \Delta t$ (eq. 4.13). Note how the first term in the numerator causes the snow density to lose all dependency on the exisiting snowpack if more snow falls in a timestep than what was already there.

$$\rho''_s = \frac{\left(W_S^i - P_S \Delta t\right) \rho'_S + P_S \Delta t \; \rho_{Snew}}{W_S^i} \tag{4.12}$$

$$W_S^i = \begin{cases} W_S & \text{if } W_S > P_S \Delta T \\ P_S \Delta T & \text{if } W_S < P_S \Delta T \end{cases} \tag{4.13}$$

Finally, this "fresh-snow snowpack" is subjected to the refreezing of liquid water within (eq. 4.14). ρ_i is the relative density of ice (ρ_i=0.9).

$$\rho_s\left(t\right) = \frac{W_S \; \rho''_s + freez_S \Delta t \; \rho_i}{W_S + freez_S \Delta t} \tag{4.14}$$

4.2.2 Model inputs and outputs

The main inputs required to drive the model are shown in table 4–2. Most of these are measured on a continuous basis by automated instrumentation. The remainder are either calculated from that data or are obtained from the

Table 4–2: Forcing variables input to the snow model.

Symbol	Forcing variable	Units	Source
T_{rain}	Temperature of incident rainfall	K	measured
T_a	2m air temperature	K	measured
P_{atm}	Atmospheric pressure	Pa	measured
q	Specific humidity	$\frac{kg_{water}}{kg_{air}}$	measured
ρ_a	Air density	kg m^{-3}	Calculated value
V_{MOD}	Wind speed (Low level)	$m\ s^{-1}$	measured
$V_a^{\S}$	10m **u**	$m\ s^{-1}$	calculated
$V_a^{\S}$	10m **v**	$m\ s^{-1}$	calculated
$K_{\downarrow}$	Incoming solar radiation	$W\ m^{-2}$	measured
$L_{\downarrow}$	Incoming longwave radiation	$W\ m^{-2}$	measured
P_S	Snowfall rate	$m\ s^{-1}$	Environment Canada
P_r	Rainfall rate	$m\ s^{-1}$	Environment Canada

§: V_a used in the calculation of the density of freshly fallen snow (ρ_{Snew}) is the modulus of the 2D vector to which these are the components.

nearest Environment Canada meteorological measurement station in Dorval, Québec Canada.

Output from the model quantifies snow properties and energy fluxes over the snowpack as shown in table 4–3. Those variables indicated as "In-Out" are "fed back" into the model at each timestep to provide information on the current timestep, ensuring continuity in the evolution of that snow property. Note how there is no single output for snow water equivalent. It is calculated from the solid and liquid snowpack masses as

$$SWE = \nu\,(W_S + W_L) \tag{4.15}$$

Where ν is a conversion factor to pass from a mass of water over a unit area to the height of that same column of water. When m^2 is chosen as the unit area and SWE is given in mm, then $\nu = 1$.

4.2.3 Model execution

The snow module of ISBA was run for each snow cover type at both the urban and suburban site. The model timestep was set to 30 minutes which

Table 4–3: Model outputs and prognostic variables of the snow model

Output	Units	In / Out
Depth	m	In-Out
Density	$kg\ m^{-3}$	In-Out
Albedo	(No units)	In-Out
Liquid water content	kg	In-Out
Solid snow mass	kg	In-Out
Bulk temperature	K	In-Out
Surface temperature	K	In-Out
Sensible heat flux	$W\ m^{-2}$	Out Only
Latent heat flux	$W\ m^{-2}$	Out Only
Conductive heat flux	$W\ m^{-2}$	Out Only
Net radiation	$W\ m^{-2}$	Out Only
Runoff	$kg\ s^{-1}$	Out Only

was short enough to resolve rapid changes in snow properties that can arise during precipitation events or melt periods but without requiring excessive computer resources.

Runs were performed without a"spinup" period and were started on the 23$^{\text{rd}}$ of January 2008 (DOY 23) and run until the 30$^{\text{th}}$ of April, 2008 (DOY 121); snow measurements having been stopped on April 26 due to complete ablation of the snowpack. There are two exceptions to the start-date: the run for urban undisturbed snow was started on January 15 (DOY 15) due to a missing data point for January 23 (equipment failure) and the simulation of urban snowbanks was started on January 31 (DOY 31) in order to exclude the municipal snow clearing operation that took place between the 23$^{\text{rd}}$ and the 31$^{\text{st}}$ of January, 2008.

For a particular site, the snow model was run for each of the different snow cover types using the same forcing data from the meteorological sensors at the flux measurement station. Each run was initialized with the snowpack properties observed on the model start day for the snow cover type of interest. Thus, it is the sensitivity of the model to initial conditions that permits the

simulation of different snow cover types despite there being no collection of transect-specific meteorological forcing data. It is therefore assumed that there is no location-specific dependency on the input parameters (e.g. incoming solar radiation or rate of snowfall) and that the measurements made from the observation tower adequately represent all of the transects.

4.3 Snow validation dataset

The dataset used for validation of the snow model in this study was acquired during the snow property observations campaign described in chapter 3. SWE, depth, albedo and aerial coverage were measured around established transects; the location of each of these having been chosen in order to sample as many different snow cover types as possible. The latter including street, alley and sidewalk shoulders, front lawns, backyards and parks. Each transect was comprised of a series of depth measurements in a straight line. SWE measurements were obtained at each end of the transect and albedo was measured at a point along the transect that appeared to the operator to best represent the snow conditions and had the most even illumination. Measurements with multiple repetitions were arithmetically averaged to provide a single value for that property for the transect.

Measurements were conducted on a once-a-week basis at two sites on the island of Montreal: A suburban site in the burough of Pierrefonds-Roxboro in the north-western portion of the island and an urban site in the burough of Rosemont-Petite-Patrie to the north-east of the downtown core. Sunny days were selected for data collection outings because of the sensitivity of albedo measurements to varying proportions of diffuse vs. direct insolation due to cloud cover. To minimize the effects of surface melting and solar zenith angle on snow albedo, albedo measurements were alternated between the morning

and the afternoon at both sites and were always acquired between 10:30 and 13:30 LST.

4.4 Results

Timeseries from each of the simulation runs are presented in figures 4–1 through 4–3. Model validation statistics (Wilmott, 1981) were computed (table 4–4) and scatter plots were drawn (figs. 4–4, 4–5 and 4–6) in order to better quantify and visualize the fit of the simulated data to the observed values.

4.4.1 Overall trends

Simulation output closely tracks observed data for both depth and SWE runs up until the beginning of the spring melt (≈DOY 90) (figs. 4–1 and 4–2), after which, the decline in simulated values consistently lags behind measured values by four to twelve days. This lag often causes extreme points corresponding to observed values near zero in the scatter-plots. Density (fig. 4–3) exhibits overall less conformity between observed and simulated variables. For the majority of snow types examined, simulated density values are quite close to those observed in the field up until the beginning of March (≈ DOY 60). After which discrepancies become more obvious to visual inspection. Most scatter plots of SWE and density show little range along both the observed and modelled data axis within each snow cover type in comparison to the total range for all snow types. Conversely, depth scatter plots demonstrate a much larger relative spread within each snow type.

Appropriate validation statistics (table 4–4) can be used to compare the general performance of the model at simulating a given snow property relative to another. These must be normalized because of the large differences in the ranges covered by each variable. This allows the use of the index of agreement (d), the systematic proportion of mean squared error (MSE_S/MSE), the slope

Table 4–4: Key model validation statistics describing the agreement between simulated and observed snow properties

Snow Water Equivalent

Validation statistic	sub-backyards	sub-front-lawns	sub-snowbanks	sub-undisturbed	urb-alleys	urb-snowbanks	urb-undisturbed	urb-backyard	urb-front lawns
d	0.90	0.78	0.67	0.91	0.67	0.69	0.86	0.82	0.81
MBE	-3.59	43.38	51.97	-6.07	-46.93	23.24	9.48	7.03	31.66
MSEs/MSE	0.47	0.72	0.83	0.74	0.88	0.32	0.54	0.74	0.49
RMSE	34.71	55.04	90.17	36.99	112.65	45.29	49.92	67.96	49.28
Slope	0.64	0.71	0.37	0.59	0.31	0.68	0.55	0.44	0.75
Intercept	50.54	110.71	227.21	43.72	125.03	39.15	52.13	131.04	58.05
r^2	0.73	0.68	0.50	0.85	0.54	0.29	0.63	0.64	0.57

Depth

Validation statistic	sub-backyards	sub-front-lawns	sub-snowbanks	sub-undisturbed	urb-alleys	urb-snowbanks	urb-undisturbed	urb-backyard	urb-front lawns
d	0.95	0.81	0.61	0.93	0.90	0.87	0.82	0.93	0.84
MBE	5.42	15.95	28.30	6.43	-1.44	8.20	11.95	3.47	11.26
MSEs/MSE	0.48	0.70	0.80	0.34	0.59	0.60	0.57	0.60	0.53
RMSE	9.12	21.14	35.92	11.58	15.47	11.40	16.10	12.65	15.51
Slope	0.85	0.70	0.47	0.91	0.61	1.24	1.15	0.68	0.96
Intercept	12.30	36.54	63.29	9.60	25.07	2.56	8.28	26.22	12.79
r^2	0.90	0.71	0.41	0.83	0.78	0.84	0.74	0.86	0.73

Density

Validation statistic	sub-backyards	sub-front-lawns	sub-snowbanks	sub-undisturbed	urb-alleys	urb-snowbanks	urb-undisturbed	urb-backyard	urb-front lawns
d	0.69	0.73	0.15	0.62	0.48	0.61	0.63	0.81	0.80
MBE	16.58	26.33	-4.93	-19.66	-56.57	-61.54	-80.23	0.90	-30.67
MSEs/MSE	0.26	0.36	0.86	0.36	0.61	0.46	0.95	0.12	0.69
RMSE	74.75	44.08	84.22	77.54	94.97	107.02	136.90	45.68	82.60
Slope	0.47	1.00	-0.41	0.34	0.22	0.50	0.26	0.71	0.48
Intercept	171.75	27.84	519.09	180.29	232.60	89.59	180.70	90.15	145.01
r^2	0.19	0.48	0.34	0.10	0.05	0.20	0.57	0.46	0.61

Table 4–5: Average of normalized goodness of fit statistics (d, slope and r^2).

Validation statistic	SWE	Depth	Density
d	0.79	0.85	0.61
MSE_S/MSE	0.64	0.58	0.52
Slope	0.56	0.84	0.40
r^2	0.60	0.75	0.33

of the regression and the coefficient of determination (r^2). The average value of each of these statistic variables for the different snow types is shown in table 4–5. Based on these quantifiers, the snow model simulates depth the best, followed by snow water equivalent and finally by density. However, it should be noted that errors in both depth and SWE values are more systematic in nature than those simulated for density.

4.4.2 Best model run performance

Useful information can be obtained from comparing model output for the same property from runs for different snow cover types. Output for backyard and undisturbed snow types at the suburban site yield the best conformity between observed and predicted values for both depth and snow water equivalent. This is reflected in the two highest values of the index of agreement (table 4–6) and two lowest values of RMSE (table 4–7) for each of these snow properties.

Table 4–6: Index of agreement (d) for best fitting snow types concerning snow depth and water equivalent. Values are without units.

Snow property	Suburban backyard	Suburban undisturbed
SWE	0.90	0.91
Depth	0.95	0.93

Table 4–7: Root mean squared error (RMSE) for best fitting snow types concerning snow depth and water equivalent. Values are given in mm.

Snow property	Suburban backyard	Suburban undisturbed
SWE	34.71	36.99
Depth	9.12	11.58

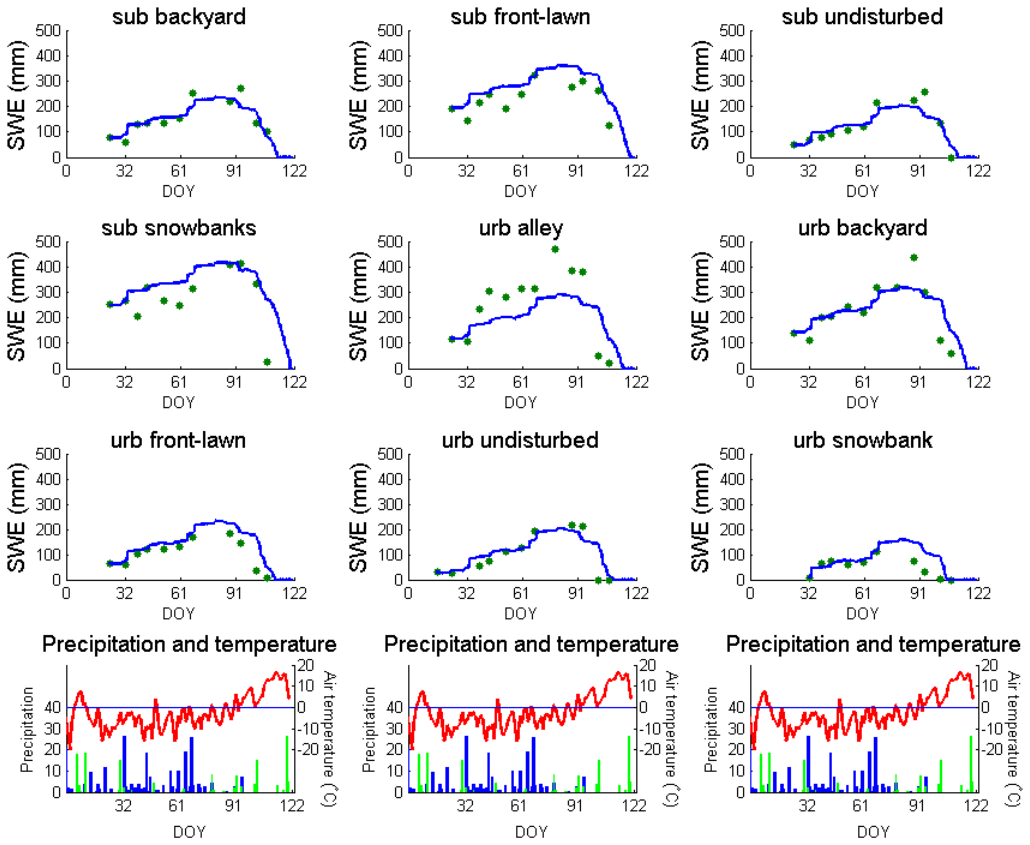

Figure 4–1: Snow water equivalent model timeseries for all 9 snow cover types. The solid line represents modeled data and points are observed values. The bottom plots show daily average precipitation and air temperature values measured at Dorval international airport. Blue and green bars represent snow in cm and rain in mm respectively. The red line is air temperature in °C.

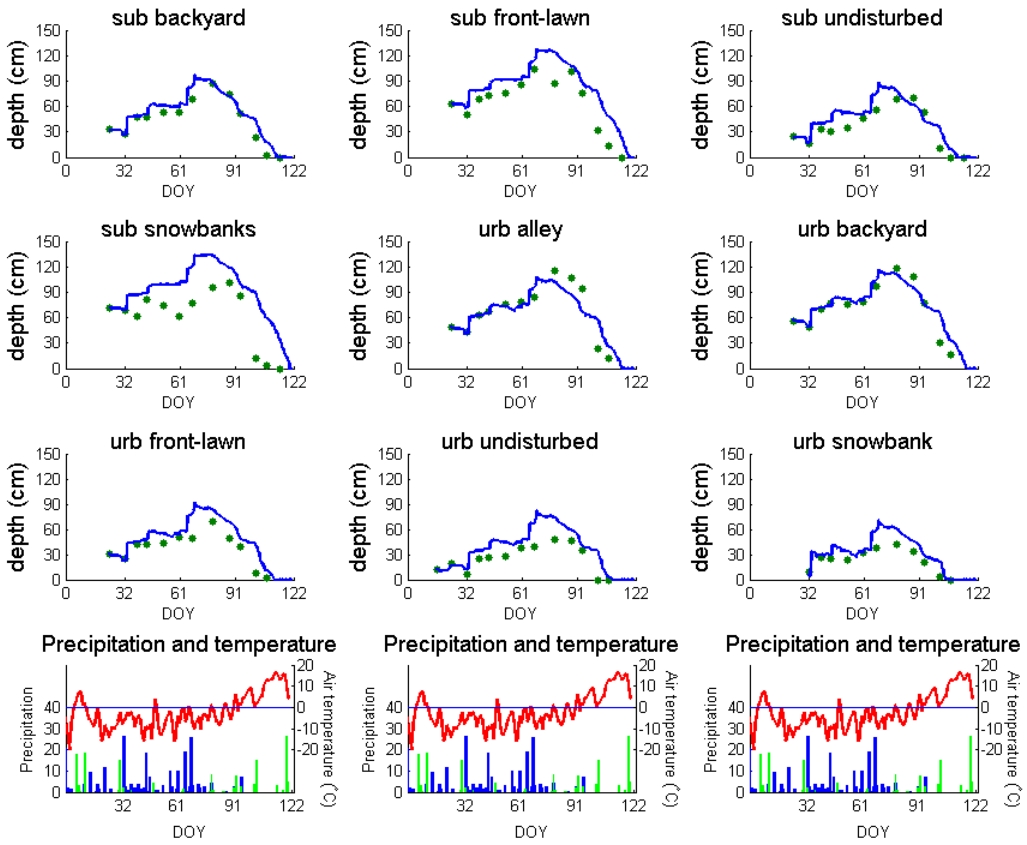

Figure 4–2: Depth model output for all 9 snow cover types. The solid line represents modeled data and points are observed values. The bottom plots show daily average precipitation and air temperature values measured at Dorval international airport. Blue and green bars represent snow in cm and rain in mm respectively. The red line is air temperature in °C.

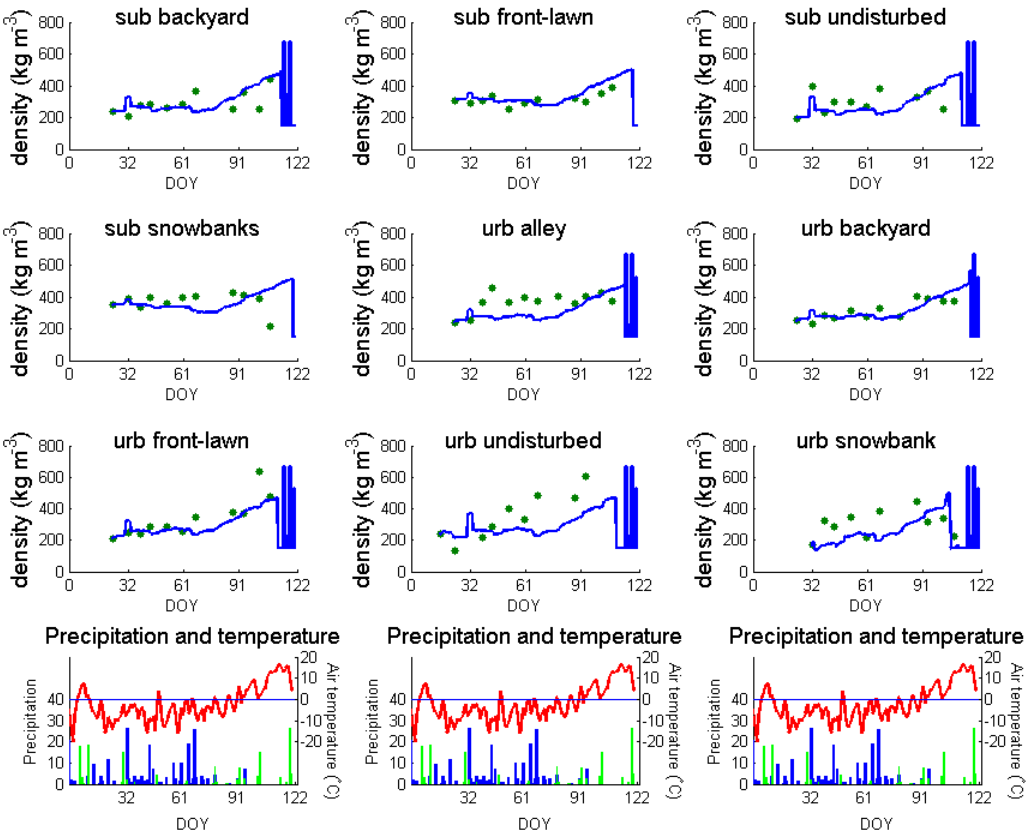

Figure 4–3: Density model output for all 9 snow cover types. The solid line represents modeled data and points are observed values. The bottom plots show daily average precipitation and air temperature values measured at Dorval international airport. Blue and green bars represent snow in cm and rain in mm respectively. The red line is air temperature in °C.

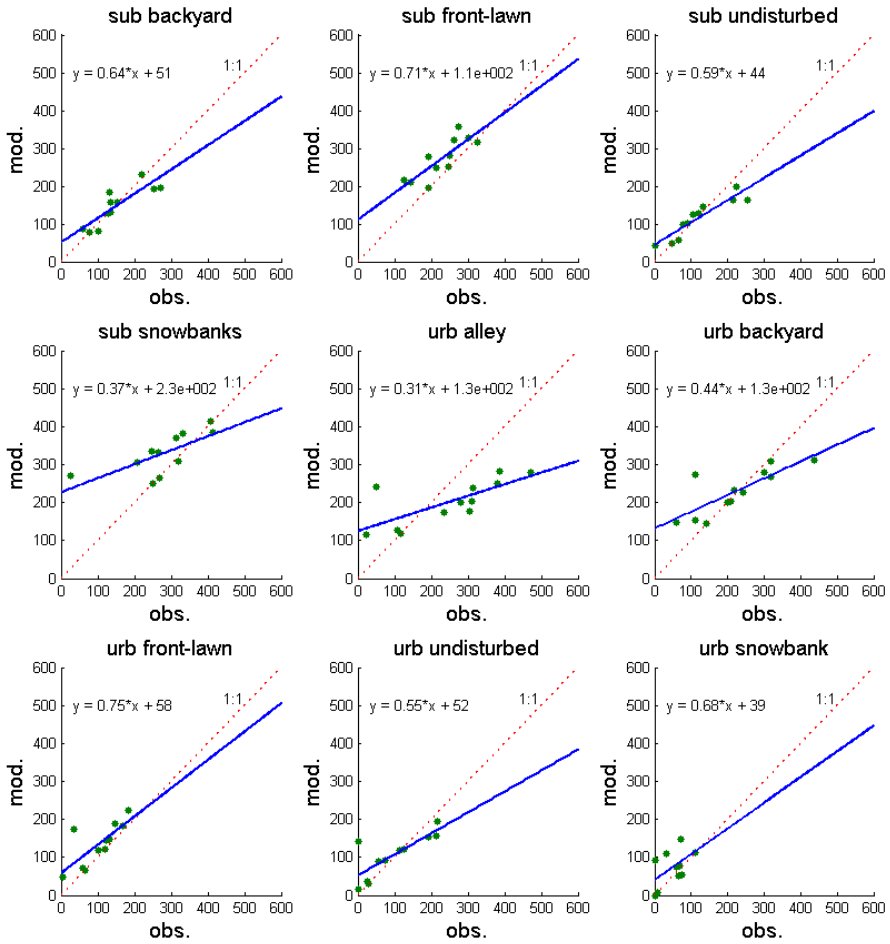

Figure 4–4: Scatter-plots of snow water equivalent output for all snow cover types. Data is represented by points, a linear fit to these points is represented by the solid blue line and the red dotted line is a 1:1 relationship.

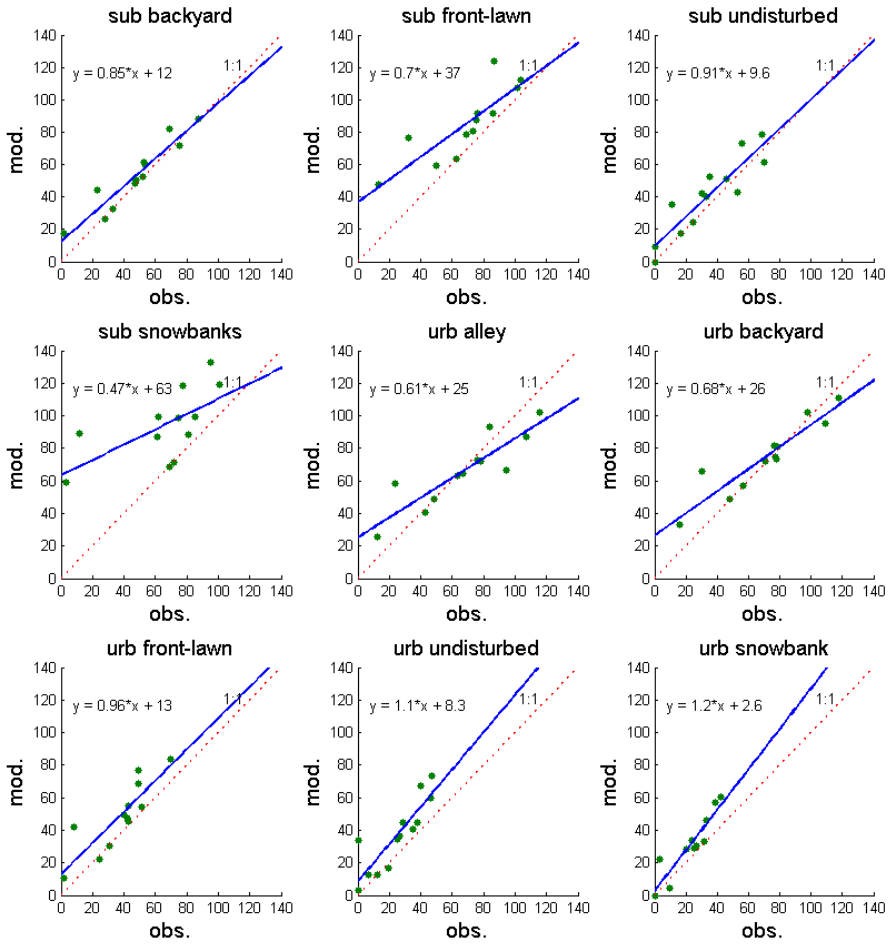

Figure 4–5: Scatter-plots of depth output for all snow cover types. Data is represented by points, a linear fit to these points is represented by the solid blue line and the red dotted line is a 1:1 relationship.

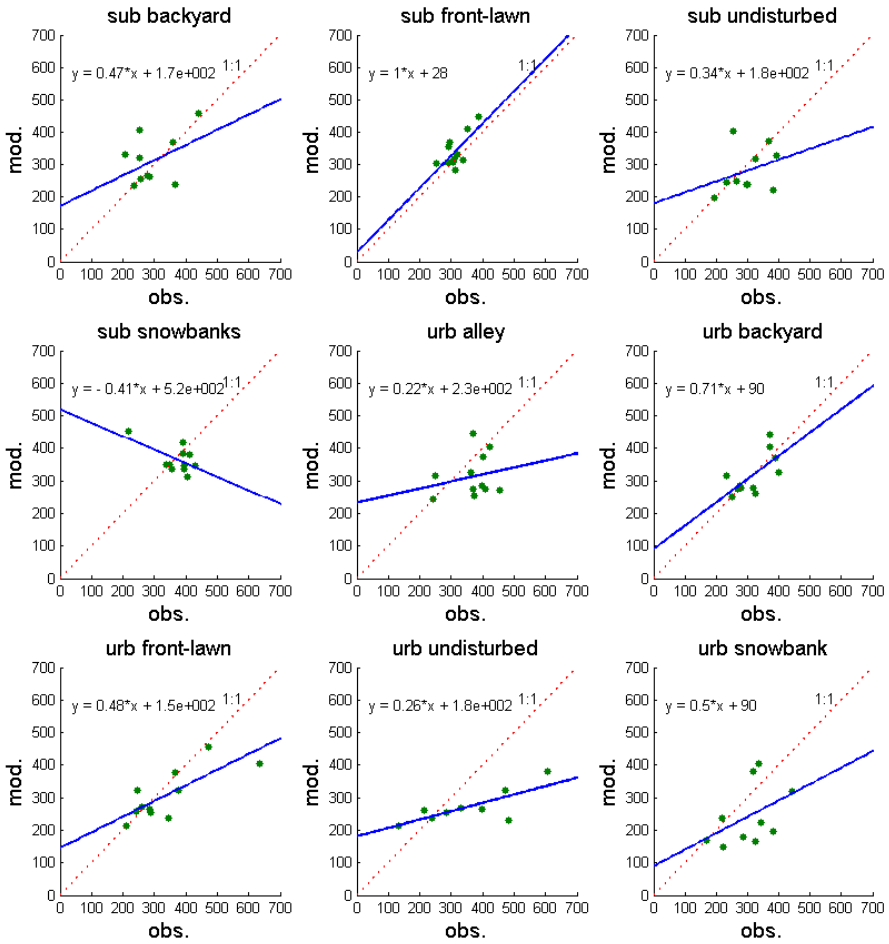

Figure 4–6: Scatter-plots of density output for all snow cover types. Data is represented by points, a linear fit to these points is represented by the solid blue line and the red dotted line is a 1:1 relationship.

One of these two snow cover types also figures among the top two values for the intercept ($\text{Intercept}_{\text{undisturbed}} = 43.72$) and r^2 ($r^2_{\text{undisturbed}} = 0.85$) of SWE and the slope($\text{Slope}_{\text{undisturbed}} = 0.91$) and r^2($r^2_{\text{backyards}} = 0.90$) of depth.

The best model output in terms of density was found for runs of suburban front-lawns and urban backyards. These showed the best ($d_{\text{urb-back}} = 0.81$) and third best ($d_{\text{sub-front}} = 0.73$) values for the index of agreement, one of the lowest systematic proportions of mean squared error ($\text{MSE}_S/\text{MSE}_{\text{urb-backyards}} = 0.12$), the two lowest RMSE ($\text{RMSE}_{\text{sub-front}} = 44.08$ and $\text{RMSE}_{\text{urb-back}} = 45.68$), the best slope ($\text{slope}_{\text{sub-front}} = 1.00$) and the lowest intercept ($\text{intercept}_{\text{sub-front}} = 27.48$). Timeseries of the density output for these two model runs show excellent conformity between predicted and observed values up until day of year 80. After this point, the simulated density of suburban front lawns adopts a visible positive bias for the last four points, despite increasing with a slope similar to observed values. On the other hand, modelled values for urban backyards exhibit an increasing trend, while the observations are seen to decrease. During this time, the average value for the last four observation points is similar to that of the simulation output.

4.4.3 Worst model run performance

Runs for the above mentioned snow cover types show cases of good model performance and offer information into the successes of the model to simulate certain aspects of urban snow. Conversely, examining cases of poor performance can provide insight as to lacking processes or just a need to refine model parameters. The snow model performs consistently poorly when it comes to simulating suburban snowbanks and, to a lesser extent, urban alley shoulders. For SWE, these two runs possess the lowest index of agreement ($d_{\text{sub-snowbanks}} = d_{\text{urb-alleys}} = 0.67$), the two highest systematic proportions of MSE ($\text{MSE}_S/\text{MSE}_{\text{urb-alley}} = 0.88$ and $\text{MSE}_S/\text{MSE}_{\text{sub-snowbanks}} = 0.83$), the two

highest root mean squared errors ($\text{RMSE}_{\text{urb-alley}} = 112.65$ and $\text{RMSE}_{\text{sub-snowbanks}} = 90.17$) and the two flattest slopes ($\text{slope}_{\text{urb-alleys}} = 0.31$ and $\text{slope}_{\text{sub-snowbank}} = 0.37$). Examination of the timeseries of the snow water equivalent of both of these snow cover types shows that while urban alleys are severely underpredicted both at the time of peak accumulation (DOY 78) and following a large snowfall in mid-february (DOY 43), suburban snowbank simulations tend to overpredict the snow water equivalent, especially just near the beginning of march (DOY 60).

In the case of depth, results for urban alleys are not remarkable. However, output from the suburban snowbank run yields the worst values of any snow cover type for each of the model validation statistics explored (details in table 4–4). Timeseries of the model run show a systematic over-prediction of depth for this snowtype throughout the year but especially at the beginning of March (DOY 60) and during the spring melt period (DOY 100-115).

For density, although it is less obvious which runs perform poorer than others, it is again suburban snowbanks that gives the lowest index of agreement ($\text{d}_{\text{sub-snowbanks}} = 0.15$), one of the highest systematic proportions of mean squared error ($\text{MSE}_{\text{S}}/\text{MSE}_{\text{sub-snowbanks}} = 0.86$), the lowest slopes on its linear regression ($\text{slope}_{\text{sub-snowbank}} = -0.41$) and, by far, the highest intercept value ($\text{intercept}_{\text{sub-snowbanks}} = 519.09$). The timeseries for both of these model runs show a significant underprediction occurring mid-winter; much more so in the case of urban alleys.

The snow model also has difficulty simulating density of undisturbed snow at the urban site. Model runs for this snow type yield the highest RMSE ($\text{RMSE}_{\text{urb-undisturbed}} = 136.90$) the highest proportion of which is systematic in nature($\text{MSE}_{\text{S}_{\text{urb-undisturbed}}} = 0.95$). Inspection of the model run's timeseries

shows much too slow of a density increase as of mid-February (≈ DOY 45) to keep up with what was observed in field measurements.

4.5 Discussion

4.5.1 Highlights

It was remarked upon in the results that there exists a slight lag between the observed complete ablation of the snowpack and the time for which it is predicted by the snow model. This occurs consistently for all snow cover types, independently of whether the peak accumulation prior to the melt period was over or under predicted. A possible cause for this is the greater input of heat to the urban and suburban snowpacks than what is assumed in the (rural) snow model. This "new energy" supplied to the melting snowpack comes from nearby buildings and from the much lower albedo caused by patchy snowcover over dark substrate materials (pavement). Patchy urban snowcover is different from that occurring in natural settings only near the end of the melt period by how it is present winter-long due to mechanical snow removal operations. When temperatures are still well below freezing, it isn't sufficient to significantly melt the snowpack, however as the spring melt begins (≈ DOY 100), melt rates are compounded by this extra contribution to the local energy budget. Moreover, this implementation of the snow model is not spatially resolved, "patchiness" of snowcover is thus never considered and the snowpack is always assumed to be homogenous snow until complete ablation occurs. Therefore, this process lacking, it can be expected for melting in the model for take more time.

Table 4–5 shows overall, the best model performance for depth, followed by snow water equivalent and finally, the overall poorest performance for density output. This significant discrepancy in the model's ability to predict one

snow property's behaviour compared to another is unexpected: although density and snow water equivalent at each timestep are calculated directly from the values at the previous timestep based on relationships outlined in the model description (section 4.2.1), depth for the given timestep is calculated from the current values of snow density and SWE. Thus, it would be expected to find problems in the simulation of density or snow water equivalent reflected in the quality of the output for depth. A possible explanation is that such discrepancies stem not from the model, but from the quality of the observational dataset. As pointed out in the previous chapter, there are many more samples taken for snow depth than there is for SWE or density. This results in much greater uncertainties on the observed density and SWE values that are not accounted for in the calculation of the model validation statistics presented in table 4–4.

4.5.2 Low and medium distubance snow types

Undisturbed snow cover and backyards at the suburban site constitute the least disturbed snow types examined throughout the entire measurement campaign. Human traffic or activity of any kind is almost completely absent during the winter from any of the backyards and the recreational field designated as the undisturbed location that were sampled. Therefore, it is not surprising that the ISBA snow model which has previously been rigorously tested in rural conditions, is able to model snow depth and SWE in these locations with good to excellent accuracy. The main factors that differentiate these two snow types is the proximity of buildings and porous fences or hedges in the case of the suburban backyard. While the former act as minor heat sources, they are also effective at blocking some of the incoming solar radiation incident to the snowpack. Both the buildings and the fences act like

"snow-fences", increasing the collection of windborne snow precipitation on their leeward side (Steppuhn, 1981).

What is less expected is that density output for these same snow types is not distinctly better than any other snow types, instead suburban front-lawns and urban backyards are simulated best. These snow types are what can be qualified as being subjected to a medium anthropogenic disturbance. In the case of suburban front lawns, this classification is due to the sheltering by neighbouring buildings as there is with backyards and to the snow shovelled onto a portion of the front lawn from the driveway by homeowners. Otherwise, there is generally little to no traffic. Urban backyards where snow was measured are of similar size to suburban front lawns but are occupied by many obstacles such as sheds and footpaths along which all pedestrian traffic is directed. Backyards receive an input of snow at one end through shovelling from the alleyway analogous to that brought to suburban front lawns from the driveway. High, porous fences act like the hedges and fences around backyards at the suburban site to capture more windborne snow within the backyard. A hypothesis lies in the higher observed values for density at the start of and throughout the season for snow types of medium human intervention compared to those that are completely undisturbed (figs. 4–7 and 4–3). The greater initial value limits the amplitude of fluctuations in modelled snow density throughout the cold period of the winter, allowing for better conformity with the reasonably constant observed values; the latter undergo very little variation due to the regular human interference that acts to homogenize the snow's density over time.

4.5.3 Roadside snowbanks and alley shoulders

It was earlier observed that model runs of two of the three highly disturbed snow types involved in this study were the most difficult to model for at least

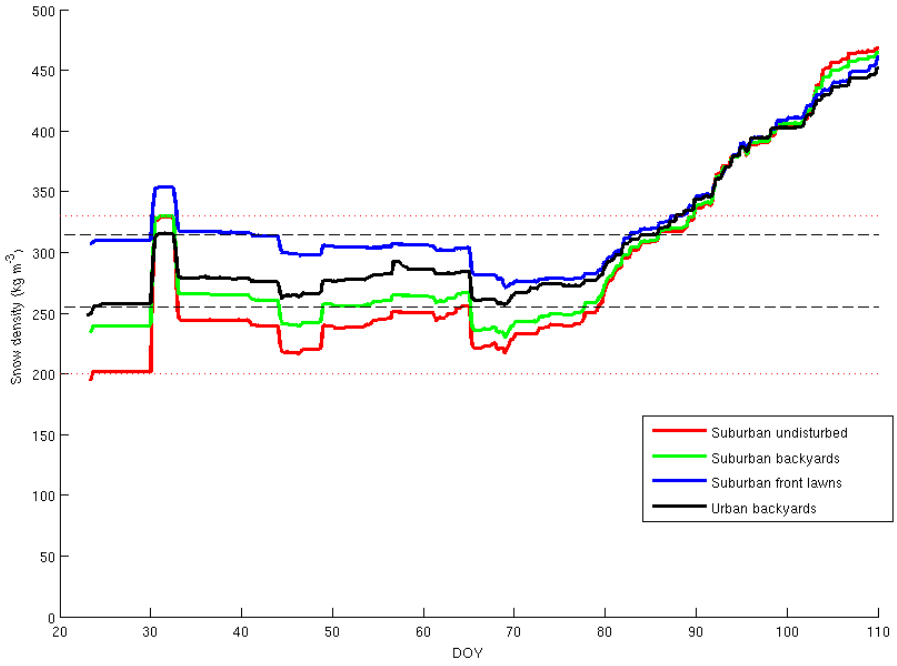

Figure 4–7: Overlay of modeled density timeseries for snow cover types undergoing medium and minimal disturbance. Note higher initial densities and less variability before the final rise for snow types undergoing medium disturbance (i.e. suburban front lawns and urban backyards).

one snow property: suburban roadside snowbanks and, to a lesser extent, urban alleys. Output for urban roadside snowbanks, however, was not cause for particular attention. All three of these snow types are not expected to be well simulated by the snow model because of the strong influence of extra processes working to change the snowpack that are not included in the ISBA snow model (e.g. snow relocation and removal, exposure to salts and abrasives, ...). An explanation as to why urban roadside snowbanks do not figure among the poorest performing model runs of depth and snow water equivalent is that although snow is relocated there from the driving surface of streets and sidewalks after snowfall events, it is periodically completely removed from the site by municipal workers to make room for more snow. In a winter such as 2007-2008, when significant snowfall events were frequent and buildup of snow on roadside snowbanks was rapid, relocation and removal operations existed in a balance that made snow depth seem to behave as though under natural conditions. In terms of density, frequent removal implies that the snow currently on the ground does not have a chance to mature before being taken away; this counteracts with the physical compaction undergone by the snow.

4.5.4 Urban undisturbed snowcover type

An important case to call attention to is undisturbed snow at the urban site. This transect is located along the edge of Molson park in an area of low pedestrian traffic to ensure the most natural snow conditions available in an urban setting. Considering this, performance of the ISBA (rural) snow model should be very good for this snow cover type or at least similar to that for suburban undisturbed. However, while comparison of snow water equivalent data yields reasonable accord, output for snow density does not fit experimental data. Part of the problem here, may not be with the snow model: visual inspection of the validation dataset shows abnormally high density values for

an area considered to be undisturbed. These are more consistent with those of glacial firn (McKay and Gray, 1981) or particularly contaminated urban snow (Sundin et al., 1999). This could be due to unexpected pedestrian traffic that was subsequently camouflaged by snowfall events, flow-through (and refreezing) of runoff from the adjacent urban park area or splashing of contaminants from the nearby street. The term "undisturbed" must therefore be taken with a note of caution when analyzing these results.

4.5.5 Model bias

For non-zero values of mean bias error (MBE), its sign can be indicative of missing processes requiring attention in the model. When absolute values of MBE are too small, then model predictions are more equally partitioned above and below the observed values, making error more attributable to the model's inability to follow finer oscillations.

For depth, mean bias error is positive for all snow types save for urban alley shoulders. Therefore, the model is generally predicting more snow than what is found on the ground. A similar tendency is observed for snow water equivalent, with only 3 of the explored snow cover types showing negative bias, only one of which is significant: urban alleys. This is unexpected because all of the snow cover types explored in this study are subjected to minimal disturbance or receive relocated snow from adjacent cover types. Meaning that these locations should have more snow than the typical rural area that the snow model is designed and parameterized to simulate. The cause may be rooted in the choice of initialization values: if SWE or depth were measured to be anomalously high or low on the day chosen for the start of the model run, all further model output will have a constant offset corresponding to that with which the run was started. The offset remains until a melt event removes all snow cover and "resets" the model. The magnitude of MBE for snow water

equivalent and depth has a rather large range and doesn't seem to follow any kind of tendency except perhaps that low values of model bias are associated with low RMSE, showing little propensity for simulated values to be "as wrong one way as the other".

For density, sign follows a different general behaviour depending on the site. At the suburban site, two of the four snow cover types exhibit a positive bias, leaving suburban snowbanks and undisturbed as negative. Model runs for snow at the urban site, on the other hand, predict density with a negative bias in four out of five snow cover types leaving only urban backyards with an essentially zero bias. The latter coincides with the lowest root mean squared error.

4.6 Summary and Conclusions

This study sought to evaluate the performance of a standalone version of the ISBA snow model in the simulation of different snow cover types found in the urban and suburban environments. Local atmospheric conditions measured at the sites were used as inputs to the model. Simulation runs were differentiated by the model's high level of sensitivity to initial conditions. Initialization data and the validation dataset were taken from the urban snowcover observation campaign performed over the winter of 2007-2008 as outlined in the previous chapter.

The model was shown to perform best on the least disturbed snow cover types available when comparing snow water equivalent and depth output to observations. This is consistent with the aim of the model to replicate rural snow properties. Simulated density values, however, were more appropriate to snowcover undergoing medium levels of human intervention. This was attributed to the equations governing cold-weather density evolution in the model: starting with high initial values limits the range available to variations

in simulated density. This matched well with the minimally but consistently managed suburban front lawns and urban backyards.

Runs of the most disturbed snow cover types performed poorly as expected. This implies that significant disturbance from human sources in the urban environment may need to somehow be included in a reparameterization of the model or a revision of density and SWE evolution equations. Fortunately, as shown in chapter 3, these snow cover types account for only a very small proportion of the total area in the urban and suburban environments. Therefore, any poor prediction of snow cover properties is lost by the weighting scheme when spatial averaging is performed.

Future work to be performed consists of a sensitivity analysis to optimize model performance through a careful adjustment of its parameters. If further improvement is required, a snow type dependent mechanism to account for snow relocation and compaction may be required. However, this would involve an element of human behaviour which may unnecessarily complicate model development.

CHAPTER 5
Summary and Conclusion

Greater urban populations than ever before in Canada have increased the demand for more accurate and precise weather forcasting in cities. These same urban centers and the heat islands they produce (Oke, 1981, 1982) also have documented effects on weather in rural areas downstream (Bornstein and Lin, 2000). These factors, in turn, have emphasized the necessity for an appropriate land surface scheme for use in such environments. Before one can be deployed operationally, however, it must undergo the proper parameterization followed by rigorous testing and validation. These operations require the use of observational data relevant to the system being simulated.

One of the EPiCC Network's goals was to acquire an appropriate energy flux dataset for the preparation of a land surface scheme in two contrasting cities in Canada, Montreal and Vancouver, but with the results being applicable to urban areas everywhere in Canada (EPiCC, 2010). Although observations focus mainly on surface energy fluxes, attention is also given to the properties of the urban and suburban snowpacks in Montreal as these are thought to be involved in processes governing such fluxes (Bélair et al., 2003a).

The research for this thesis was completed within the framework of EPiCC's Montreal observations campaign. The objectives it sought to fulfill were to collect as complete as possible of a dataset of snow property evolution in urban and suburban Montreal for the winter of 2007-2008, to scale up these measured snow properties to the convective source area of a nearby energy budget measurement system, attempt to infer links between changes in the snowpack and energy fluxes and to use the acquired observations in the validation of the

snow submodel of the ISBA land surface scheme in order to qualify the ability of this rural model at simulating snow in urban conditions.

General behaviour of the examined snowcover properties in the urban and suburban environments was similar to that expected for rural areas although differences were seen in the values of density and albedo. Densities were much higher than those usually reported in natural snowpacks but were consistent with the limited number of previous urban studies (Sundin et al., 1999). Mid-winter values of albedo for low disturbance locations (e.g. suburban backyards, urban and suburban recreational areas, etc.) were similar to those observed in rural areas (Conway et al., 1996) but high disturbance locations, such as the driving surfaces of streets and alleys showed much lower albedo values.

The net radiative flux density was shown to be sensitive to the decrease in albedo at the time of melt in the spring. Sensible heat flux density, although clearly driven by any changes in the net radiation, showed no sign of being directly influenced by snow properties. The latent heat flux density showed slightly lower values during the melt period followed by a return to its earlier trend. Repartitioning of the energy budget to melt the snowpack was brought forward as a possible cause.

Simulation work with the snow submodel from the ISBA land surface scheme showed good performance in modelling snow water equivalent and depth in low-disturbance snow types and density in medium-disturbance snow types. Model runs of the most disturbed snow cover types performed the poorest relative to observations. A notable exception to these observations was the case of urban undisturbed snow for which the fit of density output to observed values was very poor. This was attributed to the difficulty in defining a truly undisturbed snowpack in the urban environment.

Overall, the observation campaign provided a winter-long dataset of snowpack evolution for the complete set of snowcover types and properties. The modelling work constituted a first attempt at validating the snow subroutine of ISBA in urban conditions, showing a need for improvement in the case of more disturbed snow types.

Future work to be performed should be twofold. In terms of observations, a multi-year comparison using snow data collected during the second winter of the EPiCC campaign should be done in order to increase the overall available data on snow evolution in urban Montreal and to reduce the possibility of making coincidental links between snow properties and energy budget measurements. On the modelling side, this additional snow data could be put towards further validation of the ISBA model in the context of a different year. A reparameterization or redesign of the model, involving the inclusion of snow type dependent mechanisms to account for snow relocation and compaction may also be required.

References

Arya, P. S. (**2001**). *Introduction to Micrometeorology*, volume 79 of *International Geophysics Series*. Academic Press, San Diego, California London, UK, 2 edition.

Baldocchi, D. D. (**2003**). "Assessing the eddy covariance technique for evaluating carbon dioxide exchange rates of ecosystems: past, present and future." *Global Change Biology*, 9(4): 479–492.

Barnett, T. P., menil, L., Schlese, U., Roeckner, E., and Latif, M. (**1989**). "The effect of eurasian snow cover on regional and global climate variations." *Journal of the Atmospheric Sciences*, 46(5): 661–686.

Bélair, S., Brown, R., Mailhot, J., Bilodeau, B., and Crevier, L.-P. (**2003**a). "Operational implementation of the ISBA land surface scheme in the Canadian regional weather forecast model. Part II: cold season results." *Journal of Hydrometeorology*, 4(2): 371–386.

Bélair, S., Crevier, L.-P., Mailhot, J., Bilodeau, B., and Delage, Y. (**2003**b). "Operational implementation of the ISBA land surface scheme in the canadian regional weather forecast model. Part I: warm season results." *Journal of Hydrometeorology*, 4(2): 352–370.

Bergeron, O., Margolis, H. A., Coursolle, C., and Giasson, M.-A. (**2008**). "How does forest harvest influence carbon dioxide fluxes of black spruce ecosystems in eastern North America?" *Agricultural and Forest Meteorology*, 148(4): 537–548.

Blöschl, G., Gutknecht, D., and Kirnbauer, R. (**1991**). "Distributed snowmelt simulations in an alpine catchment. 1. Model evaluation on the

basis of snow cover patterns." *Water Resource Research*, 27(12): 3171–3179.

Boone, A., Habets, F., Noilhan, J., Clark, D., Dirmeyer, P., Fox, S., Gusev, Y., Haddeland, I., Koster, R., Lohmann, D., Mahanama, S., Mitchell, K., Nasonova, O., Niu, G. Y., Pitman, A., Polcher, J., Shmakin, A. B., Tanaka, K., van den Hurk, B., rant, S., Verseghy, D., Viterbo, P., and Yang, Z. L. (**2004**). "The Rhône-aggregation land surface scheme intercomparison project: an overview." *Journal of Climate*, 17(1): 187–208.

Bornstein, R. and Lin, Q. (**2000**). "Urban heat islands and summertime convective thunderstorms in Atlanta: three case studies." *Atmospheric Environment*, 34(3): 507–516.

Brandt, R. E. (**1993**). "Solar-heating rates and temperature profiles in Antarctic snow and ice." *The Journal of glaciology*, 39(131): 99.

Brest, C. L. (**1987**). "Seasonal albedo of an urban & rural landscape from satellite observations." *Journal of Applied Meteorology*, 26(9): 1169–1187.

Brown, R., Bartlett, P., MacKay, M., and Verseghy, D. (**2006**). "Evaluation of snow cover in CLASS for SnowMIP." *ATMOSPHERE-OCEAN*, 44(3): 223–238.

Brun, E., Martin, E., Simon, V., Gendre, C., and Coleou, C. (**1989**). "An energy and mass model of snow cover suitable for operational avalanche forecasting." *Journal of Glaciology*, 35(121): 333–342.

Buttle, J. M. and Xu, F. (**1988**). "Snowmelt runoff in suburban environments." *Nordic Hydrology*, 19: 19–40.

Canada, G. O. (**2007**). "Portrait of the Canadian population in 2006, 2006 census."

Christen, A. (**2009**). "Urban flux network - IAUC." Internet website. URL `http://www.geog.ubc.ca/urbanflux/index.html`.

Cobos, D. R. and Baker, J. M. (**2003**). "In situ measurement of soil heat flux with the gradient method." *Vadose Zone J*, 2(4): 589–594.

Colbeck, S. C. (**1989**). "Snow-crystal growth with varying surface temperatures and radiation penetration." *The Journal of glaciology*, 35(119): 23.

Conway, H., Gades, A., and Raymond, C. F. (**1996**). "Albedo of dirty snow during conditions of melt." *Water Resource Research*, 32(6): 1713–1718.

Deardorff, J. W. (**1978**). "Efficient prediction of ground surface-temperature and moisture, with inclusion of a layer of vegetation." *Journal of Geophysical Research-Oceans and Atmospheres*, 83(Nc4): 1889–1903.

Degunther, M., Meerkotter, R., Albold, A., and Seckmeyer, G. (**1998**). "Case study on the influence of inhomogeneous surface albedo on UV irradiance." *Geophysical Research Letters*, 25(19): 3587–3590.

Douville, H., Royer, J. F., and Mahfouf, J. F. (**1995**). "A new snow parameterization for the Météo-France climate model. Part I: validation in stand-alone experiments." *Climate Dynamics*, 12(1): 21–35.

EPiCC (**2010**). "Environmental Prediction in Canadian Cities." internet website. URL `http://www.epicc.uwo.ca/`.

Essery, R., Martin, E., Douville, H., Fernández, A., and Brun, E. (**1999**). "A comparison of four snow models using observations from an alpine site." *Climate Dynamics*, 15(8): 583–593.

Foken, T. and Leclerc, M. Y. (**2004**). "Methods and limitations in validation of footprint models." *Agricultural and Forest Meteorology*, 127(3-4): 223–234.

Fuchs, M. and Tanner, C. (**1968**). "Calibration and field test of soil heat flux plates." *Soil Science Society of America Proceedings*, 32: 326–328.

Goodison, B. E., Ferguson, H. L., and McKay, G. A. (**1981**). "Measurement and data analysis." In D. M. Gray and D. H. Male, editors, "Handbook of Snow. Principles, Processes, Management & Use," pages 191–274. Pergamon Press, Willowdale, Ontario.

Grenfell, T. C., Warren, S. G., and Mullen, P. C. (**1994**). "Reflection of solar-Radiation by the antarctic snow surface at ultraviolet, visible, and near-infrared wavelengths." *Journal of Geophysical Research-Atmospheres*, 99(D9): 18 669–18 684.

Haenel, H. D. and Grünhage, L. (**1999**). "Footprint analysis: a closed analytical solution based on height-dependent profiles of wind speed and eddy viscosity." *Boundary-Layer Meteorology*, 93(3): 395–409.

Ho, C. L. I. and Valeo, C. (**2005**). "Observations of urban snow properties in Calgary, Canada." *Hydrological Processes*, 19(2): 459–473.

Horst, T. W. (**1999**). "The footprint for estimation of atmosphere-surface exchange fluxes by profile techniques." *Boundary-Layer Meteorology*, 90(2): 171–188.

Hsieh, C.-I., Katul, G., and Chi, T.-w. (**2000**). "An approximate analytical model for footprint estimation of scalar fluxes in thermally stratified atmospheric flows." *Advances in Water Resources*, 23(7): 765–772.

Kljun, N., Rotach, M. W., and Schmid, H. P. (**2002**). "A three-dimensional backward lagrangian footprint model for a wide range of boundary-layer Stratifications." *Boundary-Layer Meteorology*, 103(2): 205–226.

Kondo, J. and Yamazaki, T. (**1990**). "A prediction model for snowmelt, snow surface temperature and freezing depth using a heat balance method." *Journal of Applied Meteorology*, 29(5): 375–384.

Kormann, R. and Meixner, F. (**2001**). "An analytical footprint model for non-neutral stratification." *Boundary-Layer Meteorology*, 99(2): 207–224.

Kung, E. C., Bryson, R. A., and Lenschow, D. H. (**1964**). "Study of a continental surface albedo on the basis of flight measurements and structure of the earth's surface cover over North America." *Monthly Weather Review*, 92(12): 543–564.

Langham, E. J. (**1981**). "Physics and properties of snowcover." In D. M. Gray and D. H. Male, editors, "Handbook of Snow. Principles, Processes, Management & Use," pages 275–337. Pergamon Press, Willowdale, Ontario.

Leclerc, M. Y., Meskhidze, N., and Finn, D. (**2003**). "Comparison between measured tracer fluxes and footprint model predictions over a homogeneous canopy of intermediate roughness." *Agricultural and Forest Meteorology*, 117(3-4): 145–158.

Leclerc, M. Y. and Thurtell, G. W. (**1990**). "Footprint prediction of scalar fluxes using a Markovian analysis." *Boundary-Layer Meteorology*, 52(3): 247–258.

Lemonsu, A., Bélair, S., Mailhot, J., Benjamin, M., Chagnon, F., Morneau, G., Harvey, B., Voogt, J., and Jean, M. (**2008**). "Overview and first results of the Montreal urban snow experiment 2005." *Journal of Applied Meteorology and Climatology*, 47(1): 59–75.

Loth, B., Graf, H.-F., and Oberhuber, J. M. (**1993**). "Snow cover model for global climate simulations." *Journal of Geophysical Research*, 98(D6): 10 451–10 464.

Lynch-Stieglitz, M. (**1994**). "The development and validation of a simple snow model for the GISS GCM." *Journal of Climate*, 7(12): 1842–1855.

Male, D. H. and Gray, D. M. (**1981**). "Snowcover ablation and runoff." In D. M. Gray and D. H. Male, editors, "Handbook of Snow. Principles, Processes, Management & Use," pages 360–436. Pergamon Press, Willowdale, Ontario.

Manabe, S. (**1969**). "Climate and the ocean circulation 1." *Monthly Weather Review*, 97(11): 739–774.

Marshall, S., Roads, J. O., and Glatzmaier, G. (**1994**). "Snow hydrology in a general circulation model." *Journal of Climate*, 7(8): 1251–1269.

Masson, V. (**2000**). "A physically-based scheme for the urban energy budget in atmospheric models." *Boundary-Layer Meteorology*, 94(3): 357–397.

Maxwell, G. B. (**1971**). *Spatial and temporal variations in urban air temperatures*. Master's thesis, McGill.

McFarlane, N. A., Boer, G. J., Blanchet, J. P., and Lazare, M. (**1992**). "The canadian climate centre second-generation general circulation model and its equilibrium climate." *Journal of Climate*, 5(10): 1013–1044.

McKay, G. A. and Gray, D. M. (**1981**). "The distribution of snowcover." In D. M. Gray and D. H. Male, editors, "Handbook of Snow. Principles, Processes, Management & Use," pages 153–190. Pergamon Press, Willowdale, Ontario.

Messier, F. (**1995**). "Is there evidence for a cumulative effect of snow on moose and deer populations." *Journal of Animal Ecology*, 64(1): 136–140.

Nanni, B. E. (**2008**a). "Aerial photograph of EPiCC Montreal suburban site." Personal Communication.

Nanni, B. E. (**2008**b). "Aerial photograph of EPiCC Montreal urban site." Personal Communication.

Noilhan, J. and Planton, S. (**1989**). "A simple parameterization of land surface processes for meteorological models." *Monthly Weather Review*,

117(3): 536–549.

North, G. R. and Coakley, J. A. (**1979**). "Differences between seasonal and mean annual energy balance model calculations of climate and climate sensitivity." *Journal of the Atmospheric Sciences*, 36(7): 1189–1204.

Obled, C. and Rosse, B. (**1977**). "Mathematical models of a melting snowpack at an index plot." *Journal of Hydrology*, 32(1-2): 139–163.

Oke, T. R. (**1981**). "Canyon geometry and the nocturnal urban heat island: Comparison of scale model and field observations." *International Journal of Climatology*, 1(3): 237–254.

Oke, T. R. (**1982**). "The energetic basis of the urban heat island." *Quarterly Journal of the Royal Meteorological Society*, 108(455): 1–24.

Oke, T. R. (**1987**). *Boundary layer climates*. Routledge, Abingdon, Great Britain; New York, United States, 2nd edition.

Oke, T. R. (**1997**). "Surface climate processes." In W. Bailey, T. R. Oke, and W. R. Rouse, editors, "The Surface Climates of Canada," McGill Queen's University press, Montreal & Kingston, London, Buffalo.

Pomeroy, J. W. and Goodison, B. E. (**1997**). "Winter and snow." In W. Bailey, T. R. Oke, and W. R. Rouse, editors, "The Surface Climates of Canada," McGill Queen's University press, Montreal & Kingston, London, Buffalo.

Pomeroy, J. W. and Gray, D. M. (**1995**). *snowcover accumulation, relocation and management*. National Hydrology Research Institute, Saskatoon, Saskatchewan.

Ripley, E. A. and Archibold, O. W. (**2002**). "Accuracy of Canadian short- and medium-range weather forecasts." *Weather*, 57(12): 448–457.

Rotach, M. W., Gryning, S.-E., and Tassone, C. (**1996**). "A two-dimensional Lagrangian stochastic dispersion model for daytime conditions." *Quarterly Journal of the Royal Meteorological Society*, 122(530): 367–389.

Schmid, H. P. (**1994**). "Source areas for scalars and scalar fluxes." *Boundary-Layer Meteorology*, 67(3): 293–318.

Schmid, H. P. (**1997**). "Experimental design for flux measurements: matching scales of observations and fluxes." *Agricultural and Forest Meteorology*, 87(2-3): 179–200.

Schmid, H. P. (**2002**). "Footprint modeling for vegetation atmosphere exchange studies: a review and perspective." *Agricultural and Forest Meteorology*, 113(1-4): 159–183.

Schmid, H. P. and Oke, T. (**1990**). "A model to estimate the source area contributing to turbulent exchange in the surface layer over patchy terrain." *Quarterly Journal of the Royal Meteorological Society*, 116(494): 965–988.

Schuepp, P. H., Leclerc, M. Y., MacPherson, J. I., and Desjardins, R. L. (**1990**). "Footprint prediction of scalar fluxes from analytical solutions of the diffusion equation." *Boundary-Layer Meteorology*, 50(1): 355–373.

Semádeni-Davies, A. and Bengtsson, L. (**1998**). "Snowmelt sensitivity to radiation in the urban environment." *Hydrological Sciences Journal-Journal Des Sciences Hydrologiques*, 43(1): 67–89.

Semádeni-Davies, A. F. (**1999**). "Snow heterogeneity in Luleå, Sweden." *Urban Water*, 1(1): 39–47.

Semádeni-Davies, A. F. (**2000**). "Representation of snow in urban drainage models." *Journal of Hydrologic Engineering*, 5(4): 363–370.

Soux, A., Voogt, J., and Oke, T. (**2004**). "A model to calculate what a remote sensor 'sees' of an urban surface." *Boundary-Layer Meteorology*,

112(2): 401–424.

Steppuhn, H. (**1981**). "Snow and agriculture." In D. M. Gray and D. H. Male, editors, "Handbook of Snow. Principles, Processes, Management & Use," pages 60–126. Pergamon Press, Willowdale, Ontario.

Stull, R. B. (**1989**). *An introduction to boundary layer meteorology*. Atmospheric Sciences Library. Kluwer Academic Publishers, Dodrecht Boston London.

Sundin, E., Andreasson, P., and Viklander, M. (**1999**). "An energy budget approach to urban snow deposit melt." *Nordic Hydrology*, 30(1): 39–56.

Tanner, C. and Thurtell, G. (**1969**). "Anemoclinometer measurements of Reynolds stress and heat transport in the atmospheric surface layer." Technical Report ECOM-66-G22F, University of Wisconsin, Madison, WI.

Tarboton, D., Blöschl, G., Cooley, K., Kirnbauer, R., and Luce, C. (**2001**). "Spatial snow cover processes at Kühtai and Reynolds Creek." In R. Grayson and G. Blöschl, editors, "Spatial Patterns in Catchment Hydrology," pages 158–186. Cambridge University Press, Cambridge, UK New York, USA Melbourne, Australia Madrid, Spain Cape Town, South Africa.

Thomson, D. J. (**1987**). "Criteria for the selection of stochastic models of particle trajectories in turbulent flows." *Journal of Fluid Mechanics Digital Archive*, 180(-1): 529–556.

Ueno, K., Tanaka, K., Tsutsui, H., and Li, M. (**2007**). "Snow cover conditions in the Tibetan plateau observed during the winter of 2003/2004." *Arctic, Antarctic, and Alpine Research*, 39(1): 152–164.

Valeo, C. and Ho, C. L. I. (**2004**). "Modelling urban snowmelt runoff." *Journal of Hydrology*, 299(3-4): 237–251.

Verseghy, D. L. (**1991**). "Class - A Canadian land surface scheme for GCMS. I. Soil model." *International Journal of Climatology*, 11(2): 111–133.

Verseghy, D. L., McFarlane, N. A., and Lazare, M. (**1993**). "Class - A Canadian land surface scheme for GCMS, II. Vegetation model and coupled runs." *International Journal of Climatology*, 13(4): 347–370.

Ville de Montréal (**2010**). "Montréal en statistiques." Internet website. URL `http://ville.montreal.qc.ca/portal/page?_pageid=2077,2454913&_dad=portal&_schema=PORTAL`.

Warren, S. G. and Wiscombe, W. J. (**1980**). "A model for the spectral albedo of snow. II: snow containing atmospheric aerosols." *Journal of the Atmospheric Sciences*, 37(12): 2734–2745.

Webb, E. K., Pearman, G. I., and Leuning, R. (**1980**). "Correction of flux measurements for density effects due to heat and water vapour transfer." *Quarterly Journal of the Royal Meteorological Society*, 106(447): 85–100.

Wilmott, C. J. (**1981**). "On the validation of models." *Physical Geography*, 2: 184.

Wiscombe, W. J. and Warren, S. G. (**1980**). "A model for the spectral albedo of snow. I: pure snow." *Journal of the Atmospheric Sciences*, 37(12): 2712–2733.

Wuttke, S., Seckmeyer, G., and Konig-Lang, G. (**2006**). "Measurements of spectral snow albedo at Neumayer, Antarctica." *Annales Geophysicae*, 24(1): 7–21.

Yang, Z.-L., Dickinson, R. E., Hahmann, A. N., Niu, G.-Y., Shaikh, M., Gao, X., Bales, R. C., Sorroshian, S., and Jin, J. (**1999**). "Simulation of snow mass and extent in general circulation models." *Hydrological Processes*, 13: 2097–2113.

Yang, Z.-L., Dickinson, R. E., Robock, A., and Vinnikov, K. Y. (**1997**). "Validation of the snow submodel of the Biosphere-Atmosphere Transfer Scheme with Russian snow cover and meteorological observational data." *Journal of Climate*, 10(2): 353–373.